THE DEVELOPMENT OF THE TONER DENSITY SENSOR FOR CLOSED-LOOP FEEDBACK LASER PRINTER CALIBRATION

by

Keisha Josephine Thomas

A dissertation submitted to the faculty of
The University of North Carolina at Charlotte
in partial fulfillment of the requirements
for the degree of Doctor of Philosophy in
Electrical Engineering

Charlotte

2009

Approved by:

_____
Dr. Ivan Howitt

_____
Dr. Tom Weldon

_____
Dr. Yogendra Kakad

_____
Dr. Andrew Willis

_____
Dr. Xintao Wu

ABSTRACT

KEISHA JOSEPHINE THOMAS. The development of the toner density sensor for closed-loop feedback laser printer calibration. (Under the direction of DR. IVAN L. HOWITT)

A new infrared (IR) sensor was developed for application in closed-loop feedback printer calibration as it relates to monochrome (black toner only) laser printers. The toner density IR sensor (TDS) was introduced in the early 1980's; however, due to cost and limitation of technologies at the time, implementation was not accomplished until within the past decade. Existing IR sensor designs do not discuss/address:

- EMI (electromagnetic interference) effects on the sensor due to EP (electrophotography) components
- Design considerations for environmental conditions
- Sensor response time as it affects printer process speed

The toner density sensor (TDS) implemented in the Lexmark E series printer reduces these problems and eliminates the use of the current traditional "open-loop" (meaning feedback are parameters not directly affecting print darkness such as page count, toner level, etc.) calibration process where print darkness is adjusted using previously calculated and stored EP process parameters. The historical process does not have the ability to capture cartridge component variation and environmental changes which affect print darkness variation. The TDS captures real time data which is used to calculate EP process parameters for the adjustment of print darkness; as a result, greatly reducing variations uncontrolled by historical printer calibration. Specifically, the first and primary purpose of this research is to reduce print darkness variation using the TDS. The second goal is to mitigate the TDS EMI implementation issue for reliable data accuracy.

DEDICATION

To my husband Paul, and children, Jasmine, Paul-Louis Jr., and Christian, for their love and support through my journey to achieve this significant milestone in my life.

ACKNOWLEDGMENTS

I would like to thank Dr. Ivan L. Howitt, for his steady encouragement and assistance through this process. He's someone I look up to and try to model. He continued to guide me and steadily provided me with great guidance through professional and personal circumstances. I would also like to thank Dr. Yogendra Kakad for his guidance through my Master's program and motivating my decision to pursue my Ph.D. Furthermore, I would like to thank my committee for allowing me the opportunity to share my interest and research with them. I extend an especially warm thanks to Lexmark International, Inc., for the opportunity to work and apply what I am learning towards a valuable Ph.D. research application. This includes my managers, Ben Newman and Bob Tulenko, along with the rest of the Mono EP Cartridge Technology Development team, and other expert engineers at Lexmark that assisted me with my research.

TABLE OF CONTENTS

LIST OF TABLES

LIST OF FIGURES

LIST OF ABBREVIATIONS

1-D	one-dimensional
A/D	analog to digital
AIO	all-in-one
AlGaAs	aluminum gallium arsenide
AMP	amplifier
AWGN	additive white Gaussian noise
BJT	bipolar junction transistor
CIE	Commission Internationale de l'Eclairage (International Commission on Illumination)
CMOS	complimentary metal oxide semiconductor
CMYK	cyan, magenta, yellow, black
COMP	comparator
DC	direct current
dpi	dots per inch
DTFT	discrete-time Fourier transform
E_g	gap energy
EMI	electromagnetic interference
EP	electrophotography
ESD	electrostatic discharge
EXLT	extra light
FFT	fast Fourier transform
FIR	finite impulse response

GaAs	gallium arsenide
HP	Hewlett-Packard
HVPS	high voltage power supply
IBM Corp.	International Business Machines Corporation
IC	integrated circuit
IIR	infinite impulse response
IR	infrared
JST	Japan Solderless Terminal
LED	light-emitting diode
LSU	laser scanning unit
LTV	light-to-voltage
LUT	look-up table
LXK	Lexmark
MFP	multifunction printer
MOCVD	metalorganic chemical vapor deposition
mono	monochrome
NPN	majority carrier electrons-majority carrier holes-majority carrier electrons
op amp	operational amplifier
PCB	printed circuit board
PC drum	photoconductor drum
POR	power on
PPM	pages per minute
PSD	power spectral density

PWM	pulse-width modulation
QWIP	quantum well infrared photo detector
RC	resistor-capacitor
REF	reference
RGB	red, green, blue
RH	relative humidity
RRO	rail-to-rail output
TDS	toner density sensor
TPS	toner patch sensor
TRC	tone response curve
w.r.t.	with respect to

CHAPTER 1: INTRODUCTION

Monochrome laser printers are known for the ability to produce high quality prints at fast speeds with little maintenance. Laser printing adopts the concept of electrophotography (EP) to produce robust prints. The EP process involves the transfer of surface charges to create electrostatic images. EP process parameters of the printer are utilized to control print darkness. As a result of part to part variation in EP components (discussed in chapter 2 section 2) along with environmental changes and device degradation affecting the printer cartridge, parameters controlling print darkness no longer maintain consistent darkness throughout the life of a cartridge. Consequently, there is a great deal of variation in print darkness. The desire is to produce an embedded sensing mechanism that captures real-time data utilized to adjust print darkness variation.

1.1 Goals of Printer Calibration

Printer calibration is the process of maintaining consistent print darkness over the life of the cartridge. Printer calibration has been performed since the inception of printers. The main goals of printer calibration are to:

- **Maintain consistent print darkness through the life of a cartridge from the first print to the last print in room temperature.** This is found by empirical testing in room temperature environment. Basic toner carries various shapes and without any printer calibration, prints are darker over the life of a cartridge.

- **Maintain print darkness through cartridge and component changes.** The print darkness must be the same when changing out a defective component or a worn component. Also mentioned previously, EP component part-to-part variation is very high.
- **Maintain print darkness through environmental changes surrounding the printer.** As mentioned before, EP components are heavily dependent upon environmental conditions which affect print darkness. EP components are also affected by thermal conditions induced by the printer's process speed. Today, high-end laser printers can operate faster than 60 pages per minute (PPM). Such speeds cause EP component characteristics to change.
- **Maintain adequate print darkness through different media types.** Since media have different elemental components, color, thickness, and size and shape, the print darkness also shifts. Even within each media type, there exist characteristic variations that affect print darkness.

The current print darkness calibration system tries to address these goals; however, the traditional system is not very effective in maintaining consistent print darkness.

1.2 The Current Printer Calibration Process and Challenges

The current open-loop calibration process involves using EP process parameters to adjust print darkness. LUTs (look-up tables) are developed by empirically testing optimal values for each EP process parameter for every L* change in print darkness over cartridge life. L* is a CIE (Commission Internationale de l'Eclairage or International Commission on Illumination) [1] standard parameter used to measure change in lightness or darkness seen by the human eye. This is performed unknown of actual real-time print

darkness level and unknown of variation from part to part.

The LUT concept presents many problems:

1) The change of optimal values to adjust print darkness does not actually coincide with actual print darkness level. This is because there is no feedback relationship in the printer's change of print darkness level.
2) Part to part variation is not considered
3) LUT's are universal and does not represent characteristics of all cartridges under all varying environmental conditions.
4) The outcome is print quality not being optimized resulting in darker or lighter prints over the life of the printer cartridge

Several challenges are faced when trying to effectively perform printer calibration using the traditional process. Higher demand for producing faster speed printers is another one of the major challenges. The current printer calibration process maintain less error for slower print speeds; however, with increasing speeds and printer options such as duplexing, the current printer calibration process must be altered or a new calibration process must be introduced. This has become necessary to effectively calibrate print darkness for today's features, speeds, and applications.

1.3 Goals of the Toner Density Sensor Design

The toner density sensor (TDS) or (also termed) the toner patch sensor (TPS) measures toner developed on the PC (photoconductor) drum. Collected data from the TDS is used in an algorithm to adjust EP process parameters that control print darkness over the life of a cartridge.

Since the TDS is positioned in the midst of EP components, electromagnetic

interference (EMI) can affect the TDS output signal. EMI exist in the printer due to motors rotating electrophotographic components (discussed in the Electrophotography section chapter 2 section 2).

The first goal of the toner density sensor is to reduce current print darkness variation through the life of a given printer cartridge. The second goal of the TDS is to mitigate electromagnetic interference (EMI) affecting the TDS output signal during implementation. The new toner density sensor design meets these goals, functions well under environmental changes, maintains a fast response and requires little additional resource to implement.

The dissertation addresses the methods in which the toner density sensor was designed and tested to verify its performance while experiencing EMI and various environmental conditions. Also discussed is the reduction of print darkness variation using the TDS. Reduction of print darkness variation and EMI experienced by the TDS helps to provide consistent image quality over the life of every cartridge through the life of the printer.

1.4 Dissertation Structure

The dissertation describes previous research, accomplishments, and current techniques to improve print quality which drives the design of the toner density sensor. Included in this document are techniques proposed to improve print quality including utilization of real-time closed-loop feedback data to adjust EP component process parameters. The dissertation describes the solution of the toner density sensor and its function specifically towards the printer calibration process. Theory behind the design process and implementation is explained in detail. The sensor design process includes

circuit analysis and control theory.

The dissertation's background (in chapter 2 section 1) describes the history of laser printers. The electrophotograhy (EP) section (section 2) describes the science behind laser cartridge technology and halftoning (section 3) describes the process of converting a continuous toned image into a reproduced digital image. The color science section (chapter 2 section 4) highlights common aspects and metrics applied in printer technology. The printer calibration section (section 5) mentions issues causing print variation which introduce various calibration methods applied to printers. Section 6 of chapter 2 identifies past applications of sensors in laser printers and highlights differences with the proposed toner density sensor. The last section of chapter 2 (section 7) discusses band-gap engineering advancements and the great impact these recent advancements have made regarding the toner density sensor.

Chapter 3 discusses previously explored printer calibration techniques including the traditional open-loop calibration and the new closed-loop calibration process. These processes are then compared to the TDS design. Chapter 4 goes into the details of related work regarding an infrared (IR) sensor used for closed-loop feedback printer calibration. It compares and analyzes the details. The TDS design is discussed in detail in chapter 5 with theoretical analysis. The design reduces the common problems of EMI and environmental changes. Chapter 6 is the implementation and interpretation where it describes how the sensor was positioned in the printer and it is actually applied for calibrating print darkness. Chapter 6 also discusses challenges in implementing the sensor and test results (including actual print samples taken for comparison of print darkness variation). Test results of the sensor implementation results are then compared

to the previous traditional printer calibration results.

The final Assessment of the toner density sensor performance is discussed in chapter 7. Challenges with implementation, test results, and comparison to previous printer calibration methods are summarized. The conclusion (chapter 8) summarizes the toner density sensor's use in monochrome laser printers and the benefits which can greatly impact the laser printing industry.

CHAPTER 2: BACKGROUND

The background chapter describes the laser printer industry, electrophotography, halftoning, color science, printer calibration, previous sensor applications in printers, and advancements in optics. The sensor is a contribution to each of these areas and each area has opportunity for future applications to improve printing using the toner density sensor. Each section elaborates each topic and finally links its relevance to the TDS.

2.1 The Laser Printing Industry

Today's industries and businesses use laser printers for their high-quality prints at fast speeds. The first laser printer was produced by Gary Starkweather from Xerox Corporation [2] in 1970 where a copier was converted to a printer. The first commercially produced laser printer was the IBM [3] model 3800 in 1976.

Xerox Laser Printer Model 9700 ca. 1977

Figure 1 [2]. The Xerox laser printer model 9700 ca. 1977. The figure is a picture of one of the first laser printers manufactured.

During this period, the laser printer was used for high volume printing such as invoices and mailing labels. The first laser printer produced for computer compatibility was the Xerox Star 8010 running pages at 8 pages per minute (PPM). The printer costs ~$17,000 and resulted in relatively small sales as compared with today. Over the next several years, laser printers evolved into wide-spread applications. Other companies such as Cannon, Hewlett-Packard (HP), Brother, Samsung, and IBM's Printer Division (now Lexmark) came aboard in the laser printing business. By the late 1980's, an estimated 300 million electronic prints were being generated per day by laser printers [4].

Currently, laser printers include color laser printers, monochrome (black toner only) laser printers, multi-function laser printers (MFP's) and all-in-one (AIO) laser printers. Within each laser printer type are low-end, mid-range, and high-end models (typically determined by maximum print speed). Laser printers are continuing to replace ink jet printers (home-use printers) as improvements and attempts are made to reduce the cost and size of laser printer components (such as cartridges and other maintenance items). Furthermore, laser printers are increasingly displaying improvement in photographic and graphic prints (where ink jets are currently more favorable). All of these improvements are translating to increasing popularity of the laser printer for home use.

2.2 Electrophotography

The laser printer adopts the concept of electrophotography to effectively produce an image unto different types of media (such as paper, transparencies, or envelopes). Electrophotography (EP) is the use of electrostatics to create images on photosensitive material. During the turn of the 20th century, several attempts were made to create a

process that will combine electricity with photography to create images. In 1938, Chester Carlson from Haloid Corporation (which became Xerox Corporation) [5] was the first to successfully create a practical electrophotographic system.

Electrophotography and laser technologies first appeared in the late 1950s [6]. As mentioned previously, the first printers to combine the technologies did not occur until the 1970s. The total monochrome (mono) EP process includes the sub-processes of exposure, charge, development, transfer, clean, and fuse [7] to effectively produce an image unto media. Figure 2 is a cross-sectional outline of the main EP components utilized to perform the sub-processes listed above.

Basic EP Components of the Mono Laser Printer

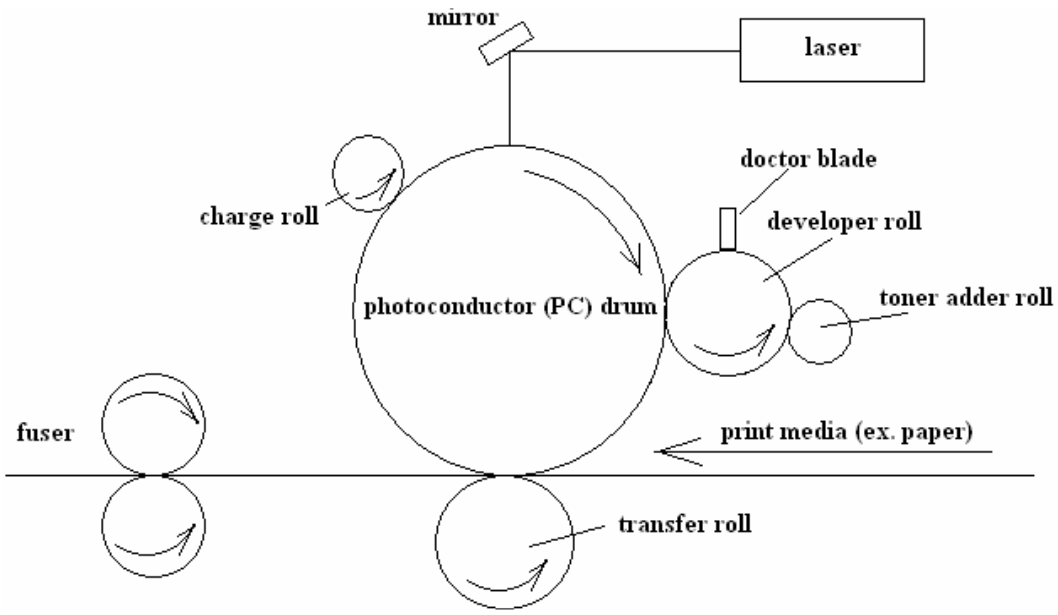

Figure 2 [5], [6], [7]. The basic EP components of a monochrome laser printer. The electrophotography (EP) components displayed are the main components that produce an image unto media (such as paper). The PC drum is charged highly negatively by the charge roll. The laser emits small dots (in the form of the image) onto the PC drum discharging those areas. The toner adder roll transfers toner to the developer roll which is smoothed and charged by the doctor blade. The charged toner is transferred to the PC drum where the transfer roll attracts the toner unto the media. The media finally goes through the fuser rolls to “fuse” the toner unto media creating the final printed product.

In the charge process, the charge roller or corona is charged by the printer's high voltage power supply to a highly negative voltage (which also supplies voltage to all other EP components of the printer). The voltage charges the light-sensitive photoconductor drum [8] for laser discharge and toner development on the drum.

A laser scanning unit (LSU) emits intensity pulse width modulated (PWM) monochrome laser light to a cylindrical photoconductor (PC) drum [9]. PC drums are typically hollow and ranges between 10-35µm in thickness with diameters averaging around 20mm [10]. The emitted light discharges spots on the drum which carries the shape of the image (shown in figure 3).

Example of a Discharged Image on the PC Drum

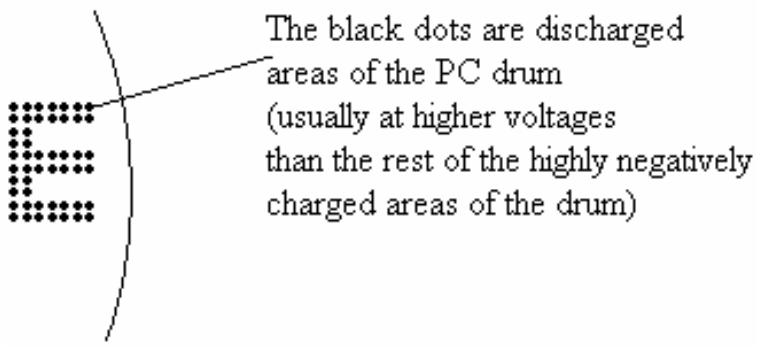

Figure 3. An example of a discharged image on the PC drum. The laser from figure 2 emits dots onto the photoconductor (PC) drum forming the image. The PC drum is discharged to a more positive negative value for toner transfer (black area) while the rest of the area around the image (white area) remains charged at a highly negative value. *The letter "E" is enlarged for display purposes only.

In the development process, toner (plastic powder-roughly 7 microns in radius [11]) is added to the developer via use of the toner adder roll. The toner adder roller transfers toner to the negatively charged developer roller where the toner is smoothed and charged by the less negative doctor blade. The photoconductor (PC) drum is made up of layers of

dielectric material on a conductive surface [12] and attracts the negatively charged toner (since the potential difference between the PC drum and developer is large enough to attract toner).

In the transfer process, media (such as paper) is transferred between the PC drum and the transfer roll where the positively charged transfer roller attracts the negatively charged toner unto the media. The media travels to the fuser (high temperature rollers) where pressure and heat is applied to "fuse" toner unto the media [13] (hence why prints are usually warm when fresh out of a laser printer).

During the clean cycle, the cleaner mechanically and electrostatically removes toner from the charge roller and PC drum (effectively cleaning these components) in order to be ready for the next print job [14]. EP components are the main components of a typical cartridge. The color EP process typically requires four cartridges [15] for each color (cyan, magenta, yellow, and black).

The EP system is continuously improved to meet the changing needs of current printing demands. Revolutionizing printer technology includes overcoming challenges for EP components to:

1. Adjust for environmental changes, including temperature and humidity [16], [17]
2. Incorporate faster print speeds
3. Adjust for improved halftoning techniques (chapter 2 section 3)
4. Combine multiple functions such as duplexing, scanning and copying
5. Adjust for toner size changes and new toner technology (i.e. chemically produced toner [18])

These are on-going issues for printer development. The toner density sensor assists in overcoming some of these challenges (mentioned in the Assessment chapter 7) and was designed around many of these limitations.

2.3 Halftoning

Halftoning is the process of creating a digital image from a continuous tone image while maintaining the illusion that the image is still a continuous tone [19],[20],[21],[22]. This concept is applied across the laser printing industry. Halftoning is also referred to as spatial dithering [23]. This technique is mainly applied in printing and dates back to the mid 1800's when William Henry Fox Talbot [24] captured an image on to a printing plate using a sensitized plate. Talbot used a black woven cloth (acting as a screen) that separated the image into small dots on a printing plate. Halftoning is built on the concept of converting an image into small dot patterns. The level of quality in a halftone algorithm is judged by the image quality to the end user.

Various Halftone Images

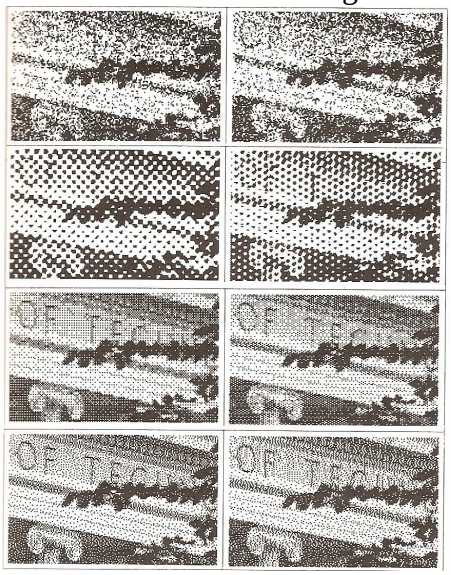

Figure 4 [20]. A variety of halftone images. Halftoning converts a continuous image into dots. Shown above are the results of various methods to create a halftone image.

Halftone dot patterns are classified into two categories: amplitude modulation (AM) and frequency modulation (FM or Stochastic screening) [25], as applied in radio communications. The dot size is modulated within a fixed frequency space in AM and the frequency is modulated within a fixed dot size space in Stochastic screening.

The process of halftoning takes the separated image and breaks the image into small dots (from 0 to 1 where 0 = white and 1 = black) and compares the dot to a threshold value of 1/2. If the dot is lighter than ½, then the dot is assigned a value of 0 or the dot is darker than the threshold gray level value of ½, the dot is assigned a binary value of 1. As a result, the image is a picture of very small black and white dots.

Halftone Dots

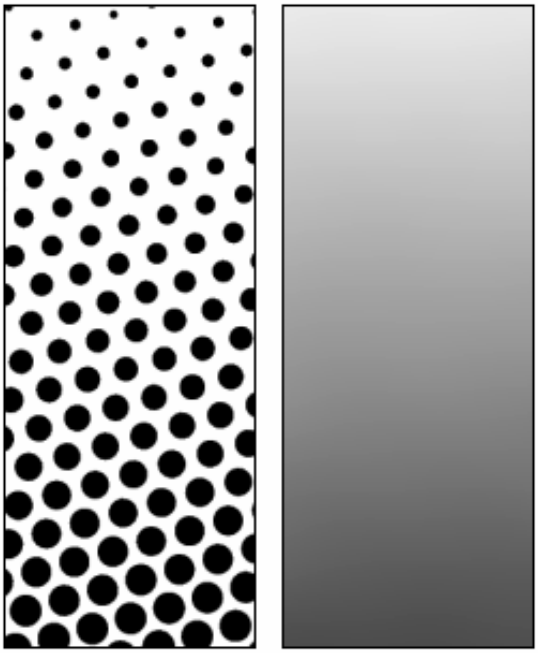

Figure 5 [25]. Halftone dot image. The figure on the left is a very close view of the image on the right.

Another popular type of the halftoning process is called error diffusion developed by Floyd and Steinberg [26]. There are two methods to error diffusion: one dimensional and

two-dimensional error diffusion. In one dimensional error diffusion, the comparison of the original value to the threshold of value of ½ is performed, and the difference between the original value and the threshold value is applied to the next pixel on the image.

In one of the simpler two-dimensional error diffusion algorithms, the error is applied by dividing the error in half and applying to the next pixel. The error is also divided into quarters (i.e. 0.25 = error propagation) and applied to the pixels below both the current processing pixel and the next pixel as shown in equation 1.

$$\frac{1}{4}\begin{bmatrix} \# & 2 \\ 1 & 1 \end{bmatrix}$$ Eq. 1.

Various models for error diffusion include dividing the error into larger areas surrounding the current processing pixel. Some error diffusion models use random error propagation for improved print quality. However, dots are not always equal in size and perfectly square, causing dot gain (where printed dot size is larger than intended) and dot overlap to occur which distorts the image. The size of dots varies with media types (i.e. regular copy paper, card stock, transparencies, envelopes, labels, glossy paper, etc.). Many halftoning techniques include calibrating patterns for improved print darkness (as shown in figure 6).

Since the role of printer calibration is to adjust print darkness, halftoning plays a large role. Printer calibration conducted for one halftone method may not work for all other halftone algorithms including error diffusion [27], [28]. Even for one halftone method, different halftone screens (represented by dpi or dots per inch) require different calibrations. Therefore, printer calibration must have the universal ability to adjust for different types of halftoning techniques, considering that different dot gains and dot

overlaps occur according to each media type. Also, as PPM and dpi increases, algorithm complexity increases and processor speed needs to increase. Closed-loop printer calibration using the TDS can be applied universally considering that print process speed, dpi, dot variations, and halftone methods are all considered in the printer calibration algorithm (explained in chapter 3). Due to these factors, the printer calibration process has to be easily applicable toward future generations of printers.

Image Comparison of Halftone and Error Diffusion

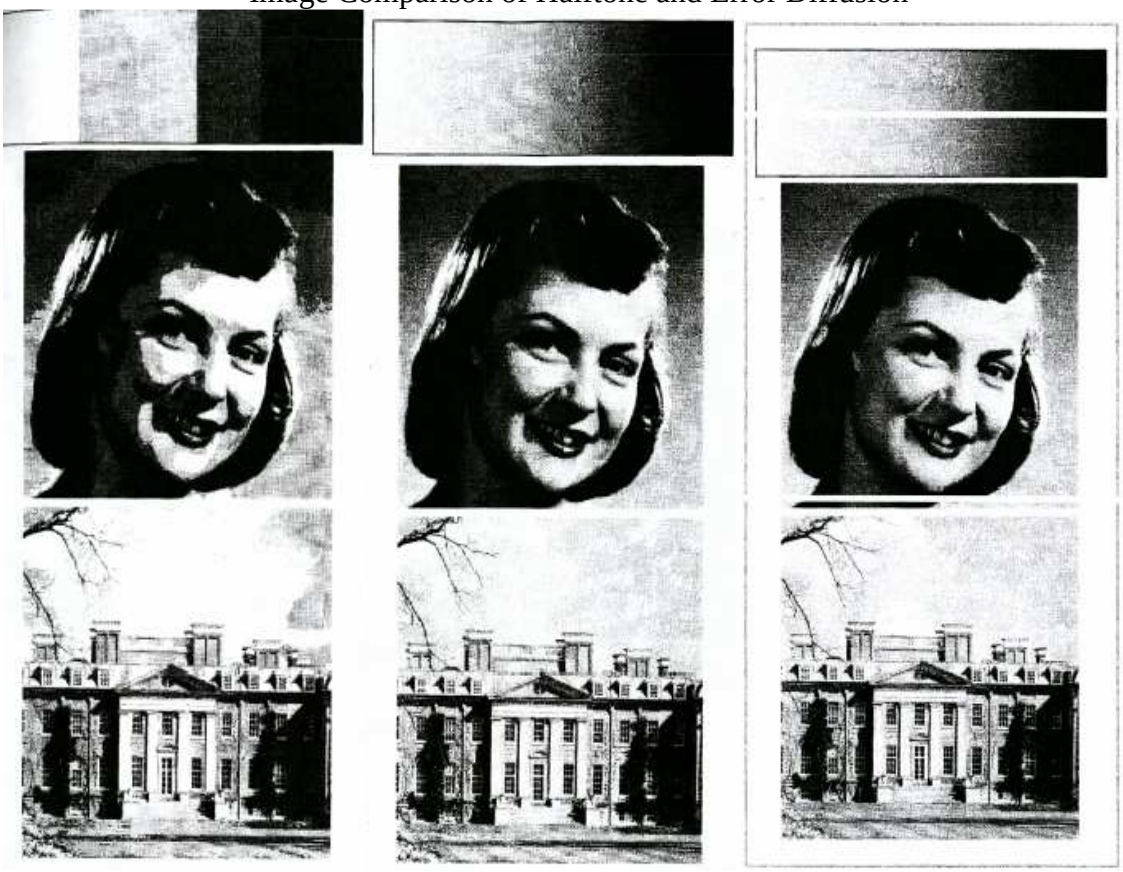

Figure 6a [23]. Basic AM halftoning applied to the image.

Figure 6b [23]. Error diffusion applied to the image. This technique is more improved than basic AM halftoning.

Figure 6c [23]. Random error (error propagation $0 < x < 0.5$. This technique is the most difficult to apply, but provides the best results.

2.4 Color Science

The color laser system has applied various techniques toward improvement of printer calibration for several years. Since past research on printer calibration mainly involved color laser and ink jet printers, this section is introduced to provide the necessary color science background required for chapter 3 (Contributions/Explored Printer Calibration Techniques). Color science also relates to metrics used in monochrome laser printing.

Monochrome laser print darkness is based on levels of gray defined by the color standard system (CIE). The CIE is responsible for developing standards for color metrics and terminology derived from color science [29],[30]. CIEXYZ was developed in 1931 to mathematically define color. X, Y, Z represents mathematical variables close to red, green, and blue respectively since it's been found that humans interpret color by red, green and blue receptors in the eye. Therefore, the three variables are required to describe a color system. The CIEXYZ system was developed by empirically testing directly from human eyes. Many color spaces are a derivation of this color space. By 1976, CIE L*a*b* (commonly seen as CIELAB) was developed in order to determine color differences not captured by CIEXYZ color metrics. This color space became very useful in imaging, where printer technology applies.

L* represents the level of lightness visually interpreted by the human eye. a* and b* represents color component dimensions [31]. L*, a* and b* applies to color laser printing technology where only L* applies to mono laser printing. The mono laser printer calibration process utilizes the defined CIE L* parameter to adjust for print darkness. Printer calibration using the TDS design proposed in this thesis can be potentially applied to the color laser printer. Figure 7 [32] is an example description of the CIELAB color

space system.

Many color spaces are transformations to characterize the device (printer) current color space to a standard mathematical interpretation of the existing color state. In the case of printers, the color space is CMY (cyan, magenta, and yellow) or CMYK (where K=black to not confuse with RGB where B=blue) [33], [34]. Even though RGB is the human perception of color space, CMYK is very useful in printing. RGB color space is additive since all colors are summed to equal white where as CMYK is subtractive where brightness is removed from white. Therefore, this process performs best on white paper since wavelengths of light are absorbed to create colors.

The CIELAB Color Space Map

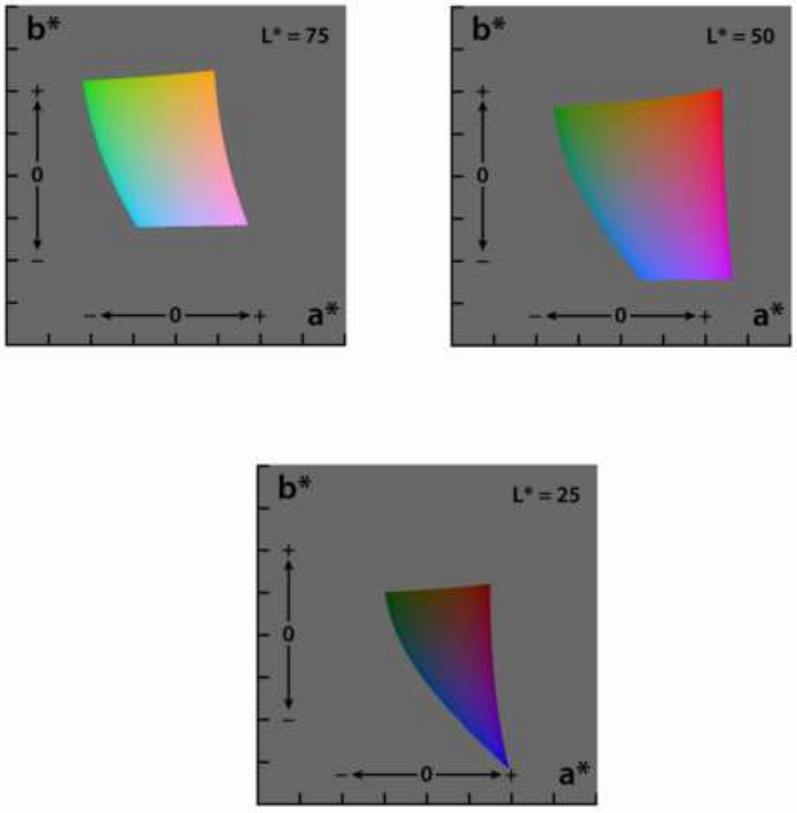

Figure 7 [32]. The CIELAB color space system. L* is the change in brightness seen by the human eye. a* represents the horizontal change from green to magenta and b* is the change from blue to yellow.

In mono laser printing, gray scales are the only level of concern which is characterized by L*. Psychophysicists have determined that the human eye can perceive at least 64 shades of gray. The shades are equal in the human visual space, and can not be performed by the printer. For adequate transformation, the levels of gray are converted to L* to be mathematically and physically useful. In mono and color laser printing system, look-up tables (LUT's) are utilized to adjust each L*, a*, and b* parameter to maintain consistent print darkness.

2.5 Printer Calibration

Temperature and humidity affects print quality of the printer. Factors such as poor toner transfer (too much or too little), background shading, and toner scatter are reported under these environments. It has also been found that each EP component have large enough variation from part to part to effect print quality. Moreover, toner charging (as explained in the section 2) has humidity dependence. As a result, print darkness "drifts" from its original state over the life of a cartridge, resulting in very dark or light prints. Printer calibration is the process of maintaining consistent print darkness over the life of the cartridge. Over the years, research involving printer calibration has evolved with several approaches to maintain consistent print darkness. Open-loop (one dimensional) and closed-loop printer calibration have been either investigated or implemented [31], [35], [36], [37], and [38]. Both of these methods are discussed in chapter 5.

While closed-loop calibration using an embedded sensor has been explored, this paper details the process in making the embedded IR sensor effective and robust for quality implementation. Development of a fast and robust method to printer calibration requires foreknowledge of the system's behavior, simple implementation (for easy

adjustment when changes are made to improve quality for future printer models), and consistent quality output response.

2.6 Sensors in the Printing Industry

Sensors have always been an integral part of the laser printing system ever since the beginning. P. Graf and W. Von Tluck [39] explained that over 70 sensors were utilized in the 1977 Siemens Laser Printer ND 2 [40]. However, the toner density sensor was not formally introduced until R.W. Pries introduced the toner patch sensor (TPS) in 1983 [41]. The TDS is a concept different from many sensor assembly systems in that the application of the sensor is designed and utilized for sophisticated closed-loop adjustment. Previous sensors utilized simpler closed-loop systems (discussed in the following paragraphs), where most feedback parameters have no direct affect on the output (such as page count, number of times a printer was powered on, etc.). Infrared (IR) light sensors have demonstrated their usefulness and versatility for solutions to existing problems and as a result, are being applied to future concepts in the printer industry. A few infrared (IR) light sensors presently used in laser printers are media sensors, environmental conditions sensor, toner concentration sensors, and toner amount sensors [42].

The toner concentration sensor is primarily used for the developer unit. In many color printers, toner is a dual component system comprised of carrier beads and toner. The carrier beads attract toner and transfers toner from the developer to the PC drum. The change in permeability is sensed by the toner concentration sensor and this change determines the concentration of toner.

Primarily in color printer systems, the toner amount sensor is used to read the

specular and diffused light from toner on the transfer belt. The toner amount provides an indication of how much additional voltage is required to attract toner to the transfer belt.

The media sensor determines the media (or most commonly paper) type [43], [44], [45], [46]. Paper can change in thickness and texture ranging from card stock to plain office paper. Paper also carries a range of sizes and shapes such as legal (11.5" X 14") or narrow. In addition, envelopes, labels, and transparencies are also media passed through printers. These types of media require different amounts of toner transfer at different EP process parameters. The media sensor allows the printer to capture the type of media that is going into the printer and may adjust the EP process parameters or may adjust the speed in which the media is running through the printer.

The thermal sensor is used to detect the fuser's heater temperature and provides an indication to turn off and on the fuser heater to maintain consistent fuser temperature during a print cycle. The environmental conditions sensor determines the temperature and humidity surrounding the printer to also adjust EP process parameters.

The commonality of these sensors is that most of them detect toner or media by brightness (density). Involved typically is the use of an emitter and receiver with an electronic circuit to convert light to a measurable output voltage (as shown in figure 8). The DC signal is then sent to an analog-to-digital (A/D) converter to be processed by the printer's engine code.

The paper sensor circuit (shown in figure 8) describes the typical circuit applied to sense various media types for appropriate amount of toner transfer. Depending on the reflection of the media, toner transfer is adjusted by changing transfer voltage to produce optimal prints. The IR signal shown is a phototransistor; however, a photodiode can also

be utilized instead.

Sensor application to improve printer calibration is a similar concept to the sensor applications previously described. The sensor has optical components (i.e. an emitter and detector and electronic components). However, the development of a sensor for closed-loop detection of micron-sized toner with high efficiency, accuracy, and speed is challenging to design.

A Typical Paper Sensor Circuit Used in Laser Printers

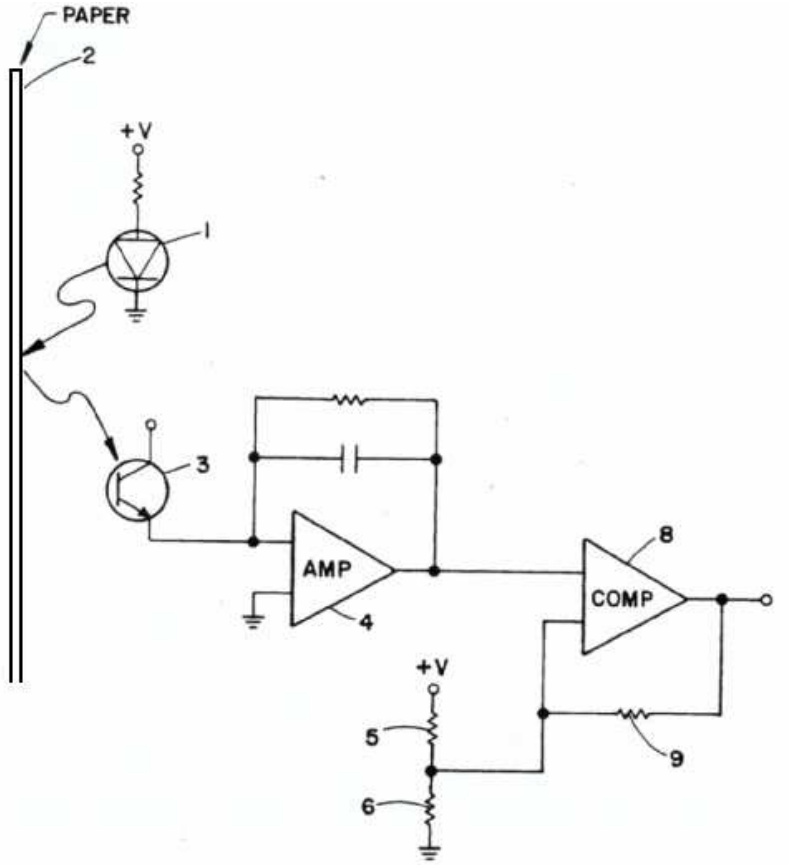

Figure 8 [47]. A typical paper sensor used in a laser printer. The sensor circuit uses a light-emitting diode (LED-4) to send a reference input signal. The reflected light is captured by a phototransistor (3). The amplifier (4) and RC circuit filters noise and amplifies the detected signal. The output of the amplifier is sent to a comparator (8) to provide the change in output in relationship with the reflected light. The output change (as displayed specifically in this figure) is a result of reflected light decrease below a predetermined threshold level (which is calculated by the resistor divider pair 5 and 6).

The TDS signal is utilized to adjust print darkness levels; therefore, strong detection accuracy is required. Captured data from the TDS is correlated to print darkness; however, in paper sensing simply requires a detectable output signal (not necessarily accurate) to verify if media is present. The TDS output signal must not only be accurate, but be free of noise and able to provide the same level of detection under varying environmental conditions. The same is not necessarily required of the paper sensor. Again, only a detectable output signal is required to determine if media is present at the paper path. If the output signal's strength is varied due to environmental conditions, this is acceptable. As long as the sensor output signal is detectable, the paper sensor is functioning.

2.7 Advancements in Optics

Optical components of a typical sensor such as the light-emitting diode (LED) must possess high-detection sensitivity. The LED has advanced from a device created in 1962 with a low efficiency (about 0.1 lm/W) to efficiencies close to 1 [47]. One of the main contributors to the IR LED and detector industry is the material combination of GaAs and AlGaAs.

AlGaAs/GaAs are formed through the concept of energy bands. As atoms of both compounds are brought together, each energy level split into two levels since the Pauli Exclusion Principle [48] states that no more than two electrons of opposite spin are allowed to occupy the same quantum state. As a result, the energy levels become bands of levels of energy. The valence band is formed and the conduction band is empty. The electrons can be excited from the valence band to the conduction band to generate energy (in the case of the LED, light energy). The addition of the AlGaAs provides greater

output power emitted from the LED and greater detection capabilities of the photodiode [49].

The gap energy (E_g) can be simply calculated with the following equation:

$$E_g = h\upsilon = hc/\lambda \qquad \text{Eq. 2.}$$

where E_g = gap energy
h = Planck's constant = 6.626 X 10 -34 m^2 kg/s
υ = frequency of light
λ = wavelength of light
and c = speed of light = 3 $X10^8$ m/s

The gap energy of GaAs is 1.42eV. This calculates the peak wavelength to equal 875nm which is in the range of IR light.

Band gap engineering has advanced where aluminum gallium arsenide (AlGaAs/GaAs) emits IR light via double heterostructure theory [50]. GaAs is a direct bandgap semiconductor as displayed in figure 9.

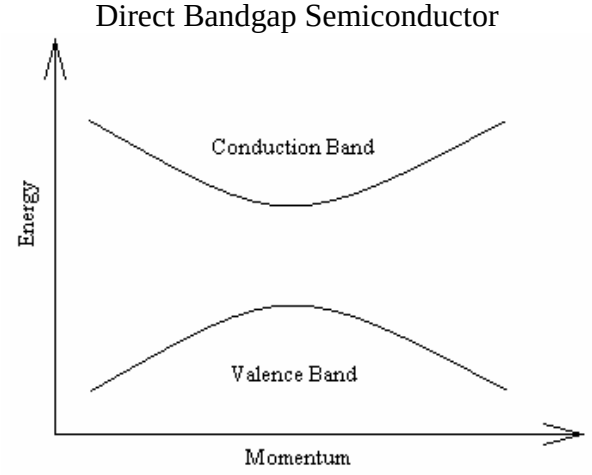

Figure 9 [51]. A direct bandgap semiconductor. The minimum conduction band energy is directly above the maximum valence band energy.

The minimum energy of the conduction band is positioned directly above the maximum energy of the valence band (shown in figure 9) so electrons and holes can

combine directly. Therefore, light is emitted while conserving momentum. Indirect bandgap materials (such as silicon crystals [51]) mainly emit phonons (not photons) to conserve momentum. Heterojunction structures (figure 11) have less absorption loss than homojunction structures (figure 10) [52].

Homojunction Structure Energy Band Diagram

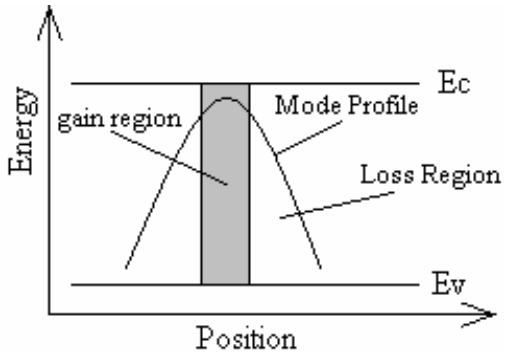

Figure 10 [52]. A homojunction structure energy band diagram. Significant energy loss (due to absorption) occurs in homojunction structures.

Figure 11 displays the general double heterostructure energy diagram for AlGaAs/GaAs.

Double Heterostructure Energy Band Diagram

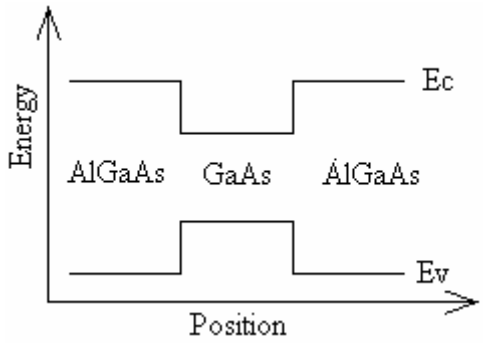

Figure 11 [52]. The AlGaAs/GaAs double heterostructure energy band diagram. The energy bandgap of the gain region (center) is smaller than surrounding materials to lessen absorption loss.

The gain occurs in the narrow band gap region, causing most absorption in this region. In homojunction structures, absorption loss occurs at the wings of the spectrum since the energy gap remains the same throughout the structure. Most double heterostructures are created via liquid-phase epitaxy and metalorganic chemical vapor deposition (MOCVD) [53], [54], [55] and [56]. Figure 12 displays the structure for a typical AlGaAs/GaAs heterojunction detector.

Typical Heterojunction IR Detector

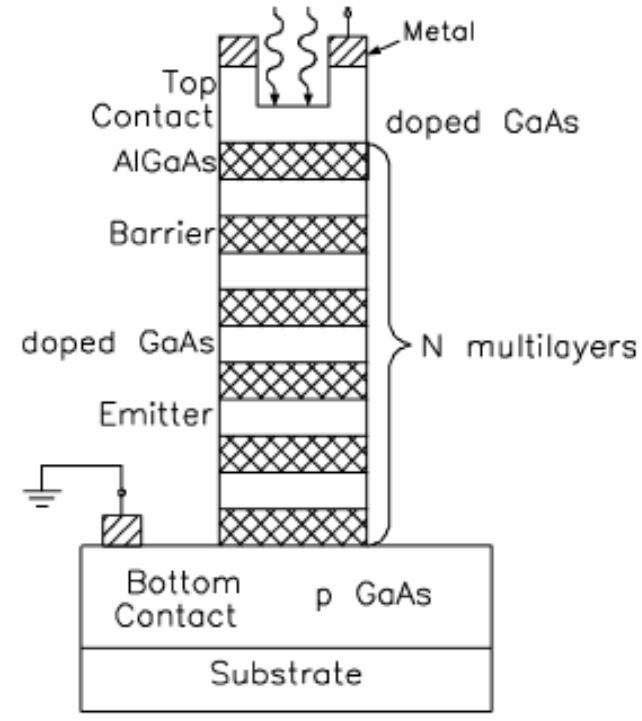

Figure 12 [49]. Structure of a typical heterojunction IR detector. Photoemission occurs through the AlGaAs barriers. Light absorption occurs at the GaAs layer.

GaAs again has narrower wavelengths with peak sensitivities around 930nm [57]. AlGaAs/GaAs IR detectors possess fast responses (with nanosecond rise times) at high efficiency, and low cost [47],[49],[53],[54]. AlGaAs/GaAs emitters and detectors are

very desirable for the design of the toner density sensor. Photodetectors, including quantum well infrared photodetectors (QWIP) [58], [59] have also evolved in the late 1980's to early 1990's to greatly improve printing for the printer industry.

The toner density sensor needs fast responding optical components in order to execute printer calibration process with little speed notice to the customer. Low costs of these AlGaAs/GaAs emitters/detectors maintain little impact to the overall cost of the printer and high efficiency of these heterostructure devices is simply an additional positive benefit.

CHAPTER 3: EXPLORED PRINTER CALIBRATION TECHNIQUES

Printer calibration is the process of maintaining consistent print darkness from the original print through the life of a cartridge. Historically, printer calibration is typically "open-loop." The term "open-loop" printer calibration is where there is no direct real-time feedback of data for adjustment of EP process parameters to improve print darkness. Many times, feedback parameters are not directly linked to print darkness, but are used to estimate print darkness through empirical testing. Examples of these parameters are print process speed, toner level, page count, etc. Therefore, environmental factors, such as temperature and humidity and toner characteristics are not captured in real-time for the adjustment of print darkness. Printer calibration involves transformation characterizing device-dependent values to device independent values [31].

This chapter discusses traditional one-dimensional printer calibration (section 1) and closed-loop printer calibration (section 2) as it relates to the color laser system (since most research is on the color system). It also compares and explains the drive for closed-loop calibration using the TDS compared to previously implemented IR sensor applications.

3.1 Traditional Printer Calibration

Printer calibration (like most calibration systems) requires a standard (reference) system for comparison. One dimensional printer calibration involves the use of developing standard LUT's to determine optimal EP process parameters. In the case

involving a color laser printer (where most printer calibration research exists), color measurements are taken to produce transformations called tone response curves (TRCs) [31]. TRC correction is usually applied to each channel: C, Y, and M (leaving out K for simplicity). This process involves using the current values for C, M, Y (determined from device characterization) and applying a defined transformation (given to the printer) to each of those values to produce the following results:

$$C' = f_1(C) \quad \text{Eq. 3} \qquad M' = f_2(M) \quad \text{Eq. 4} \qquad Y' = f_3(Y) \quad \text{Eq. 5}$$

where C', M', and Y' are correction factors for C, M and Y respectively.

The typical mono laser system uses linearization to map to the L* axis only (a* = b* = 0) as the TRC. This is due to the fact that color requires correction to hue and saturation (as mentioned previously in chapter 2 section 4).

The typical process for device dependent characterization to device independent characterization involves the following:

1. Pre-determined device control values are represented by a set of color patches
2. The values are measured in device-independent color coordinates (L*, a*, b*). (mono laser printing only requires the L* brightness function).
3. A forward transformation function is developed to map the control value to the control value response (device independent value). The function is obtained by empirical testing and/or modeling.
4. The forward transformation function is inverted to obtain the device-correction transformation function (made up of characterization and calibration shown in figure 14) which is used to determine the calibrated device output response.

The printer calibration process is summarized by the following diagram.

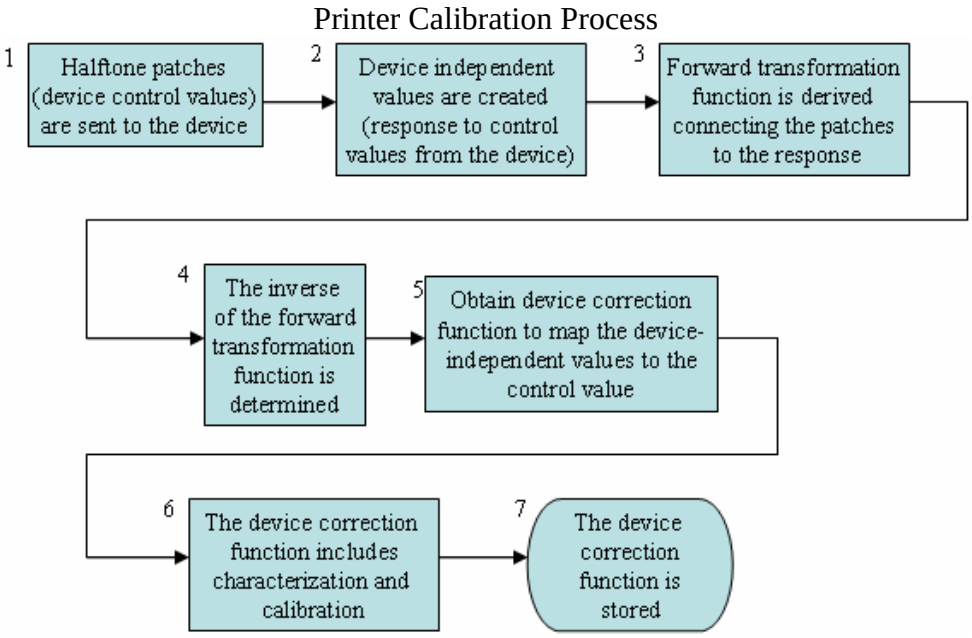

Figure 13 [31]. The existing printer calibration process. The current calibration process is empirically performed and stored in the printer. A transformation function is developed to determine the response required for accurate print darkness/color settings.

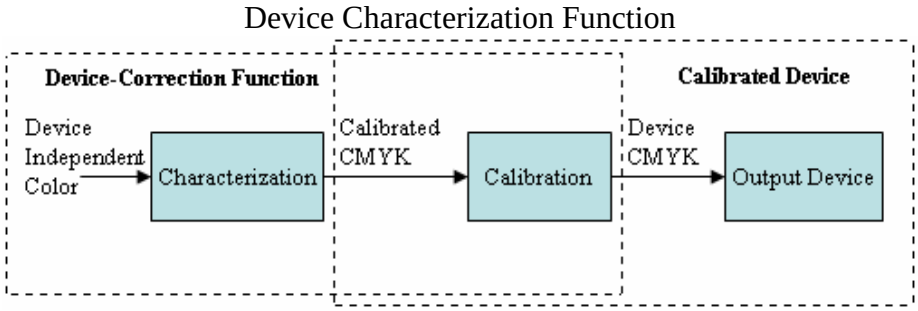

Figure 14 [31]. The device characterization process. The device independent color is a color with previously known parameters sent to the printer for development of the response (discussed in figure 13). EP print process parameters are adjusted and the calibrated output is finally sent to the device to adjust the print darkness/color settings.

Two common 1-D calibration techniques: channel-wise linearization and gray-balanced calibration are discussed in the following section.

3.1.1. Channel-wise Linearization to ΔE From Paper

The focus of this method is to use the TRC to create a relationship that links paper input value to L^*. Usually, paper values range from zero (black) to 255 (white) and the

Euclidean distance, $\Delta E = \Delta L^*$ [60] since:

$$\Delta E = \sqrt{\Delta a^{*2} + \Delta b^{*2} + \Delta L^{*2}} \quad \text{Eq. 6}$$

For mono printers,

$$\Delta a^* = \Delta b^* = 0 \quad \text{Eq. 7}$$

Therefore,

$$\Delta E = \Delta L^* \quad \text{Eq. 8}$$

L^* is defined as:

$$L^* = 116 * \left(\frac{Y}{Y_o}\right)^{\frac{1}{3}} - 16 \quad \text{Eq. 9}$$

where Y = the amount of light reflected and Y_o = the amount of incoming light

The relationship (Y/Y_o) is the reflectance fraction. The actual relationship between L^* and the input values are found to be non-linear (as displayed in figure 15). The non-linear relationship is due to the non-linear relationship between light and the naked eye's perception of light. Using the straight line drawn, the inverse L^* is found through a LUT for printer calibration (using gamma correction) [61].

Linearization Curve in 1-D Calibration

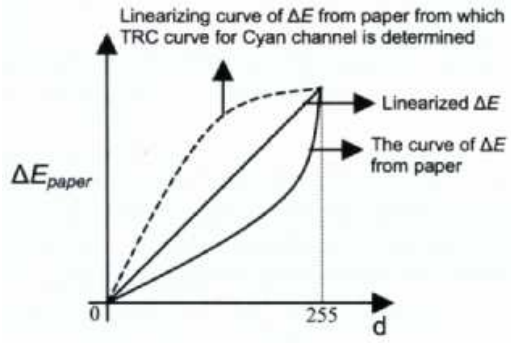

Figure 15 [60]. Linearization curve in 1-D calibration. The Euclidean distance is equal to L* for mono laser printers. The change in EP process parameters (represented by "d") versus L* can be obtained through gamma correction [61].

3.1.2. Gray-Balanced Calibration

Gray balanced calibration involves the use of mapping a medium's changes of lightness to input values. The following equation is used to capture this change:

$$L^* = 100 - (100d)/255 \qquad \text{Eq. 10}$$

where L* ranges between 0 (black) and 100 (light)

L* ideal values are inversely mapped through a LUT transformation for use towards darkness correction as described in figure 16.

Print Darkness Correction Process

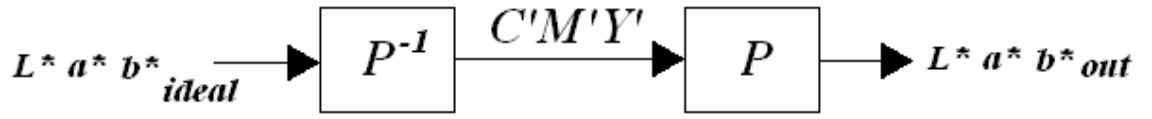

Figure 16 [60]. The print darkness correction process. The device independent values are sent through a transformation to provide the ideal C'M'Y values as it relates to the printer and its condition. The C'M'Y' values are then transformed to the adjusted values as L*a*b*.

Accurate printer calibration is achieved when:

$$L^*_{ideal} - L^*_{out} = 0 \qquad \text{Eq. 11}$$

Gray-balanced calibration is considered the preferred method of one-dimensional printer calibration since the human visual system is more sensitive to changes in gray than actual gray values. Empirical testing of these values is performed to acquire as accurate print calibration as possible.

One dimensional calibration is easy to implement and helps to maintain fast print speed; however, these systems are open-loop systems and do not capture real-time changes affecting the accuracy of printer calibration. Optimal EP process parameters may not always work in every environment (especially where there are extreme cases of

temperature and humidity). Open-loop calibration also does not capture EP component part to part variation consequently causing variation in print darkness (displayed in figures 22-24 in chapter 5 section 1). The toner density sensor is used to capture real-time closed-loop feedback with automatic adjustment of print darkness. The technique is simpler than the traditional process and the benefits include improved print quality in various environments, little impact to speed and cost, and as a result, a more robust design.

3.2 Closed-Loop Calibration

The closed-loop calibration process eliminates user intervention; reduce effects due to printer component variations and environment changes while maintaining low cost. It incorporates real-time processing with the benefit of utilizing most of the available printer's EP process parameters (used in 1-D calibration) to maintain consistent image quality.

Y. Wu [37] has described the use of an embedded IR sensor in a typical inkjet printer. Closed-loop mono printer calibration is summarized by defining a set of test gray-scale patches for measurement, calculating the ideal L* target (as done in open-loop calibration), and following the process description displayed in figure 17. The data captured by the toner density sensor provides the relationship between current L* values and ideal values. The process is repeated via a given condition (such power-on, incremental number or pages, etc.).

This process is simpler than the historical open-loop process because the IR sensor eliminates a lot of user intervention to develop LUT's and other additional print settings required to perform open-loop printer calibration.

Closed-Loop Printer Calibration Process

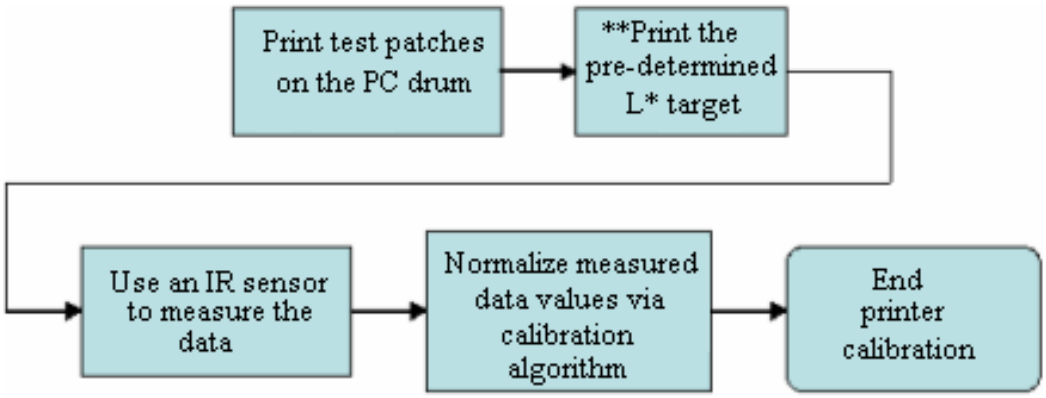

Figure 17 [62]. The closed-loop printer calibration process. This includes determining the L* target by using the sensor to measure test patches. The data is stored and normalized (calibrated) to values that adjust EP process parameters for optimal prints at accurate print darkness settings. **This step is required for ink jet printing.

3.2.1. Linearization for Ink Jet Printer Calibration

An extension of what was discussed above, Y. Wu [37] suggests the use of an embedded sensor to capture data used to generate a linearization table (similar to 1-D calibration using L* vs. gray levels) by color calibration algorithms for ink jet printing. The process includes the following steps:

- Printing a color target with a number of pre-defined color patches
- Waiting for paper to dry
- Measuring the target using an embedded sensor
- Using the data from the sensor to develop a linearization table with color calibration algorithms.

The patches are of different gray levels and are printed on paper. The more patches to measure, the better the accuracy of the calibration. However, printing patches may slow print process speeds (due to waiting for paper to dry since ink is used); therefore, suggested was to use linearization to reduce the number of patches printed while

maintaining calibration accuracy. As described previously, a non-linear relationship exists between output (L^*) and input (EP component values) PWM signals (X). Using gamma correction (based on the symbol Y), the relationship can be described as:

$$Y = aX^{\gamma} \qquad \text{Eq. 12}$$

where Y = output signal
and X = input signal

Gamma correction is applied to create linearity from a non-linear characteristic. Therefore,

$$X' = X^{\frac{1}{\gamma}} \qquad \text{Eq. 13}$$

where X = input signal

This method again requires multiple patches for accuracy of calibration. At the time of this research ([62] published 2005), an embedded sensor was costly and was not as precise as using a high-end spectrophotometer. The environmental conditions described in Y. Wu's research are nominal and doesn't introduce methods for effective printer calibration due to variations in temperature and humidity. Also, the research does not describe EMI conditions.

Even though the printer calibration process described above is for ink jet printing, it presents promise in mono and color laser printing. If an embedded IR sensor is utilized for printer calibration in ink jet printing, a similar device may be applied to color laser printers. The embedded sensor can be used to sense toner level to map a response from the ideal amount of toner to the actual amount being printed. While there is little published research in applying embedded sensors in mono laser printing, this paper establishes a basis for the use of an embedded IR sensor for mono laser printing. Also

(and mentioned previously), factors very important to accurate sensing as EMI and environmental effects are not discussed in printer calibration research. These aspects and reduced variation in print darkness are addressed in this dissertation.

CHAPTER 4: RELATED SENSOR DESIGNS AND THE NEW TDS

The focus of the proposed TDS is to determine toner density from the PC drum. Data collected from the TDS is placed into an algorithm to adjust necessary EP process parameters that control the amount of toner required for accurate print darkness. The focus of the research was to first reduce print darkness variation. The second goal (in implementation of the TDS) is to develop a TDS circuit that effectively mitigates EMI (produced by interactions between EP components) on the sensor. Section 1 discusses previous embedded IR sensors and their functions in print darkness calibration. The new TDS design is then compared to similar sensors discussed in Section 2. The first portion of the last section (section 3) explains the requirements in designing the TDS which includes the function, implementation, and design requirements for accurate TDS output data. The last portion of section 3 describes constraints on the development, implementation (including EMI), and operation of the TDS.

4.1 Previous TDS Related Work

As mentioned previously, R.W. Pries from the IBM Corporation [41], introduced the concept of the toner density sensor (known as the toner patch sensor) in 1983. The concept design of the toner patch sensor (TPS) is displayed in figure 18. The diagram displayed is a block diagram of the overall operational function of the TDS as it relates to printer calibration. The newly developed TDS design is modeled after this concept.

The TPS as Introduced by R.W. Pries

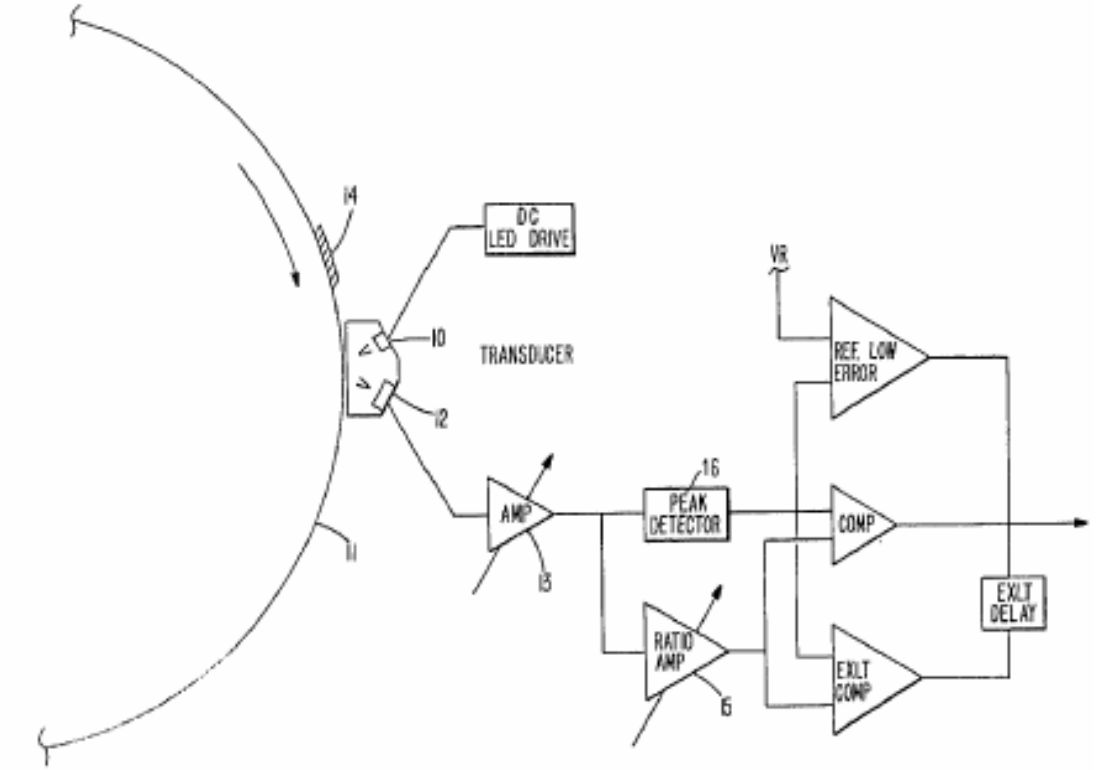

Figure 18 [41]. The TPS introduced by R.W. Pries. Light is emitted by a LED (10) and reflected by a photoconductive surface (such as the PC drum). The light is detected by a photosensor (12) and converted to a voltage signal. The output signal maintains a relationship with the light detected. The signal is amplified (13) and sent to a detector (16). The signal reflected by the untoned (bare) photoconductor (PC) is stored. When the PC has toner deposited on it (patch 14), the signal passes under sensor (12) and the value of the patch is sensed and amplified (15). The toned signal will possess a lower value than the untoned signal. Components of the circuit that's not discussed are utilized for error detection of out of range signals (such as checking for extra light (EXLT) and checking for very low signals).

The TPS function is displayed in figure 18. IR light is sent via a light-emitting diode to the bare PC drum and the reflection is captured by a photodetector. The light detected is very small and therefore must be amplified (via amplifier 15) to a measurable signal. The toned PC signal is amplified to a level equal to the untoned PC signal to normalize the signal. Therefore, the output signal will be high for low toner concentration. The comparator will produce a signal that will cause additional electrostatic fields to increase

development of toner to the PC. Error checking is also included in the diagram where the extra light (EXLT) comparator's function is to flag high output signals and the reference low error is to flag out of range low output signals detected.

Y. Wu [37] also introduced an embedded sensor used in color ink jet printing (as mentioned in chapter 3 section 2). The sensor captures four visual bands (for a color ink jet printer). Since the responses of these filters don't match the CIEXYZ color space, and as a result, are not sufficient enough to construct a spectrum curve, the idea is to use another method to restrict the curve to a known number of colors. Eventually, a subset of these colors is used toward printer calibration.

Four LEDs are used to capture C, M, Y, K respectively. The reflectance is captured by a CMOS (complimentary metal oxide semiconductor), and a light-to-voltage (LTV) converter. Calibrations including black and white point calibration, sensor to media distance variation compensation; temperature change compensation and media non-uniformity compensation are performed to optimize print quality.

4.2 The Newly Designed TDS Function, Purpose and Comparison

The basic operational overview of the new TDS implemented in the Lexmark E series is described in figure 19. As with previous IR sensors utilized for print darkness calibration, this sensor also measures the reflectance of several toned patches to determine a relationship between the ideal toner concentration and the actual toner concentration.

The sensor is positioned in line with the PC drum to capture reflectance. The 5V DC supply voltage (V_{CC}) powers the sensor's optical components and integrated circuit (IC) from the printer's controller (system) PCB card. The LED light intensity is provided by

the LED Driver Circuit (discussed in chapter 5). The reflected light signal is detected by a photodiode and converted to a voltage and amplified for a measurable output. Outputs of the TDS can range from a minimum of <0.7V to a maximum of 5V. The range of outputs can cause significant error in signal filtering accuracy (discussed later in this section). Output of the TDS is then sent through an analog-to-digital (A/D) converter (also discussed in chapter 5) and utilized in the printer calibration algorithm to adjust/correct print darkness. Error flagging components are not located on the sensor printed circuit board (PCB). Error flags and other logic operations are included in the print darkness correction algorithm.

Basic TDS Operational Overview

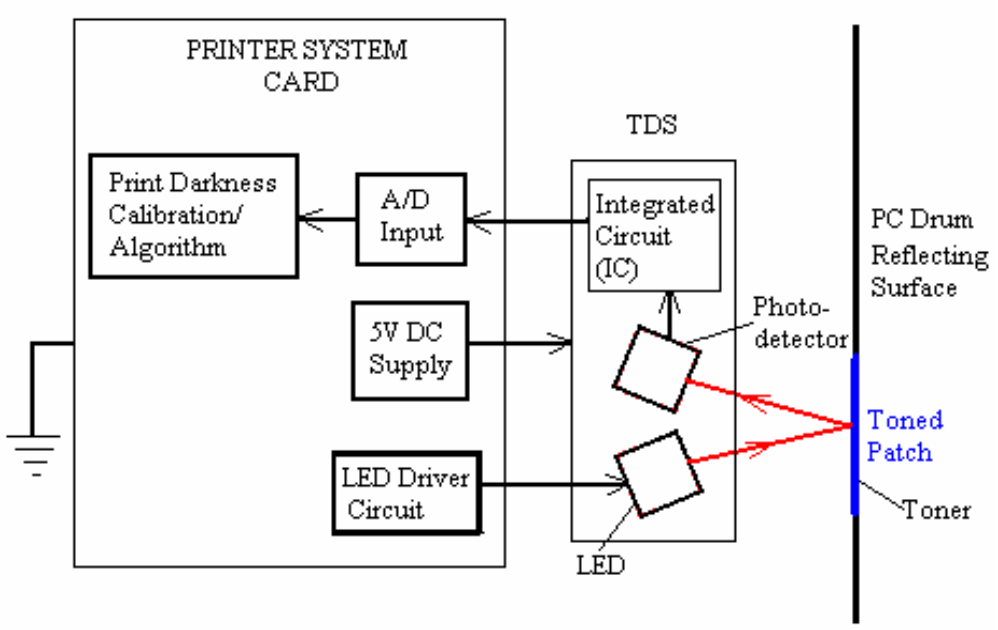

Figure 19. The basic TDS operational overview. A typical 5V DC supply is used to power the sensor. The LED driver circuit supplies variable current (described in chapter 5) that drives LED light. The light is emitted by the LED and detected by the photodiode. The light detected is converted to a measurable output voltage in proportion to the intensity of light reflected. Usually, an untoned (bare) PC drum measurement is taken and stored. A number of toned patch measurements are taken and compared to the bare PC drum measurements for accurate printer calibration. The analog measurements are converted to digital signals and utilized for print darkness correction through an algorithm.

Figure 17 defines the overview of the printer calibration process using the toner density sensor (which stated previously is the common method for closed-loop printer calibration).

The sensor's first and main purpose is to reduce print darkness variation. Currently, print darkness variation for the previous Lexmark mono laser model cartridge) is over ±8L* from the nominal print darkness of 56L* (print darkness samples are displayed in chapter 5 figures 22, 23 and 24). The desired goal of the TDS is to reduce this variation to <±5L* over the life of the cartridge. This goal was set to have the least print darkness variation impact on the customer. Hence, the toner density sensor must produce accurate signals for accurate print darkness correction.

The TDS design's second purpose for implementation is to mitigate EMI affects on the sensor and to reduce print darkness variation. EMI existence is due to the combination of motors spinning EP components and voltages supplied to the EP components used to produce required electrostatic interactions to print toner unto media (paper).

EMI may encompass an entire TDS signal. After developing the toner density sensor, figure 20 was the resulting TDS output obtained via measurement (discussed in chapter 5 section 2).

The EMI captured in figure 20 is a direct result of data captured while EP components are powered. The EP Components are powered by the high voltage power supply and are typically in the range of approximately -1500Volts to approximately +1500Volts. The transfer roll is the main EP component positioned closest to the TDS. Both the TDS and transfer roll are powered during a TDS cycle.

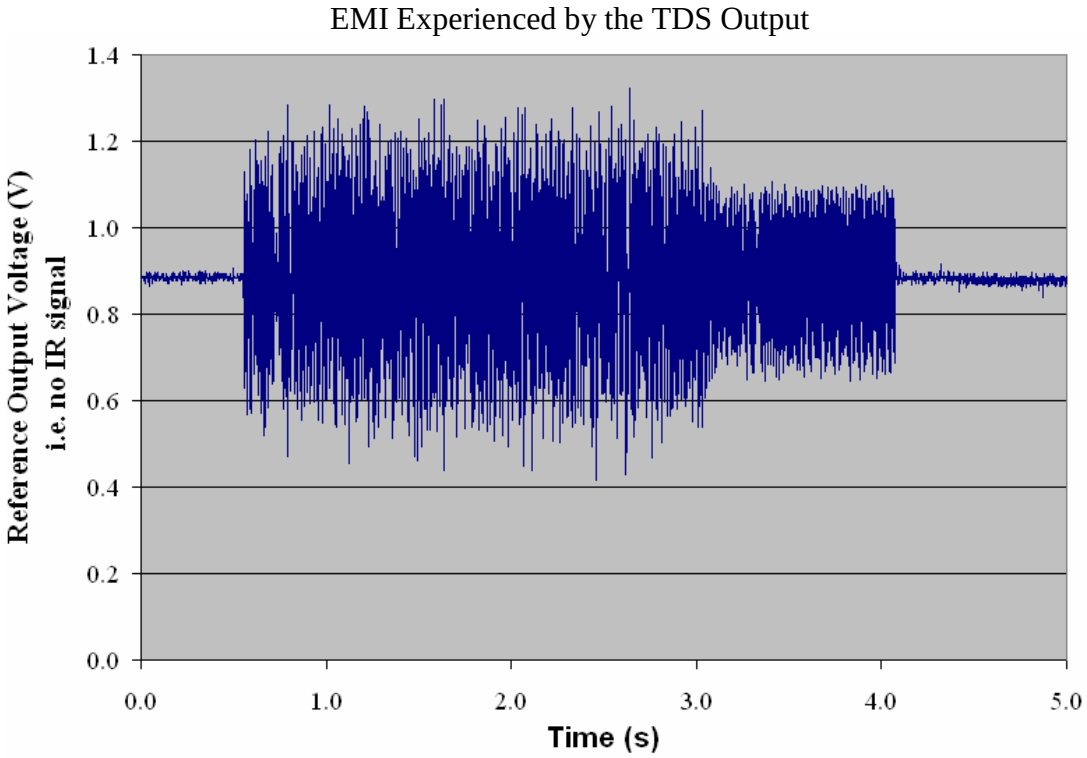

Figure 20. EMI experienced by the TDS output. EMI occurs once EP components are powered (approximately @0.6 seconds). The TDS output (for this sensor) is equal to the reference signal (discussed in chapter 5) when no light is emitted by the LED (~0.9V).

When the LED is powered and light is detected, signal filtering produces an erroneous signal. An example is shown in figure 21. The output voltage noise is clipped at ~4.7V due to the noise hitting the rail of the operational amplifier (which is specified to be within ±0.2V of the supply voltage of 5V). The TDS is positioned within 5mm of the nearest EP component (the transfer roll); therefore, EMI effects are mainly from this component due to the fact that it is positioned closest to the TDS and it has the highest voltage range (from approximately -1500V to approximately +1500V). The purpose of the TDS design described in chapter 5 is to reduce the EMI affecting the TDS output signal. As part of the design process for the development of a working design, further investigation and evaluation of EMI is demonstrated in chapter 6.

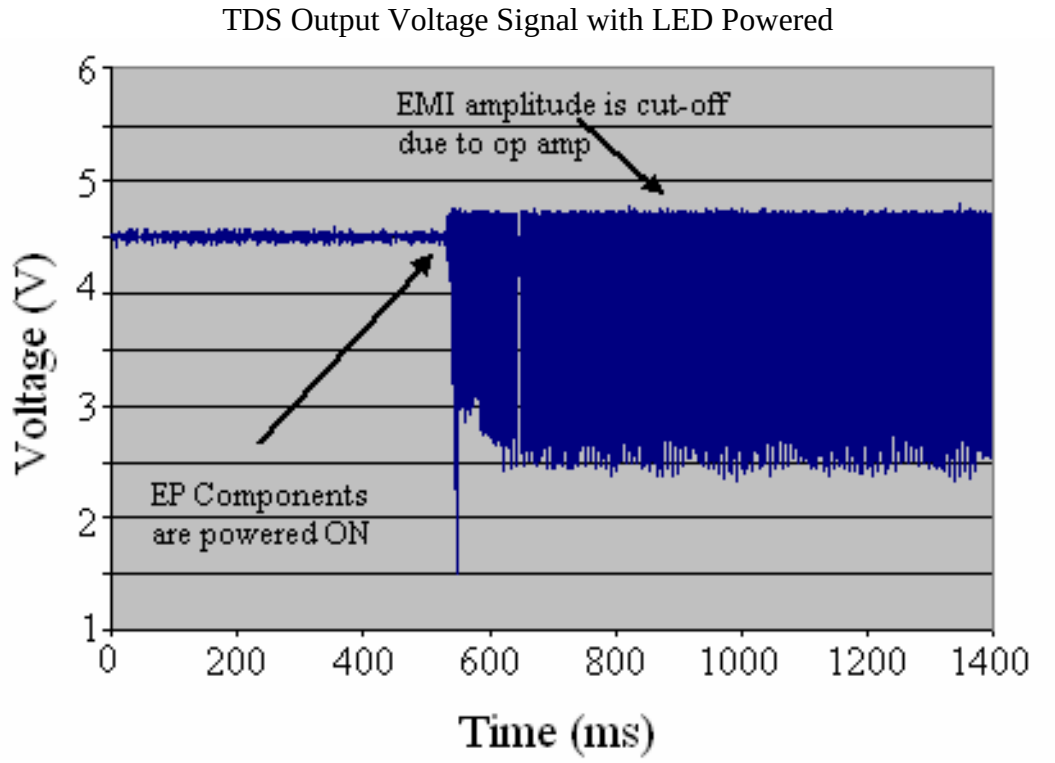

Figure 21. TDS output voltage signal with LED powered. The TDS is powered and the maximum voltage (with light detection) for this sensor output is ~4.5V. The amplitude of the interference signal was cut-off at 4.7V (which is due to EMI maximizing the operational amplifier voltage rail in the sensor circuit as discussed in chapter 5). The sensor's output due to filtering is roughly the DC average of the signal (i.e. ~3.7V). This is not the actual signal's voltage (~4.5V) and as a result, the final output is erroneous.

As mentioned in this chapter, previous research described embedded sensors require calibration for temperature change, media non-uniformity compensation, and media distance compensation. Addition of these calibrations slows print process speed. It also makes designing the sensor system more complicated. The ink jet IR sensor measures density from ink printed on the page, so media compensation is required. Card stock paper (dense paper) absorbs ink differently than regular 20lb office paper, thus requiring the additional compensation. Temperature change calibration and media non-uniformity compensation is required for sensor reflectance accuracy. Previous research shows that

each sensor shows a common purpose (i.e. to detect voltage changes by printing multiple test patches on a medium); however, past research does not present results of print darkness variation through the life of a printer cartridge. Furthermore, there is little research regarding impact on closed-loop print darkness variation using IR sensors. Lastly, past research explains little concerning EMI impact and how to address EMI (as conditions can change for every printer generation). The toner density sensor design tackle the goals of reducing print darkness variation and mitigating EMI from the sensor output signal once implemented.

4.3 TDS Requirements and Constraints

The function of the toner density sensor is to produce an accurate linear relationship between different levels of toned patches and the output voltage. Several sensor/printer performance, design, and implementation requirements/constraints are listed below.

Performance Requirements

- **The sensor must be able to detect small changes in toner concentration.** Without this sensitivity, the sensor will not provide a linear relationship between toner concentration and voltage change.
- **The sensor must be able to operate after experiencing electrostatic discharge (ESD).** In the event where ESD occurs, the sensor must have the ability to function properly.
- **An A/D converter and a developed algorithm must be in place to utilize data captured by the TDS for adjustment of print darkness**. The actual print darkness determined by the TDS is calibrated to the ideal print darkness set by the patches printed on the PC drum.

- **The sensor must be able to operate and function effectively after being shipped/stored and manufactured in extreme environmental conditions**. Some manufacturing locations experience uncontrolled environmental conditions (i.e. very little or no air conditioning at times during the day or night).

Performance Constraints

- **The sensor must be able to operate near EP components.** Since charged components are interacting electrostatically with motors running the components, EMI interferes with the TDS signal. EMI impact is further evaluated in chapters 5 and 6. As mentioned previously, EMI cause inaccurate TDS output signal filtering.
- **The TDS design should be easily transferable for future generation printers.** The design should not require significant engineering resource when designing a future generation printer.
- **The printer calibration cycle must not significantly reduce the speed of the printer.** The settling time of the sensor must be relatively fast for little speed impact to the user.

Electro-Optical Design Requirements

- **A noise-free input voltage (V_{CC} = +5V) is required to supply the circuit**. The input voltage is supplied by the printer's controller card.
- **An LED driver circuit (including an input PWM signal) is required to emit light from the LED**. The PWM signal is utilized to develop a relationship between light reflected from the toned patch and output voltage.

- **The output must have a reference voltage**. A voltage reference is the standard for most sensor designs (discussed in chapter 5).
- **IR optical components (i.e. the LED and photodiode) must be able to detect only IR light and not be affected by ambient light.** Light interference can cause erroneous detection by the photodiode**.**
- **The operational amplifier must provide a rail-to-rail (RRO) output.** Most RRO amplifiers can produce outputs close to the supply voltage (i.e. ±0.2V of the supply voltage). This is to maximize filtering capabilities (discussed in chapters 5 and 6).

Electro-Optical Design Constraints

- **Sensor components must have low tolerances for print darkness correction accuracy.** As stated previously, the sensor's accuracy is critical in reducing print darkness variation.
- **The maximum LED current rating is 50mA**. This is a standard for most LED's of the type used for the design.
- **The A/D converter input must have a maximum rating of 3.3V.** This is the specified rating for the A/D selected.
- **The design should be low cost.** The cost must (at most) balance with benefit of the sensor application.

Implementation Requirements

- **The sensor's optical housing must have a direct view of the PC drum and without obstruction from other printer components**. Light emitted and detected must not be interfered for light detection accuracy.

- **A wiper mechanism must be designed to keep the sensor's optical window free of paper dust, toner and other forms of contamination**. If the sensor's heavily contaminated, the sensor may read an inaccurate signal.
- **The sensor must be positioned <20mm away from the PC drum**. The LED and photodiode must be positioned where the signal can be detected accurately. Since the signal is a low voltage signal, the greater the distance, the greater the error in detection accuracy.

Implementation Constraints

- **The sensor size must be smaller than 100mm^2.** This is to ensure fit in the space-constrained printer. Since the sensor is positioned around EP components (where high voltage electro-static interactions take place), the sensor must have significant distance between itself and other components (discussed in chapter 6).

The goals for the toner density sensor design are to reduce print darkness variation and to mitigate EMI affecting the TDS output signal. The purpose of the TDS design is to effectively meet these goals.

CHAPTER 5: NEW TDS DESIGN

The purpose of the TDS design is to provide an accurate signal for reduction of print darkness variation and for reduction of EMI from the sensor output signal. The general concept of the toner density sensor (as described by R.W. Pries) is to use an LED to emit IR light. Light is reflected by the PC drum (untoned and toned) and captured using an IR detector with a series of electronic components to convert detected light (with varying intensities) into a measurable output voltage. Print darkness is being corrected in real-time utilizing the data provided by the TDS.

The design chapter is partitioned into six segments: print darkness characterization, EMI characterization, the selection of optical components, the LED driver circuit (converts input PWM voltage to light emission), the sensor PCB (printed circuit board) circuit (converts light detected to a measurable voltage), and the A/D converter interface circuit (filters/reduce noise and steps down voltage for input into the A/D converter).

Reduction in print darkness variation and relating the design of the TDS to this reduction is detailed in section 1. Section 2 investigates EMI properties crucial to effectively designing the TDS. The optical components section (section 3) discusses how the components were selected based on availability, manufacturer specifications and printer specifications. The LED driver circuit (section 4) provides the analysis in designing a circuit that converts PWM voltage to a variable light source. Section 5 (the sensor PCB circuit) provide details required to determine a starter circuit for the TDS.

Lastly, section 6 (the A/D interface circuit) has a similar design to section 4; therefore, selection of components and values are discussed relative to the analysis performed for the LED driver circuit.

5.1 Design of the TDS to Reduce Print Darkness Variation

Print darkness variation in the previous generation Lexmark printer was over ±8L*. This was determined by performing cartridge yield testing of three printers and three cartridges for each printer (totaling nine cartridges). The most extreme samples of print darkness variation produced were 8L*[63] from the nominal print darkness. Figures 22, 23 and 24 display the variation for the Lexmark T460 series. Based on the report, 79% of the variation is due to part-to-part variation and 21% is due to environmental variation experienced by the cartridge. To reduce part-to-part variation, the TDS output signal must be very accurate and must have the ability to calibrate for every cartridge inserted into a given printer. To accomplish this, patches are printed on the PC drum to develop the relationship between actual print darkness and the nominal patch darkness.

Since most sensors possess a reference voltage, the TDS reference voltage (i.e. minimum output) is set to 1.0V. The TDS with no light emitted and reflected must be equal to this value. When light is reflected from the untoned drum, the output must be at the maximum of 4.8V. The PC drum surface is glossy with a 68% reflectance [63] and therefore, the LED and photodiode were designed for a highly reflective surface (as discussed in section 3). As patches are placed on the PC drum for measurement, the lightest patch should have the most IR light reflected (relative to the other patches) with an output voltage closest to the maximum value and the darkest patch should have the least light reflected with an output voltage closest to the reference voltage.

Lightest Sample of Print Darkness for the Previous Generation Printer

Figure 22 [63]. The lightest sample of print darkness for the previous generation printer. The TDS was not implemented in the printer used to produce this print sample. (Print defects may appear as a result of scanning the original print sample into this document for display.)

Print Darkness of a Nominal Print Sample

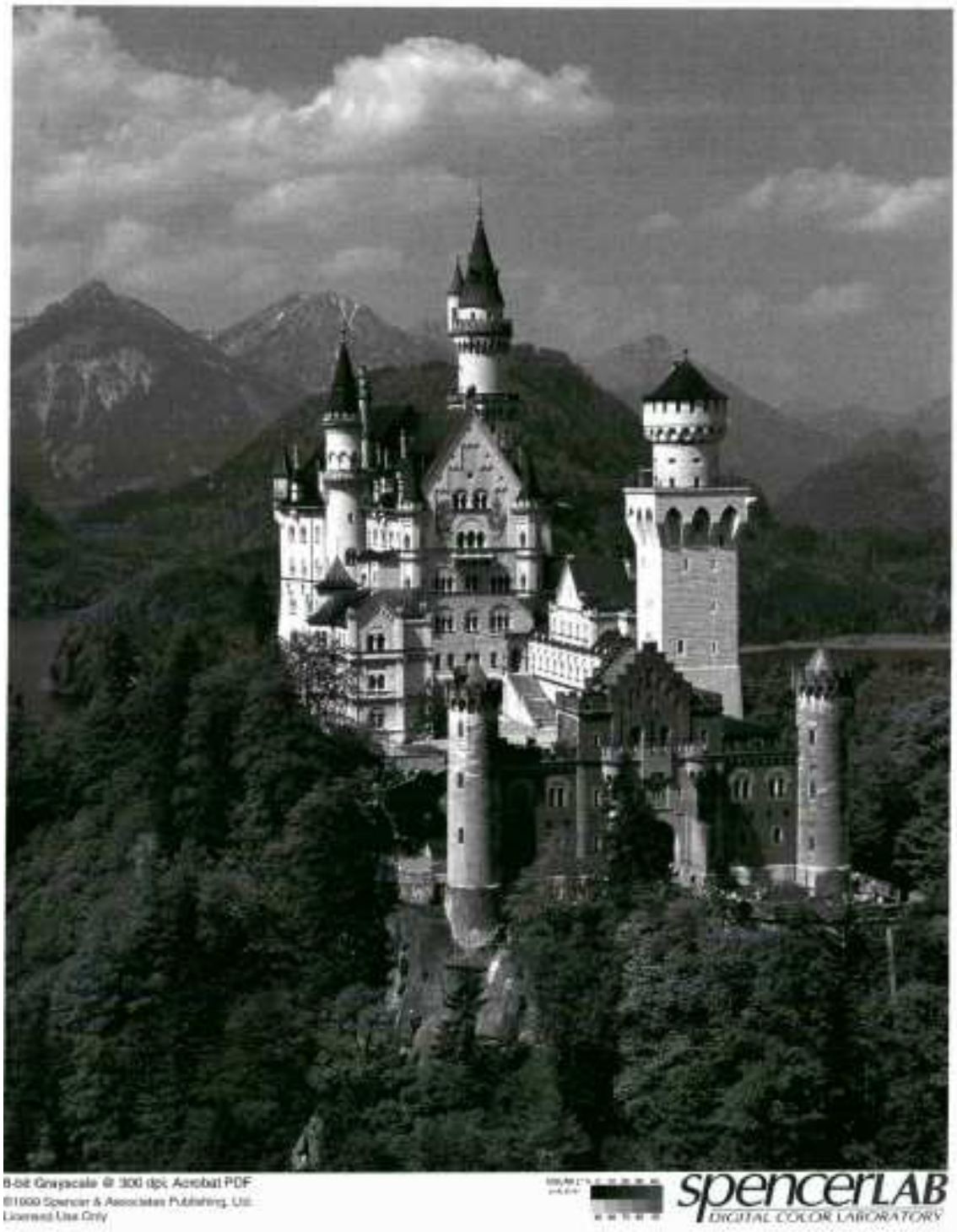

Figure 23 [63]. Print darkness of a nominal print sample. The nominal print sample is utilized to compare dark and light samples. (Print defects may appear as a result of scanning the original print sample into this document for display.)

Darkest Sample of Print Darkness for the Previous Generation Printer

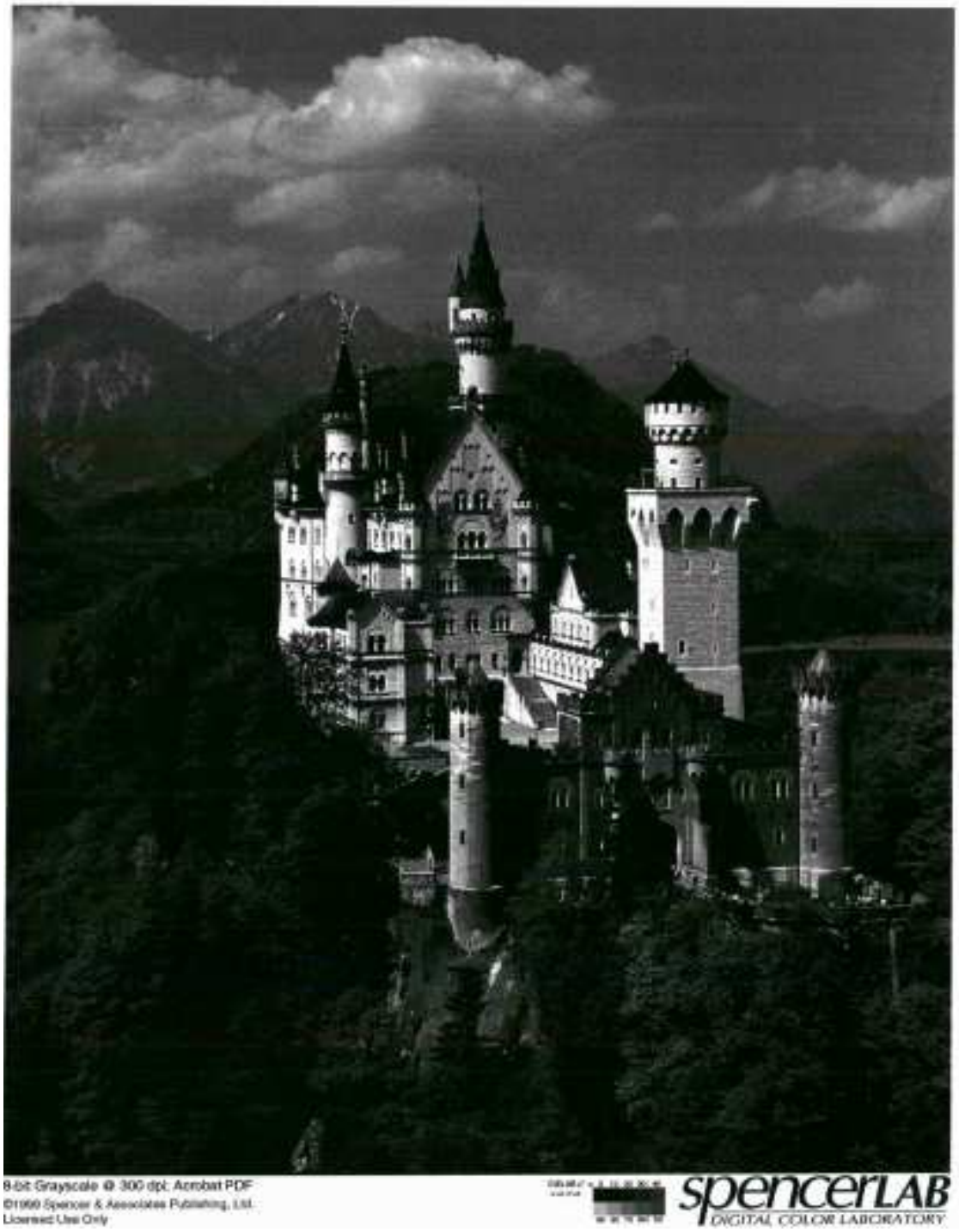

Figure 24 [63]. The darkest sample of print darkness for the previous generation printer. The TDS was not implemented in the printer used to produce this print sample. (Print defects may appear as a result of scanning the original print sample into this document for display.)

Figure 25 displays the patch/TDS output voltage relationship with constant maximum current emitted by the LED.

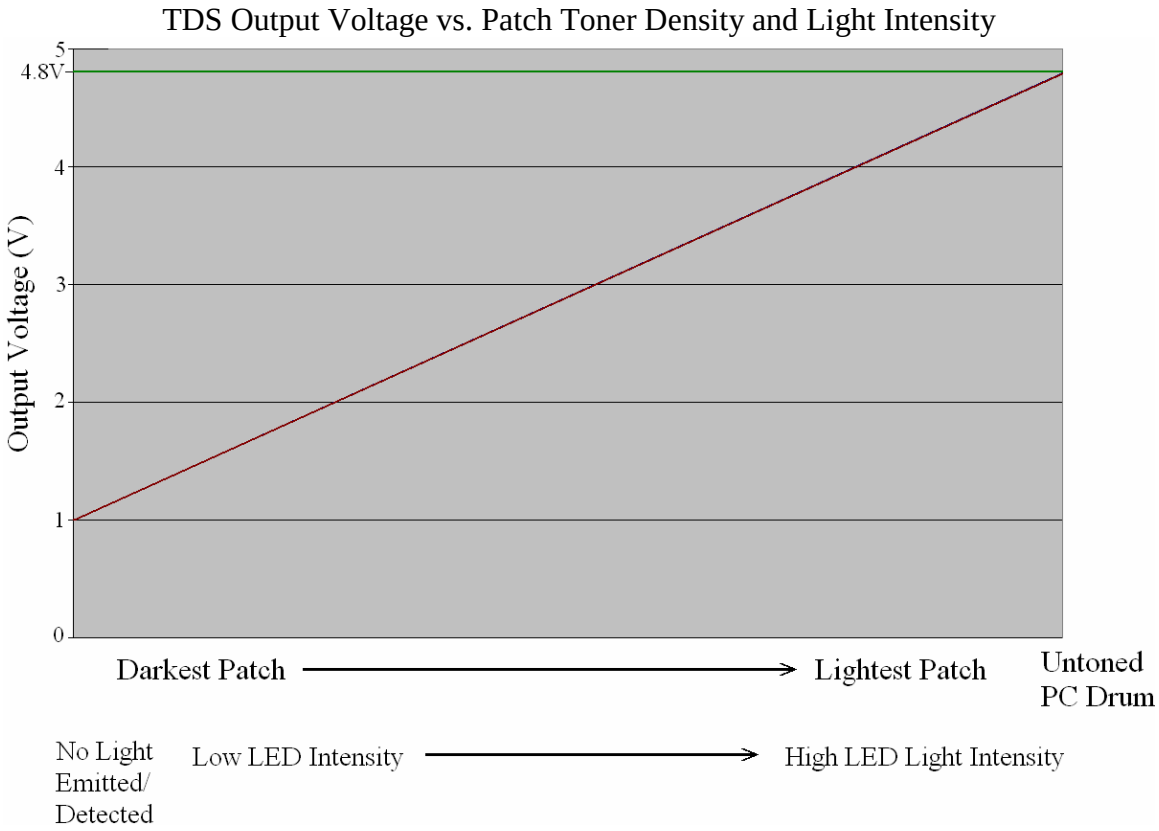

Figure 25. The TDS output voltage versus patch toner density and light intensity. The graph shown represents maximum constant light emitted to provide the output response of patches at different gray levels. Also shown is that the same relationship exists for variable light intensities emitted and reflected by an untoned PC drum.

To develop the relationship between the untoned PC drum and the output response of the sensor (including its tolerance), a relationship must be established between the sensor and the light emitted. Thus, print darkness calibration is actually a calibration of the sensor and then the toner density. A linear relationship linking LED light intensity (based on the LED forward current I_{LED}) and the output voltage has to be established for calibration accuracy. Therefore, the relationship shown in figure 25 is actually the same

relationship needed for the LED light intensity. Minimum and maximum LED forward current values are determined by the components selected (as discussed in section 3). To introduce variable light to the LED, a PWM signal (with variable duty cycle) is utilized and converted to a DC signal for variable light intensity.

In order to perform an accurate calibration algorithm, the analog TDS output signal is filtered and converted to a digital signal. Since the output signal is a voltage signal, the detected light is converted to a voltage. Output values of the TDS are divided by the maximum LED light intensity voltage for the reflectance ratio. The reflectance ratio is taken to mitigate part-to-part variation.

Based on the desired results in printer calibration, the TDS design is divided into three portions: The LED driver circuit, the detection circuit and the A/D interface circuit. The LED driver circuit produces variable light for sensor calibration, the sensor PCB circuit converts the detected light to a measurable voltage and the A/D interface circuit is utilized to filter the signal and condition it for the A/D converter.

5.2 Design of the TDS to Reduce EMI

EP components such as the charge roll, transfer roll, PC drum, etc. are charged to generate electrostatic interactions for toner transfer. Due to space constraints, the only available spacing for the new Lexmark E460 series is to place the TDS between the transfer roll and the EP frame. Figure 26 is where the TDS is positioned. Since the TDS is positioned within millimeters of the transfer roll, the assumption is that these components may affect the TDS signal. The only method to characterize the EMI is to develop a “first-pass” TDS PCB design. It was discovered (detailed in chapter 6 section 2) that electromagnetic interference (EMI) affects the TDS output signal. In the

implementation of the sensor for characterization of EMI (described in chapter 6 section 2), the initial sensor design with no filtering or shielding produced figure 21 (displayed in chapter 4). Various methods were introduced to mitigate the problem (i.e. shielding, moving the sensor further away from EP components, and placing a ground plate on the sensor); however, none of these options mitigated EMI experience by the sensor (as explained in chapter 6).

The TDS Implemented in the Lexmark E Series Printer

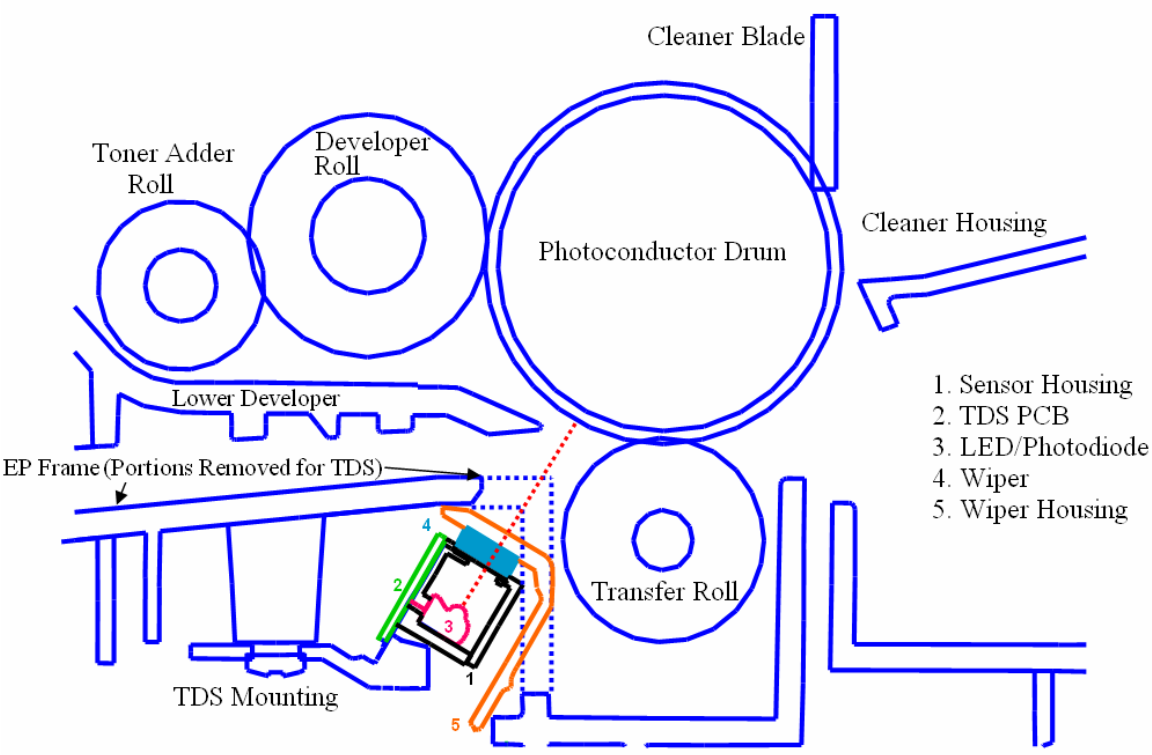

Figure 26 [63]. The TDS implemented in the Lexmark E series printer. The TDS was positioned such that there is a view of the PC drum without obstruction. The TDS was designed with a wiper to periodically wipe contaminants from the optical window (discussed in chapter 6).

Oscilloscope probes were attached to the TDS output, the transfer roll, the developer roll, and the charge roll. The EP components' data are saved for comparison and analysis of the output signal. The EMI displayed at the TDS output was characterized in Matlab

to determine its power spectral density (PSD). Figure 27 provides the TDS reference (minimum-no light detected) output with no filtering.

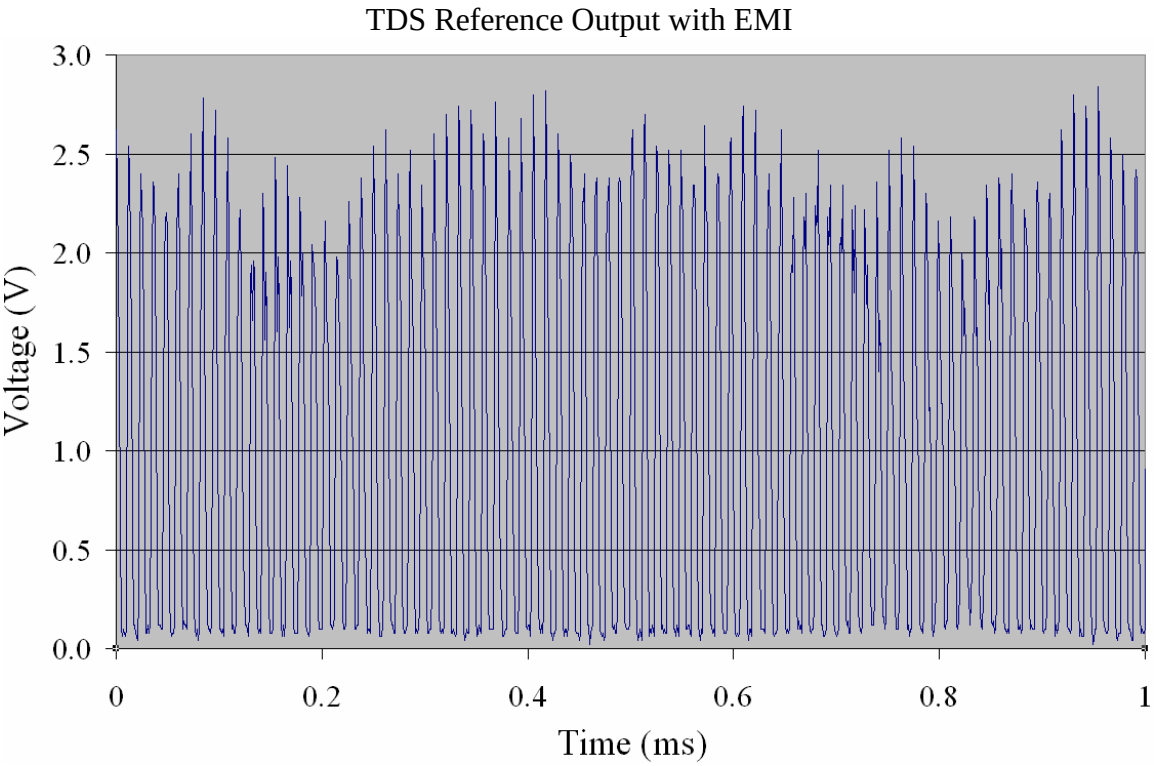

Figure 27. The TDS reference output. The positive noise displayed is the result of EMI affecting the TDS.

To verify the signal's accuracy, the sampling rate was determined based on the Nyquist frequency for prevention of aliasing.

$$\text{i.e.} \quad 2B < 1/Ts \qquad \text{Eq. 14} \qquad \text{with} \quad B \sim 83.333\text{kHz} \quad \text{Eq. 15}$$

$$\text{and } Ts = 1\mu s \qquad \text{Eq. 16}$$

$$\text{Therefore, } 166.67\text{kHz} < 1\text{MHz}$$

Further analysis of the TDS EMI was performed by finding the discrete-time Fourier transform (DTFT) via obtaining the fast Fourier transform (FFT) [64].

$$X[k] = \sum_{n=0}^{N-1} x[n] W_N^{kn} \quad \text{Eq. 17} \qquad \text{where } W_N^{kn} = e^{-j2\pi/N} \quad \text{Eq. 18}$$

N= number of samples (i.e. *N* = 181) and *x[n]* = sample sequence and *X[k]* = the DTFT

The DTFT is modeled in Matlab. Figure 28 displays the FFT for the TDS output with EMI. The peak frequencies and amplitudes displayed in figure 28 are listed in table 1.

FFT of the TDS Output with EMI

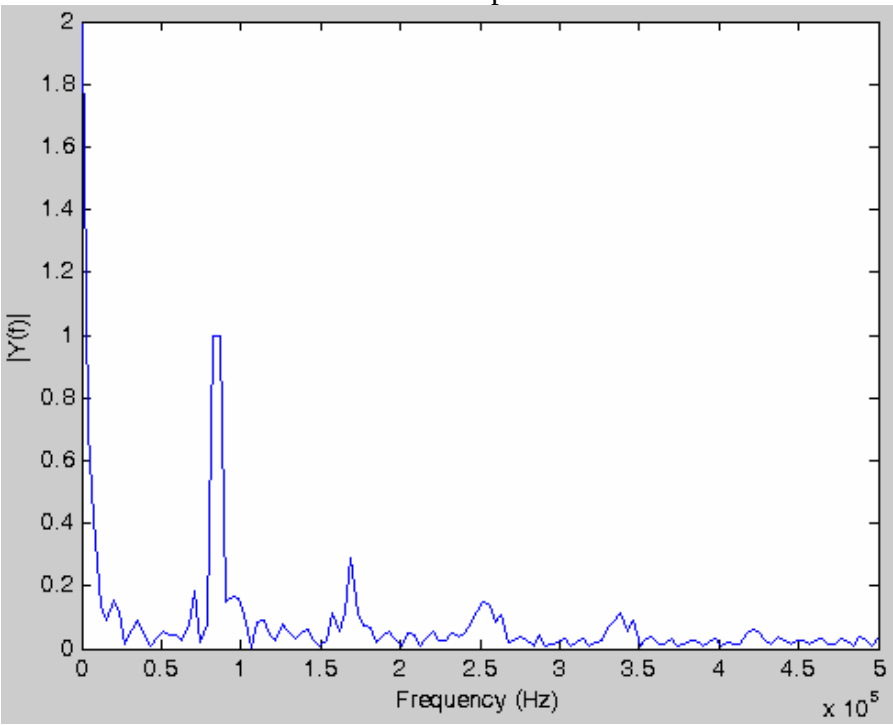

Figure 28. The FFT of the TDS output with EMI is modeled in Matlab. There are obviously multiple frequencies contributing to the EMI experienced by the TDS.

Frequencies Displaying Peak Amplitudes

F	Frequency	Amplitude
f_1	86614	0.9990
f_2	169290	0.2922
f_3	251969	0.1475
f_4	255906	0.1401
f_5	338583	0.1124
f_6	346457	0.0897
f_7	421260	0.0608

Table1. Frequencies displaying peak amplitudes. The samples are taken from the TDS output with peak amplitudes selected >0.05V.

Therefore, the mathematical representation of the signal is a sum of seven cosine functions representing the frequencies displayed in table 1. The TDS output with EMI is characterized by an additive white Gaussian noise (AWGN) summed with a series of cosine functions.

i.e. $$TDS\_Output = u(t) * [A_1 \cos(2\pi f_1 t) + A_2 \cos(2\pi f_2 t) + A_3 \cos(2\pi f_3 t) + \ldots + A_4 \cos(2\pi f_4 t) + A_5 \cos(2\pi f_5 t) + A_6 \cos(2\pi f_6 t) + A_7 \cos(2\pi f_7 t)] + n(t)$$ Eq. 19

where $n(t)$ = AWGN of zero mean with a standard deviation (σ) =1

This EMI is rectified by the op amps in the TDS design (section 5). Thus, the output signal displays only positive values. The signal is compared to the original FFT of the TDS output in Matlab (displayed in figure 29).

Amplitude Spectrum Comparison of the TDS EMI and the Characterization Function

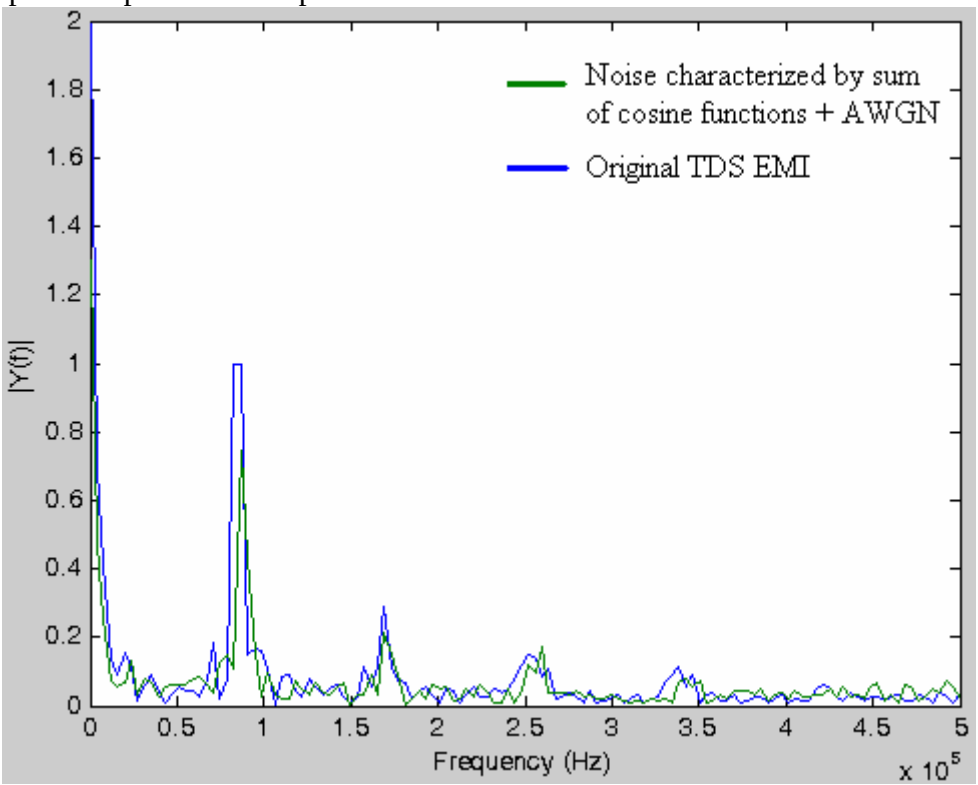

Figure 29. The FFT of both the original TDS EMI output and the characterized signal. The signals displayed are very similar.

A low-pass filter will mitigate most of the frequencies displayed in figure 30. Selecting a cut-off frequency of 70kHz and a pass-band frequency of 40kHz will generate an ideal filter to mitigate most of the EMI. Displayed in figure 30 is the filter design performed in Matlab.

The Magnitude Response of the Filter Design

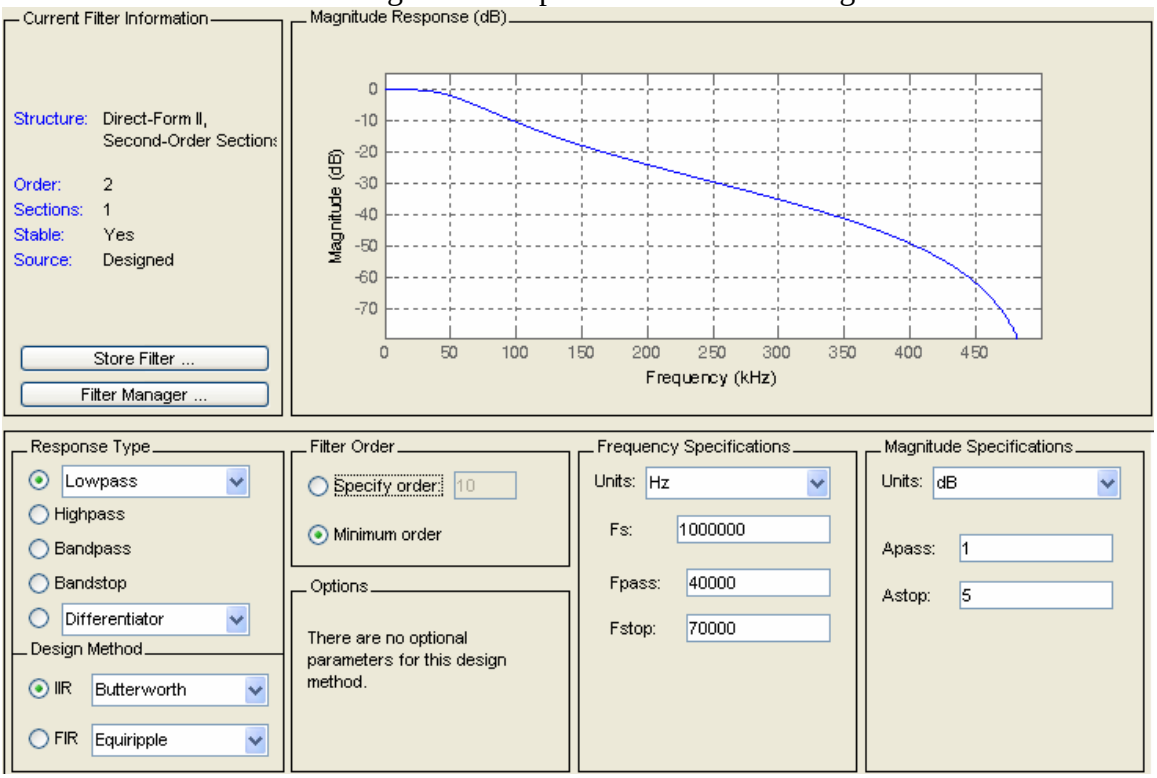

Figure 30. The magnitude response of the filter design in Matlab. The filter cuts frequencies > ~40kHz.

The filter is an infinite impulse response (IIR) 2nd order Butterworth filter. The Butterworth filter has value in that the passband is mostly flat than other filters (such as Chebyshev, and Bessel filters). Considering that the TDS PCB design involves two op amps (explained in section 5), low pass filters placed at the feedback portion of each op amp generates an active second order inverting filter. The current TDS PCB design limits placement of low pass filters; hence the reason for filtering to occur on both op

amps and not just one. The sensor PCB design section (section 5) details the placement and selection of components for optimal filtering.

5.3 Selection of Optical Components

Mentioned previously, the optical components chosen for the TDS is the IR light-emitting diode and the IR photodiode. It has been found that GaAs with doping of aluminum displays some of the best mechanical properties at fast speeds and low cost [65], [66], [67]. As mentioned previously, a phototransistor was not selected since photodiodes display a linear characteristic between its photocurrent (I_{PD}) and the irradiance (E_e) [68]. This relationship is utilized for the calibration process.

$$I_{PD} = f(E_e) \quad \text{Eq. 20}$$

$$\text{where, } E_e = \frac{d\Phi_e}{dA_E} = \frac{radiant\_power}{surface\_area} \quad \text{Eq. 21}$$

Light Incident on a Surface

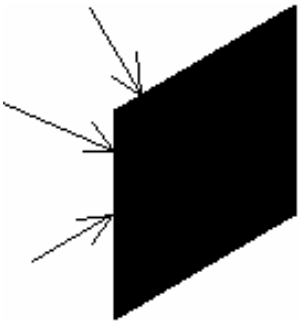

Figure 31 [68]. Light incident on a surface. Light emitted on to a photodiode surface maintains a linear relationship with its photo current (I_{PD}).

The maximum LED forward voltage must be at least 6V (since 5V is the supply voltage with at most a ±0.25V tolerance) and must be able to emit 40mW of light.

$$\text{i.e. } P_{LED} = i_{LED} * V_{LED} \quad \text{Eq. 22}$$

V_{LED} = voltage drop of a diode = 0.7V @max

and $i_{LED\ max}$ = 35mA (explained in section 4)

The photodiode was selected based on its ability to be sensitive enough for a detection range of relatively high light power. Lastly, the components were selected based on printer space availability (constraint listed in chapter 4 section 3). The components selected have peak wavelengths of 940nm for emission and detection respectively.

Drawing of a Typical Light-Emitting Diode

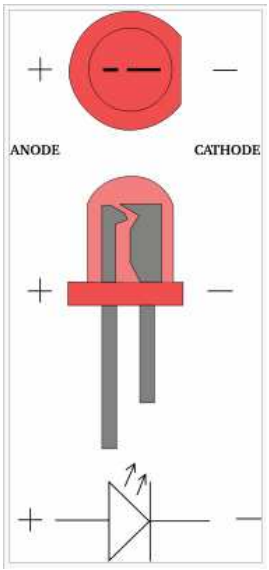

Figure 32 [69]. A drawing of a typical light-emitting LED. The LED is forward biased for light emission.

Most datasheets reviewed displayed the following range of characteristics for the LED and photodiode:

- LED maximum current rating: 40-60mA
- Maximum supply voltage: 1.5-7V
- Maximum soldering temperature: 240°C -260°C at 3s-5s

from the surface of resin edge).

Based on these stated characteristics, it is apparent that these components are very susceptible to damage under high temperatures. However, in most cases, the TDS design was determined based on these manufacturer specifications for flexibility in obtaining the optical components. Therefore, finding the right LED was not very difficult.

Some manufacturer limitations of the photodiode include:

- Maximum reverse voltage 20V
- Maximum power dissipation 75mW
- Maximum short-circuit current 2.4µA
- Maximum dark current 1.6µA
- Maximum soldering temperature: 240°C -260°C at 3s-5s

  from the surface of resin edge)

The TDS photodiodes' reverse voltage and maximum power dissipation are within manufacturer specifications. Since the supply voltage to the LED is only 5V, the light detected and converted to current will be <1µA (as described in section 5 of this chapter). Also, the power dissipation will only be in the µW range. The short circuit current is equal to the photodiode current (described in section 5) and thus current will be <1µA at maximum light detection. The dark current [70] is current flowing through the photodiode when the LED is not emitting light (i.e. $i_{LED} = 0$). Hence, the manufacturer limit of 1.6µA will not be detected since this much current will not be detected even at maximum. Like the LED, the photodiode is also sensitive to high temperatures; therefore, extensive testing must be performed to verify these components durability in operation and when being shipped and stored in extreme weather conditions.

The LED and photodiode desired will have a wavelength of 940nm. This is to allot for more light in the IR range. Optical components in the lower wavelength range may allow some lower range wavelengths to get detected. Figure 33 displays the typical LED and photodiode considered. Most LEDs and photodiodes of the characteristics listed above have similar geometries.

IR LED and Photodiode Geometry for TDS Design

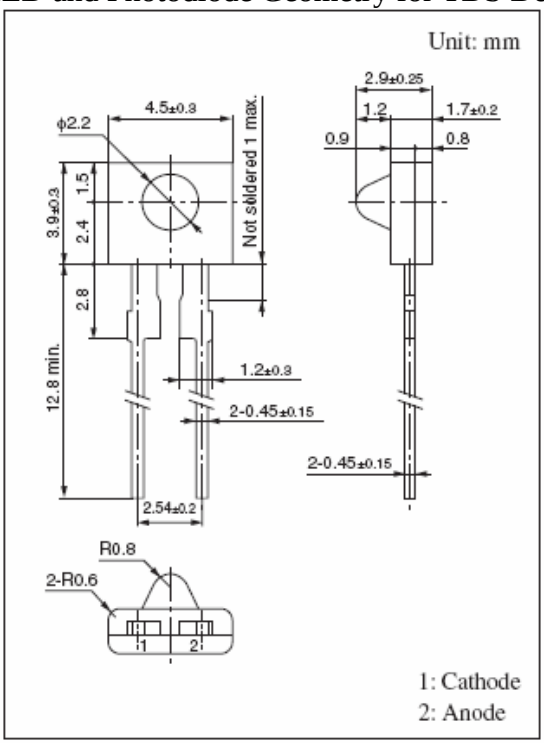

Figure 33 [70]. IR LED and photodiode geometry for the TDS design. The LED and photodiode many times have the exact same geometry shown. The total component size for both optical components does not exceed 5mm in length and 3mm in width, and 4mm in height (including maximum tolerances). Having optical components this small will make it easier to find space in the printer to accommodate the newly designed TDS.

The LED driver circuit utilizes a 5V DC signal to supply the LED and the photodiode is supplied by 1V DC signal (in the sensor PCB circuit). The 1V signal is provided by a resistor divider using the 5V supply (i.e. V_{REF}). Figures 34a-d describes LED and photodiode temperature and wavelength characteristics respectively for two

manufacturers. It is noticeable that LEDs and photodiodes share similar characteristics critical to effective operation. With two manufacturer specifications displayed, characteristics do not change considerably.

LED/Photodiode Temperature and Wavelength

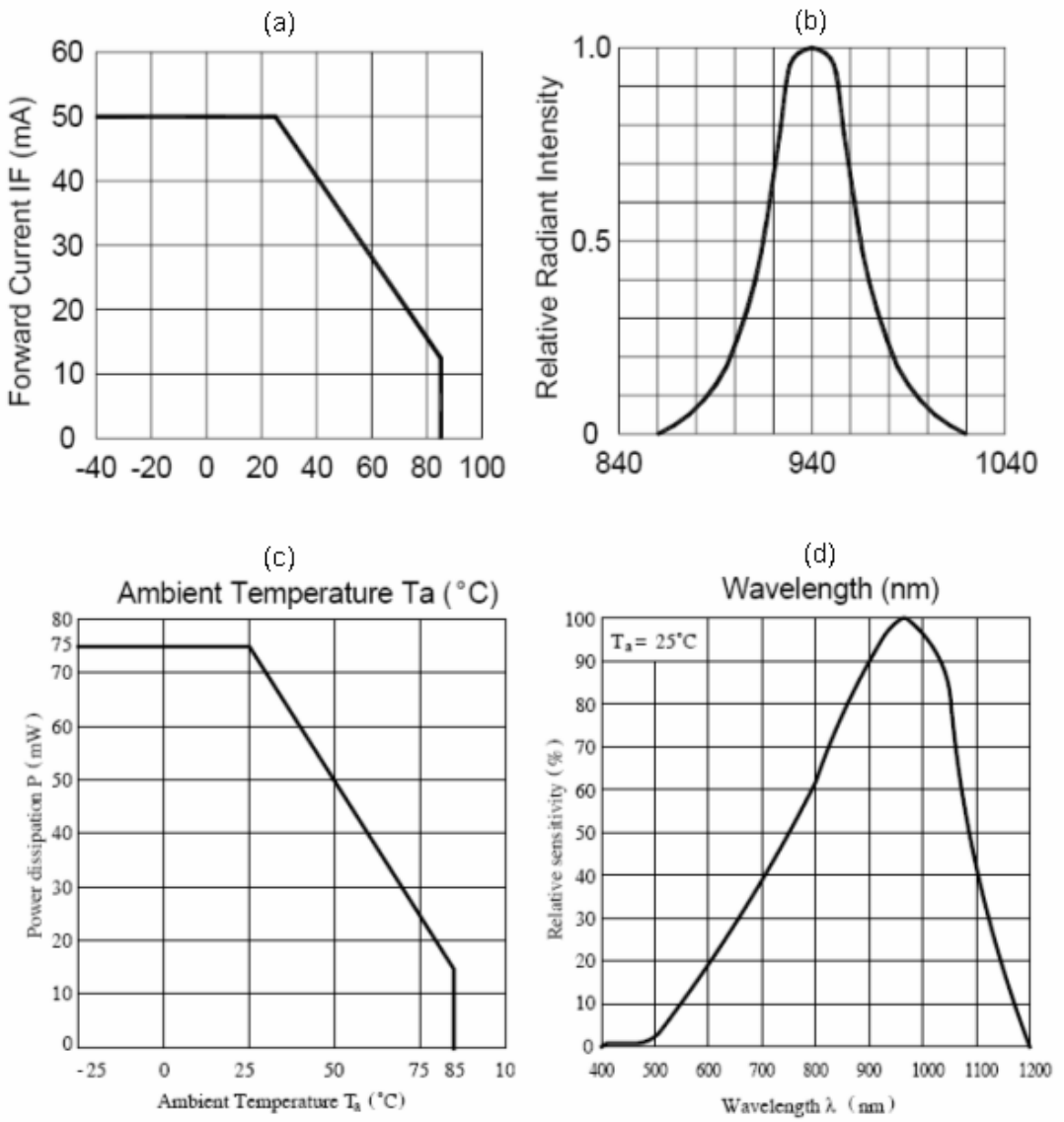

Figures 34a-d [71], [72]. LED/Photodiode temperature and wavelength specifications. Temperature and wavelength characteristics of the LED and photodiode pair provided by two manufacturers. The characteristics for many of these components with similar manufacturer specifications with identical characteristics display almost the same graphs. The optical components are sensitive to ambient temperature; however, the normalized output of the design excludes temperature effects. The peak wavelength transmission is 940nm.

The optical components are sensitive to ambient light; thus an optical housing was created to filter the light detected by the photodiode. The sensor's optical housing was designed and sent to the Materials lab for analysis to verify light transmission. The optical housing only allows transmission of IR light >800nm and completely blocks ambient light.

The LED was designed to provide a maximum output of 35mA (to be within the specified maximum LED forward current of 50mA). The circuit's voltage saturates at 20mA to allow degradation (due to temperature changes as displayed in figures 34a and 34c). The photodiode (sensor printed circuit board) circuitry was designed to provide a variable output between 1V and 5V which is linear with light transmission (discussed in section 5).

5.4 Design of the LED Driver Circuit

The purpose of the LED driver circuit is to convert the input PWM signal (used to adjust patch darkness for the PC drum) to emitted light. The LED driver design requires the following:

- A variable LED output current with a maximum amplitude of 35mA DC.
- A filter design that allows a PWM signal to be converted to a DC signal.
- A fast time constant that allows a rise time <2ms and a settling time <5ms for fast TDS calibration (with negligible notice by the consumer).

Initially, an operational amplifier was applied in conjunction with a NPN BJT for constant current in which a variable voltage signal can vary the resistance to the LED changing the LED current; however, it was found by eliminating the op amp and applying the BJT in active mode [73], the circuit can be cost-reduced and less

complicated. Figure 35 displays that when the BJT NPN transistor is in active mode [74], [75], [76], the voltage supplying the LED is independent of LED current (i_{LED}). The voltage supplying the LED is simply a switch. The LED current is (collector current) is driven by and approximately equal to the emitter current (discussed further in this section).

TDS LED Driver Circuit

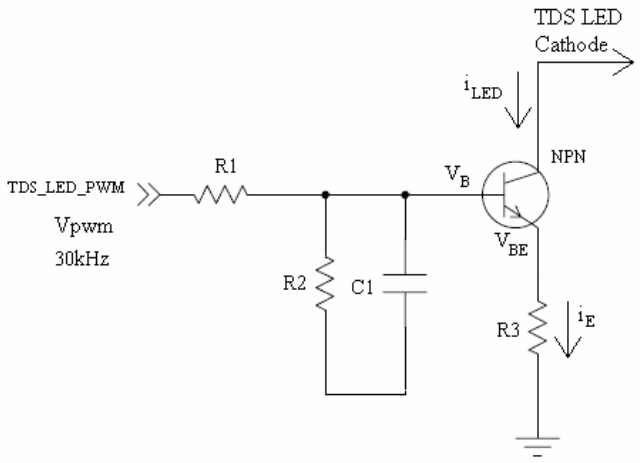

Figure 35. The TDS LED driver circuit. A filter design is applied to convert the PWM signal to a DC signal. The BJT converts the DC voltage signal to a DC current.

The LED driver circuit must maintain a rise time < 2ms and a settling time <5ms for fast sampling (which is discussed in the Implementation and Interpretation chapter 6). This system is modeled to determine optimal resistor and capacitor values for this response with given input conditions (i.e. V_{pwm} @ f = 30kHz frequency).

Laplace transformation circuit analysis [77] is utilized to determine the optimal settling time. First an equation is derived to find V_B. Kirchoff's Current law [78] is applied at the node (V_B) before the base of the NPN transistor:

$$\frac{V_{pwm} - V_B}{R_1} = \frac{V_B}{R_2} + \frac{V_B}{Z_{c1}} \quad \text{Eq. 23}$$

Let A_o = Amplitude of the square wave input V_{pwm}.

The transfer function (V_B/V_{pwm}) is found by first separating the term (on the left) and factoring out common constants:

$$\frac{V_{pwm}}{R_1} = \frac{V_B}{R_2} + \frac{V_B}{Z_{c1}} + \frac{V_B}{R_1} \Rightarrow V_{pwm} = R_1\left(\frac{V_B}{R_2} + \frac{V_B}{Z_{c1}} + \frac{V_B}{R_1}\right) \quad \text{Eq. 24}$$

V_{pwm} and V_B are isolated to convert the equation into a transfer function.

$$\frac{V_{pwm}}{V_B} = R_1\left(\frac{1}{R_2} + \frac{1}{Z_{c1}} + \frac{1}{R_1}\right) \Rightarrow \frac{V_B}{V_{pwm}} = \frac{1}{R_1\left(\frac{1}{R_2} + \frac{1}{Z_{c1}} + \frac{1}{R_1}\right)} \quad \text{Eq. 25}$$

Z_{c1} is substituted with $1/sC$ to display the equation as a function of the complex variable s:

$$\frac{V_B(s)}{V_{pwm}(s)} = \frac{1}{R_1}\frac{1}{\left(\frac{1}{R_2} + \frac{1}{\frac{1}{C_1 s}} + \frac{1}{R_1}\right)} = \frac{1}{R_1}\frac{1}{\left(\frac{1}{R_2} + C_1 s + \frac{1}{R_1}\right)} \Rightarrow \frac{V_B}{V_{pwm}} = \frac{1}{R_1}\left(\frac{1}{\frac{R_1 + R_2 R_1 C_1 s + + R_2}{R_2 R_1}}\right) \quad \text{Eq. 26}$$

$$\frac{V_B(s)}{V_{pwm}(s)} = \frac{R_2}{R_1 + R_2 + R_1 R_2 C_1 s} \quad \text{Eq. 27}$$

The complex variable s is isolated to display the equation in a standard transfer function form.

$$\frac{V_B(s)}{V_{pwm}(s)} = \frac{\frac{1}{R_1 R_2 C_1}}{\frac{1}{R_1 R_2 C_1}} \frac{R_2}{R_1 + R_2 + R_1 R_2 C_1 s} = \frac{\frac{1}{R_1 C_1}}{\frac{R_1 + R_2}{R_1 R_2 C_1} + s} \quad \text{Eq. 28}$$

Let $D = \frac{R_1 + R_2}{R_1 R_2 C_1}$ Eq. 29 and $F = \frac{1}{R_1 C_1}$ Eq. 30 Then, $\frac{V_B(s)}{V_{pwm}(s)} = F\left(\frac{1}{s + D}\right)$ Eq. 31

V_{pwm} is a periodic square wave signal having the behavior displayed in figure 36.

A Periodic Step Function

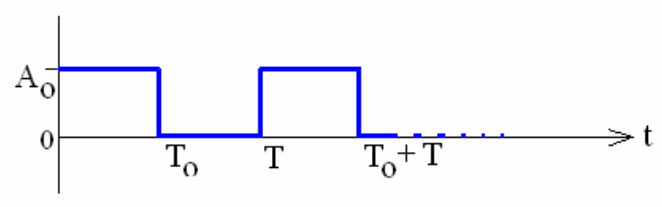

Figure 36. A periodic step function.

Where T = period of the square wave ($1/f$)

T_o = Duty Cycle* T

A_o = peak amplitude of the PWM signal

Figure 37a and b show how the equation for the periodic step function is determined.

Unit Step Function

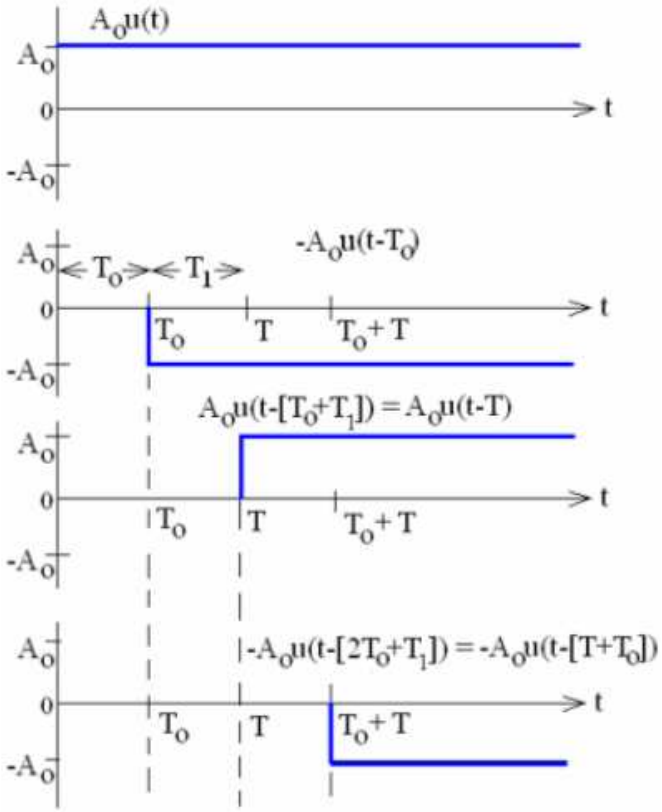

Figure 37a. The unit step function with delays. The step functions displayed above are summed to get a periodic step function.

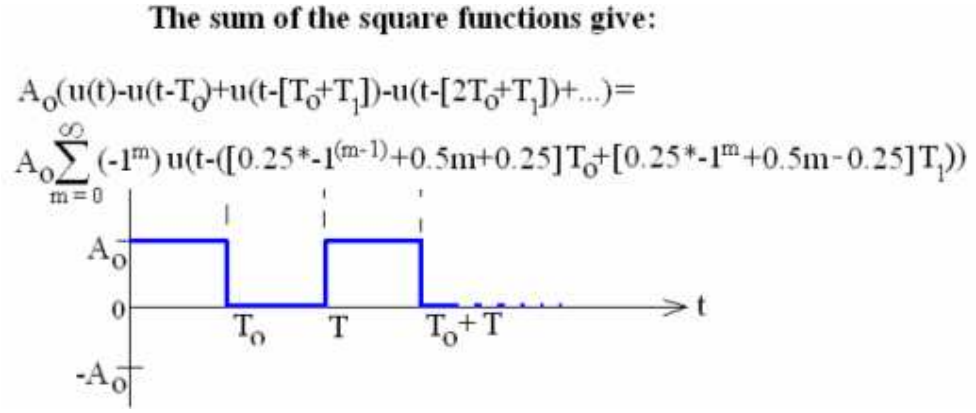

Figure 37b. Sum of the step functions. Characterization of the sum of infinite unit step functions with delays to create a square wave.

Where $T_1 = T - T_o$ thus, $T_1 + T_o = T$

Since $V_{pwm}(s)$ is a periodic step function, utilizing the step response characterizes the actual response of the periodic step function.

$$\text{i.e. } V_{pwm}(s) = \frac{A_o}{s} \qquad \text{Eq. 32}$$

Simply taking the step response of the function V_B gives:

$$V_B(s) = F\left(\frac{1}{s+D}\right)A_o * \frac{1}{s} \Rightarrow A_o F\left(\frac{1}{s(s+D)}\right) \quad \text{Eq. 33}$$

Taking the inverse Laplace function (L^{-1}) gives V_B as a function of time (from the frequency domain). The general Laplace transformation for a term similar to V_B is provided in a typical Laplace transform look-up table.

$$L^{-1}\{V_B\} = L^{-1}\left\{\frac{\alpha}{s(s+\alpha)}\right\} = 1 - \exp(-\alpha t) \quad \text{Eq. 34}$$

Applying the equation above to the function V_B provides v_B (time domain equation for frequency domain V_B).

$$L^{-1}\{V_B\} = \frac{A_o F}{D} L^{-1}\left\{\frac{D}{s(s+D)}\right\} \Rightarrow \quad \text{Eq. 35}$$

$$v_B(t) = \frac{A_o F}{D}[1 - \exp(-Dt)] \quad \text{Eq. 36}$$

The LED forward current desired is 35mA. Since the diode across the base-emitter junction possess a ~0.7V drop and the input square wave PWM signal was set at 3.3V, the maximum voltage at the base of the transistor must be set where the current through the voltage divider (after the capacitor is >98% charged) is smaller than the milliamp range for safety purposes.

$$\text{i.e. } V_B = i\frac{R_2}{R_1 + R_2}V_{PWM} \quad \text{Eq. 37}$$

$$\Rightarrow i = \frac{V_B}{V_{PWM}} * \frac{R_1 + R_2}{R_2} \quad \text{Eq. 38}$$

Also, the voltage must be large enough to experience the voltage drop while having significant voltage to divide by a resistance that will provide the maximum LED current of 35mA. Furthermore, the value of the time constant 1/D (equation 29) is dependent on the values of R_1, R_2, and C_1. Based on these factors, the values chosen for R_1, R_2, and C_1 were 1kΩ, 10kΩ, and 1μF. Values of greater orders of magnitudes cause an increase in the time constant which in turn slows the response of the LED driver circuit. Values of lesser orders of magnitude may be utilized; however, the current increases by the same orders of magnitude. This may cause issues of safety in testing and implementation. Values within the order of magnitude may be effective for this circuit. The values of 1kΩ, 10kΩ, and 1μF are common values easy to calculate and are typically available for implementation.

Applying equation 31 in Matlab (code displayed in Appendix A) provides time characteristics for V_B that are critical to fast sampling of the TDS. The main time

characteristics observed are the rise time and settling time.

The step response generated is displayed in figure 38. The rise time was within 2ms and the settling time maintained at 3.56ms (less than the 5ms specification limit).

Step Response of the LED Driver Circuit

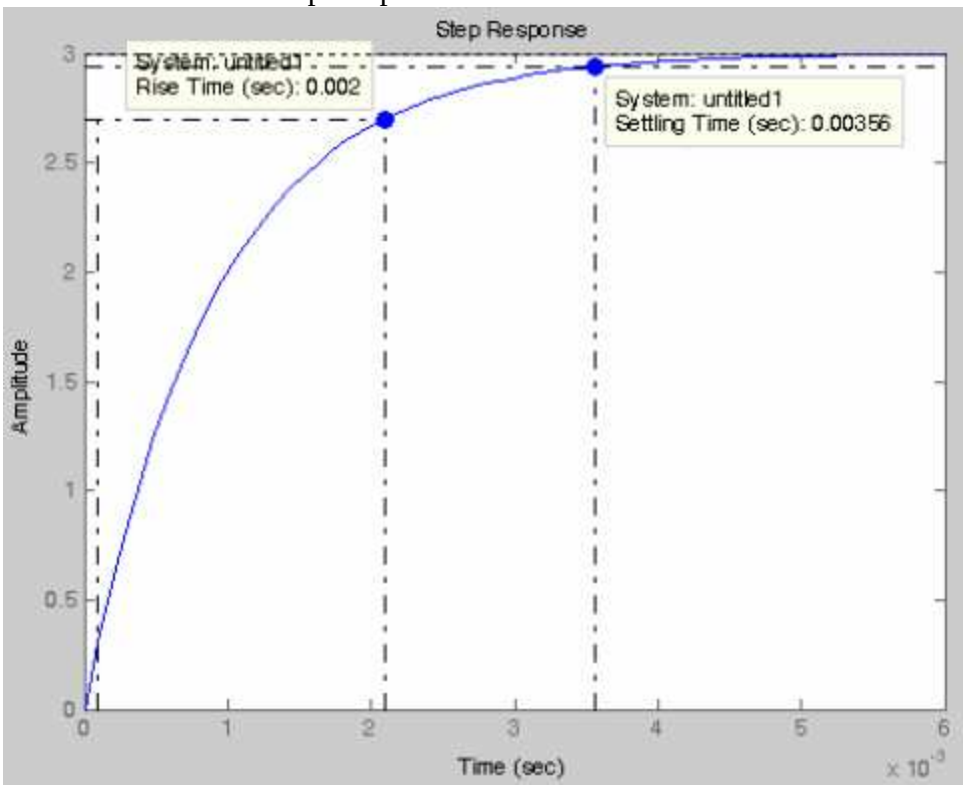

Figure 38. Step response of V_B. Rise time and settling time are within their specified limits of 2ms and 5ms respectively.

After the testing, values selected may be adjusted to reduce electromagnetic interference (EMI) and other extraneous effects.

The Bode plot of this system shows that this system is stable. The Matlab command "bode(VBdivVpwm)" was added to the end of the Matlab code in Appendix A. The resulting graph is displayed in figure 39. View of the Bode plot displays a positive phase margin (criteria required for stability) and an infinite gain margin since the phase never

crossed -180° [79].

Bode Plot of the LED Driver Circuit

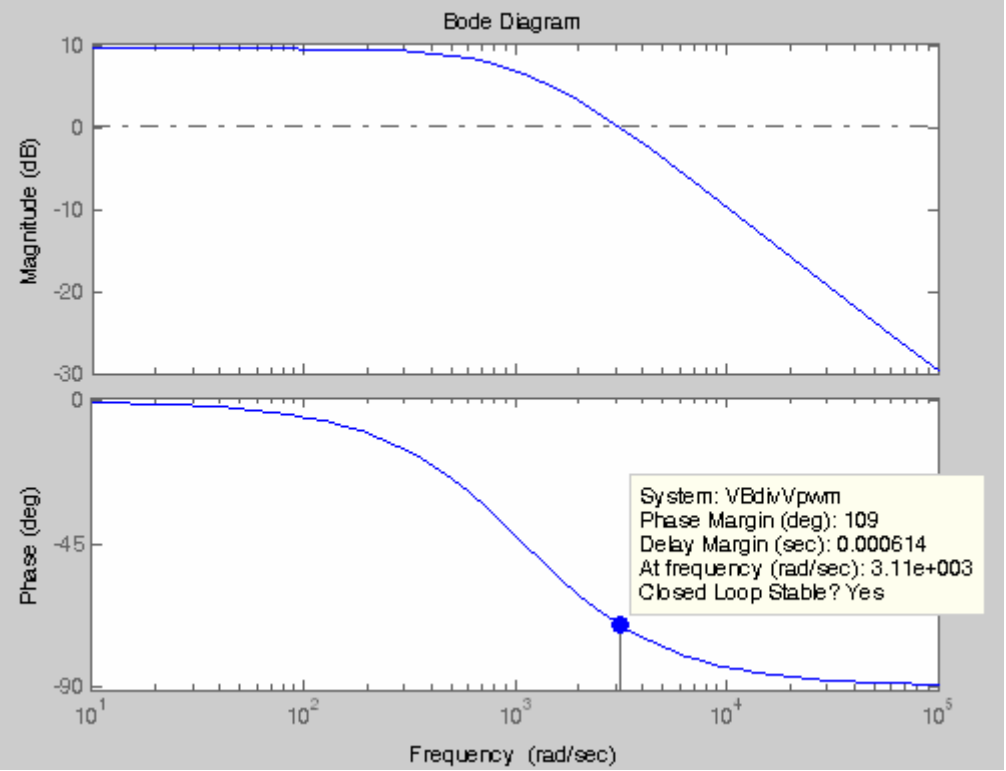

Figure 39. The Bode plot of the transfer function V_B/V_{pwm}.

Lastly, the resistor at the emitter of the transistor is calculated once finding its relationship with the LED forward current at the collector (i_{LED}). The PWM duty cycle changes V_B which therefore changes i_{LED}. The LED forward current (i_{LED}) can be found knowing: the base voltage (from equation 31), the voltage drop across the base-emitter (which is a diode drop with a maximum voltage drop V_{BE} ~ 0.7V) and the resistor at the emitter (R_3). As mentioned previously, the emitter current (i_E) is approximately equal to the collector current (i_C) when the NPN BJT is in active mode (i.e. $i_e \sim i_c$).

Since the i_{LED} is variable (used to determine TDS calibration settings) with a maximum of 35mA (as previously determined in section 3); therefore, the resistance is found by the following equation:

$$R_3 = \frac{v_B - v_{BE}}{i_{LED}} = \frac{\frac{A_o F}{D}[1-\exp(-Dt)] - v_{BE}}{i_{LED}} \quad \text{Eq. 39}$$

Taking the limit as t approaches infinity at 100% duty cycle yields the resistance.

$$R_3 = \lim_{t\to\infty}\left[\frac{\frac{A_o F}{D}[1-\exp(-Dt)] - v_{BE}}{i_{LED}}\right] \Rightarrow R_3 = \frac{\frac{A_o F}{D} - v_{BE}}{i_{LED}} \quad \text{Eq. 40}$$

$$\text{since } D = \frac{R_1 + R_2}{R_1 R_2 C_1} = 1.1e3\frac{1}{\Omega F} \quad \text{Eq. 41}$$

$$F = \frac{1}{R_1 C_1} = 1.0e3\frac{1}{\Omega F} \quad \text{Eq. 42}$$

A_O = 3.3V for 100% duty cycle

v_{BE} = 0.7V

and i_{LED} = 35mA = 0.035A

R_3 was found to be 65.7Ω for a maximum LED forward current of 35mA.

The final values were applied for implementation on the TDS system card circuit. Again, values will be selected based on testing results. Since the DC component of the square wave is simply the average of the square wave over the period, the DC component of the square wave can be used to determine i_{LED} at any given input PWM duty cycle.

$$\text{i.e.} \quad i_{LED} = \frac{v_B - v_{BE}}{R_3} \Rightarrow i_{LED} = \frac{\frac{A_o * dutycycle\% * F}{D}[1-\exp(-Dt)] - v_{BE}}{R_3} \quad \text{Eq. 43}$$

The duty cycle is dependent upon the patch darkness desired. Thus, for every patch placed on the PC drum, the duty cycle is adjusted for that particular patch. The output of the sensor is utilized to develop a linear relationship between the actual L* (brightness) to print darkness.

5.5 Design of the Toner Density Sensor PCB Circuit

The TDS PCB circuit is the only circuit on the PCB of the sensor. The circuit is basically a detector circuit utilized to convert detected light into a measurable voltage. The proposed PCB has a maximum width of 10mm and a maximum length of 50mm. Therefore, the sensor circuit components must be relatively small sized surface mounts. The sensor circuit requirements are:

- Provide a variable output with a maximum of 5V
- Maintain the specified tolerance despite changes in environment
- The variable output must have a linear relationship with the LED input current
- The sensor must be designed with a 5V DC input. This is the supplied voltage available for the sensor design.
- The maximum output voltage must equal to 4.3±0.7V. This is determined by the maximum 5V supply subtracted by a ±0.7V tolerance (which again was a random choice for tolerance until further testing).

The photodiode is capable of producing varying currents as a result of environmental conditions. Therefore, the output is always normalized to adjust for this variation. Normalization also accounts for LED variation and other extraneous effects on the TDS while under operating conditions.

To get an output close to the supply voltage, a rail-to-rail Output (RRO) dual operation amplifier design is utilized [80]. Considering the light-emitting diode (LED) and photodiode size options based on required space allotted for the sensor in the printer (<5mm for both width and height), a design was built around the LED and photodiode availability. The following circuit is a general circuit typically used for sensor detection

(discussed in chapter 2 section 6). Resistor values were determined and selected after determining the relationship between I_{LED} and I_{PD} (which is discussed later in this section).

Toner Density Sensor Electrical Circuit Representation

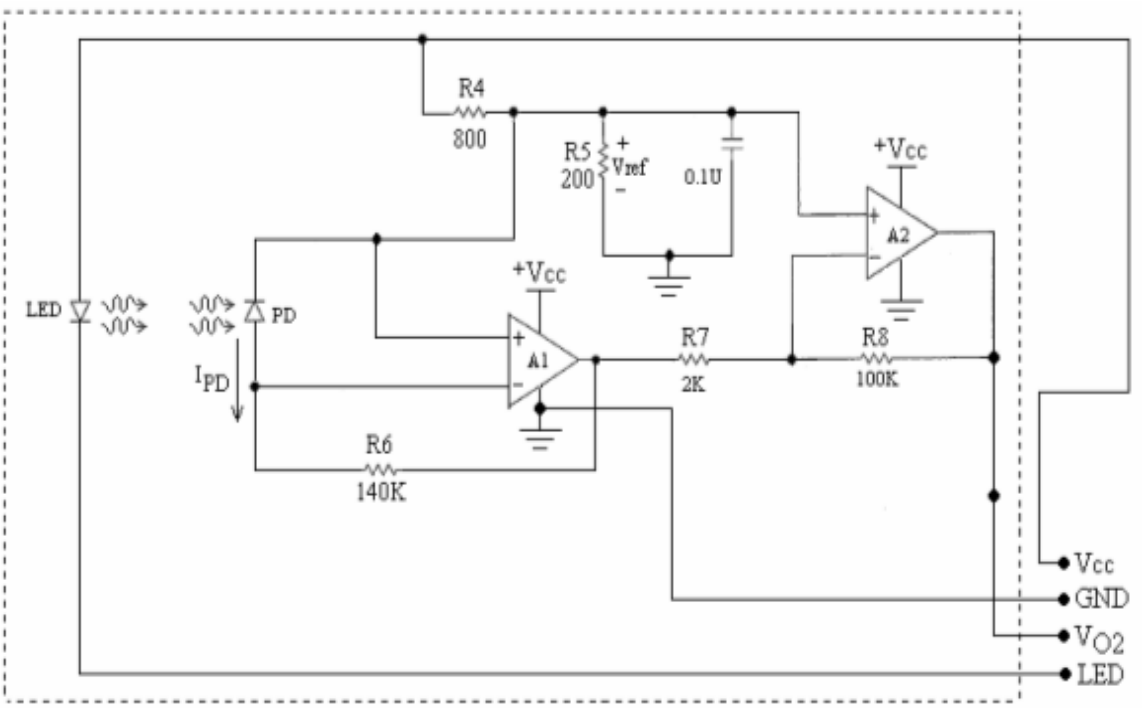

Figure 40. The toner density sensor electrical circuit. The LED light is reflected by the PC drum and received by the photodiode. The photodiode current is reversed-biased and is converted to a voltage close to the reference voltage of 1V (determined by resistor divider R_4 and R_5). The output is then amplified by the second op amp to a measurable output voltage (4.3±0.7V).

The photodiode converts received light to a small current (where $I_{PD\text{-}max}$<1μA). The current is converted to a voltage (output of the first op amp V_{O1}<1V) and is compared to the reference voltage (V_{REF} = 1.0V) entering the first op amp (A1) positive terminal. In order to maintain both the ideal op amp characteristic (where $V^+ \approx V^-$) and enough voltage difference for comparison (between V_{O1} and V_{REF}) at the op amp terminals, the value of V_{REF} must be close to the value of V_{O1} (V_{O1} <1V). Hence, V_{REF} is set equal to

1.0V by the R_4/R_5 resistor divider. The second op amp (A2) amplifies the output signal of A1. Hence, A2 must have the ability to amplify the input signal and provide a maximum output of 4.3±0.7V at a maximum current of 35mA (as stated previously).

The first op amp equation was determined to find the output voltage:

$$\frac{V_{O1} - V_{REF}}{R_6} = -I_{PD} \Rightarrow V_{O1} = (-I_{PD} * R_6) + V_{REF} \quad \text{Eq. 44}$$

$$\text{where } V_{REF} = \frac{R_5}{R_5 + R_5} V_{CC} \quad \text{Eq. 45}$$

The second op amp equation is based on the Kirchoff's current law (i.e. current entering the node between R_7 and R_8 is equal to the current leaving the node). The second op amp equation was found to be:

$$\frac{V_{REF} - V_{O1}}{R_7} = \frac{V_{O2} - V_{REF}}{R_8} \Rightarrow V_{O2} = R_8 \left[V_{REF} \left(\frac{1}{R_7} + \frac{1}{R_8} \right) - \frac{V_{O1}}{R_7} \right] \quad \text{Eq. 46}$$

Substituting the equation for V_{O1} into the second op amp equation gives:

$$V_{O2} = R_8 \left[V_{REF} \left(\frac{1}{R_7} + \frac{1}{R_8} \right) - \left(\frac{(-I_{PD} * R_6) + V_{REF}}{R_7} \right) \right] \quad \text{Eq. 47}$$

$$V_{O2} = V_{REF} + I_{PD} \frac{R_6 R_8}{R_7} \quad \text{Eq. 48}$$

The photodiode current (I_{PD}) was found using the relationship between I_{LED} and V_{O2}.

$$I_{PD} = (V_{O2} - V_{REF}) * \frac{R_7}{R_6 R_8} \quad \text{Eq. 49}$$

The TDS maximum output voltage is desired at 20mA. This is to allow more resolution within the linear portion of the LED forward current and the output voltage. The photodiode reverse current selected was calculated to detect up to 0.55µA @20mA of LED current (i_{LED}) given the values in the chart below. The current is too small to

measure; therefore, this value was calculated with knowledge of the sensor component values. This information was utilized to verify the chosen resistor values for the actual sensor circuit.

TDS Parameters Used to Determine Photodiode Current

R_6 (kΩ)	R_7 (kΩ)	R_8 (kΩ)	V_{REF} (V)	V_{O2} (V)	I_{PD} (μA)
100	2	100	1	5	0.55

Table 2. TDS parameters used to determine photodiode current. The resistor values were originally picked to get an output of 5V given that I_{PD} = 0.55μA.

The chart below describes the relationship between I_{PD} and i_{LED}. The relationship is almost perfectly linear after testing with the actual sensor developed (details discussed further in chapter 6). This linear relationship is utilized to develop the TDS calibration algorithm.

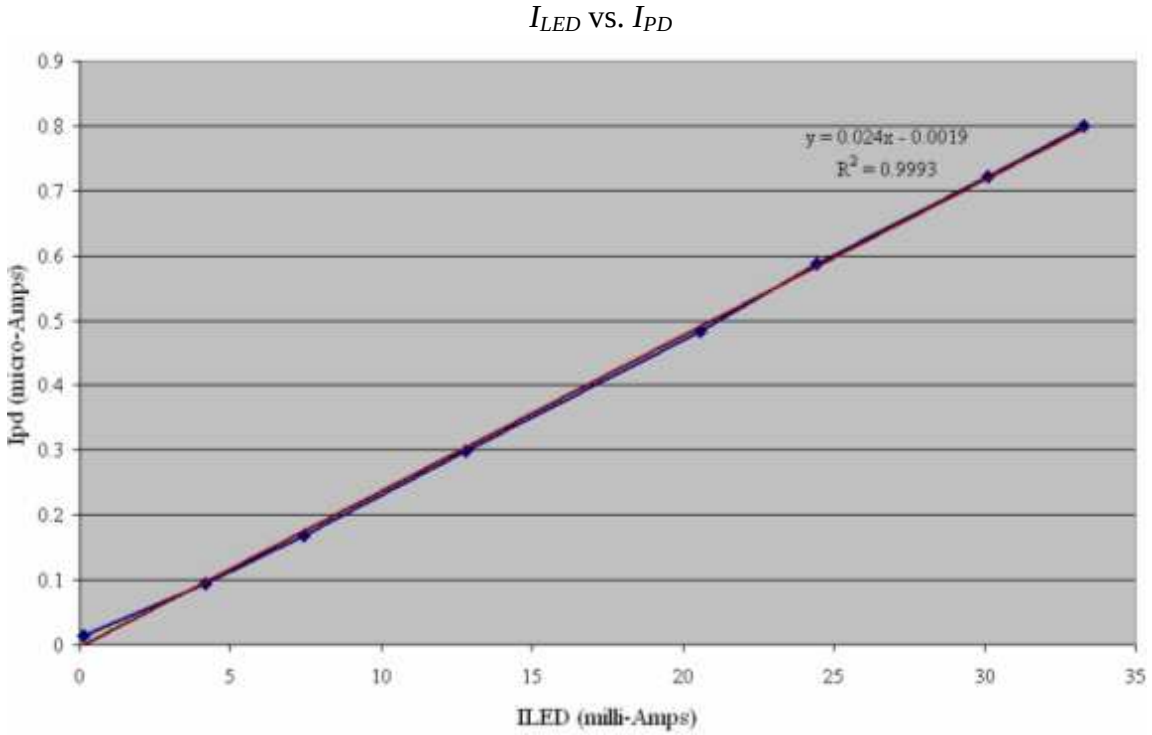

Figure 41. TDS I_{LED} vs. I_{PD}. The current of the photodiode was too small for detection by a standard ammeter. The current was calculated knowing the relationship between ILED and the sensor output voltage. The following chart helped to determine the values for the op amp design.

As mentioned in the LED Driver Circuit analysis, the TDS voltage should max at 5V @20mA and maintain 5V until the maximum forward current is reached at 35mA. Figure 42 displays an example of the TDS Output vs. LED forward current relationship.

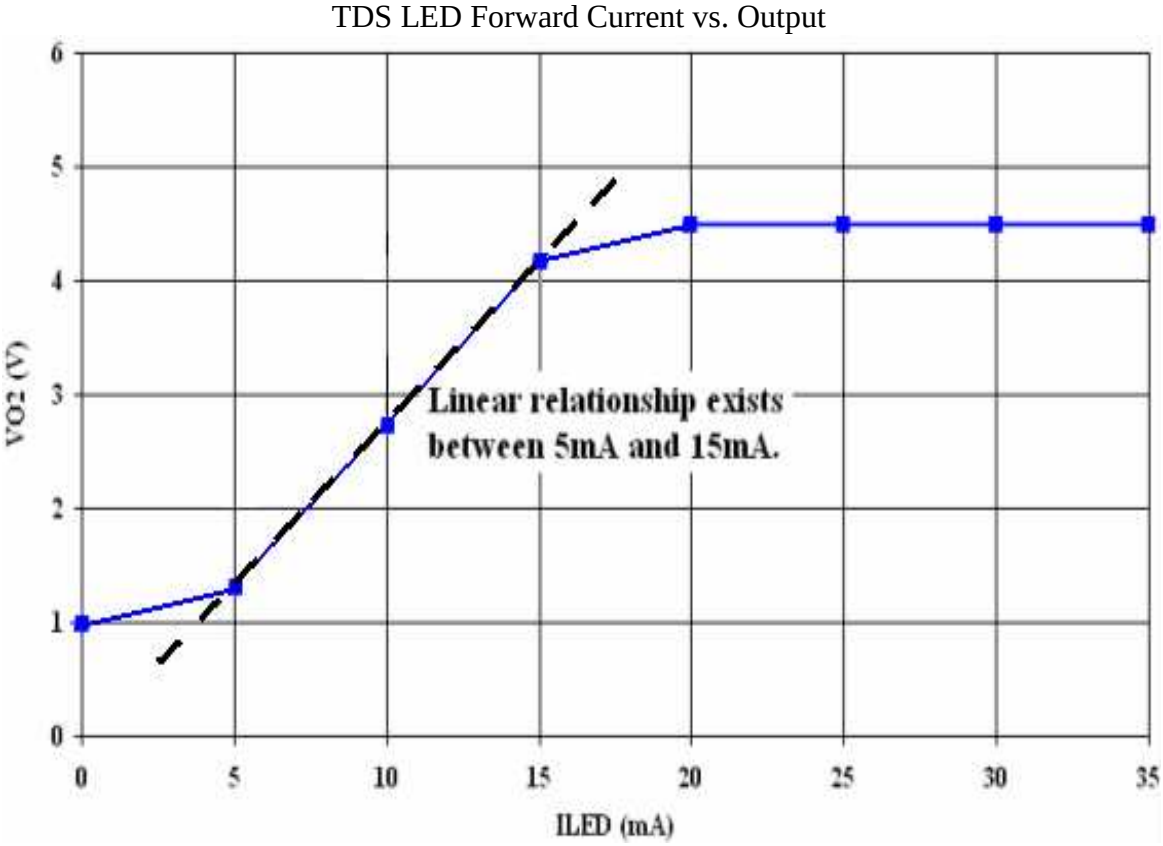

Figure 42. TDS LED forward current vs. output. The values of V_{O2} possess a large range between 5 and 15 mA; hence, only the minimum and maximum voltages are referenced in the design of the TDS sensor circuit. The slopes and their differences between 5 and 15mA are referenced to maintain a specified linear characteristic for manufacturers of the finalized toner density sensor.

Capacitors were not placed in the op amp circuit until an assessment is made regarding the noise level (due to EMI where the design is discussed in section 2). This was determined during testing of the implemented first-pass of the sensor in the printer. Based on assessment of the electromagnetic interference (EMI) and other possible noise effects, capacitors will be placed on the feedback portion of each op amp. Values of the

capacitors were selected based on the desired rise time of 5ms and settling time of 10ms and on the filtering capacity of the second order low pass filter.

Adjustments to the low-pass filter design are based on the following factors:

- The existing sensor design allows little room for design changes for optimal filtering. This is because most LTV sensor circuits possess similar circuit designs displayed in figure 40.
- The reference voltage acts as an offset to the TDS output. Therefore, the TDS must be designed to include a reference voltage (not implemented in the Butterworth filter design).
- The resistors and capacitors are selected on availability of these components given their surface mount package sizes (i.e. size 0603) and cost.
- The filter is also based on the resulting gains of the selected components, photodiode current and operational amplifier rail (i.e. most RRO amplifiers are within ±0.2V of the supply voltage).

Appendix B displays the analysis for the second order transfer function implemented. Equation 67 provides the resulting equation for the sensor PCB circuit for determination of the optimal filter design within rise and settling time specifications.

$$V_{O2} = V_{REF} + I_{PD} * \frac{R_6 R_8}{R_6 R_7 R_8 C_3 C_4 s^2 + (R_6 R_7 C_3 + R_7 R_8 C_4)s + R_7} \quad \text{Eq. 67}$$

The capacitances were originally selected based on the time constant (τ < ~1ms) and availability. The modified circuit with low pass filtering is displayed in figure 43. Code and analysis displaying the modified EMI reduction circuit is in Appendix B.

TDS PCB Modified with Capacitors

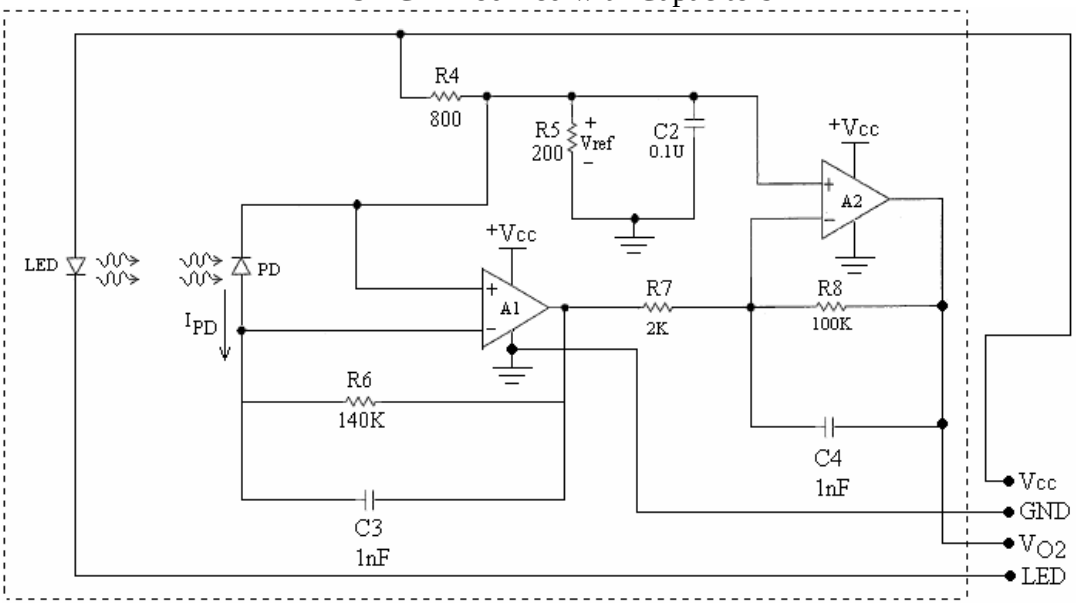

Figure 43. The TDS modified with capacitors. The capacitors are utilized for second-order low-pass filtering of EMI.

Figure 44 is the Bode plot of the transfer function acquired for the circuit above.

Modified TDS PCB EMI Reduction Circuit

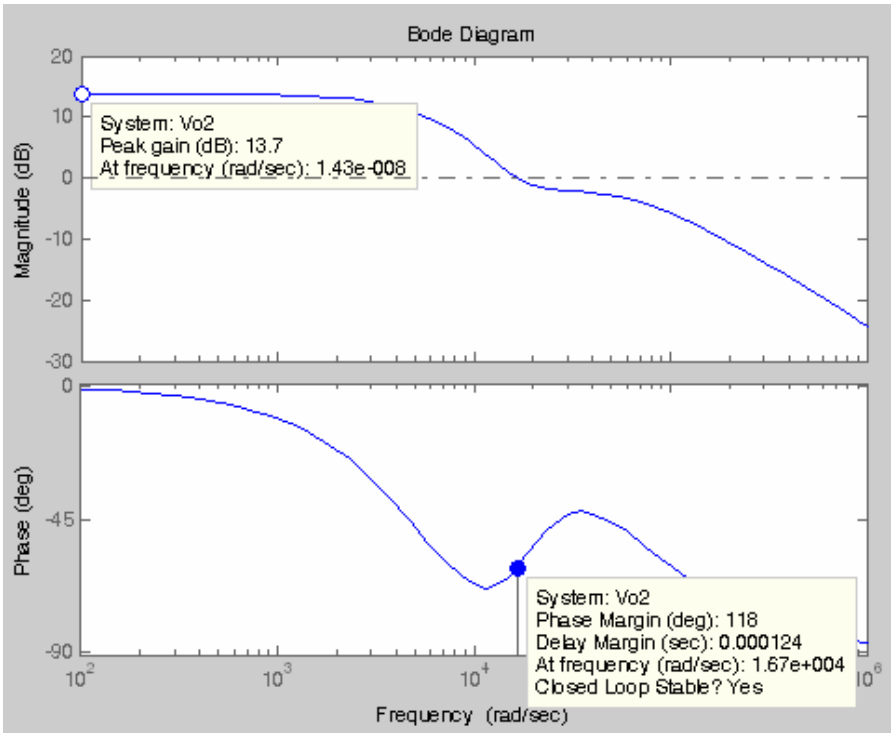

Figure 44. The modified TDS PCB EMI reduction circuit. The system is stable and the time constants for each filter are within 1ms.

This circuit is a second order low-pass filter circuit. Chapter 6 section 2 discusses details regarding implementation of the circuit.

5.6 Design of the A/D Interface Circuit

The A/D interface circuit was designed mainly to reduce potential EMI coming from the sensor cable (as it travels through EP components to the system card) and to step down the voltage from the maximum output voltage of 4.3±0.7V (proposed TDS output value) to the TDS to 2.6±0.7V (proposed A/D input value). The A/D converter used has a maximum voltage input of 3.6V. A simple voltage divider was applied at the output of the circuit.

TDS A/D Converter Interface Circuit

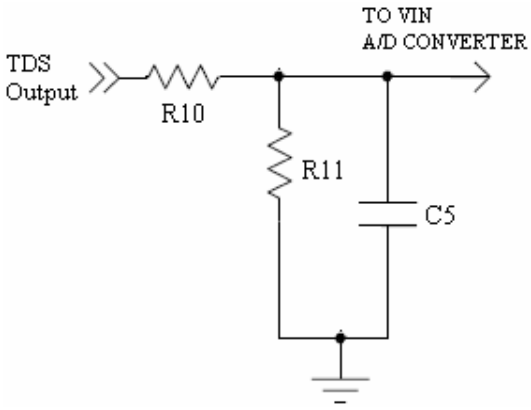

Figure 45. The TDS A/D converter interface circuit. The voltage divider filters noise from the TDS and steps down the TDS output to a maximum of 3.3V to the A/D converter.

The TDS A/D input is then equal to:

$$V_{A/D} = V_{O2} \frac{R_{11}}{R_{10} + R_{11}} \quad \text{Eq. 50}$$

The circuit analysis applied is exactly the same as what's been done with the LED driver circuit at the base of the NPN transistor (V_B). The difference is the TDS output

(V_{O2}) is replaced for A_o, R_1 is replaced R_{10}, R_2 is replaced for R_{11}, and C_5 is replaced for C_1. The capacitance will be determined based on the noise level of the sensor. Originally, C_5 was set equal to 0.1µF. R_{10} and R_{11} were set to equal 10kΩ and 20kΩ respectively. Similar to the LED driver circuit voltage divider, values orders of magnitude lower can be utilized; however, the current increases the same orders of magnitude. As a result, safety of the circuit and component ratings becomes a concern. Values orders of magnitude higher than the values selected will slow down the response time of the circuit. Matlab code was re-applied for the A/D Interface circuit (Appendix C). The step response and the Bode plot of the A/D interface circuit are displayed in figures 46 and 47 respectively.

Step Response of the A/D Interface Circuit

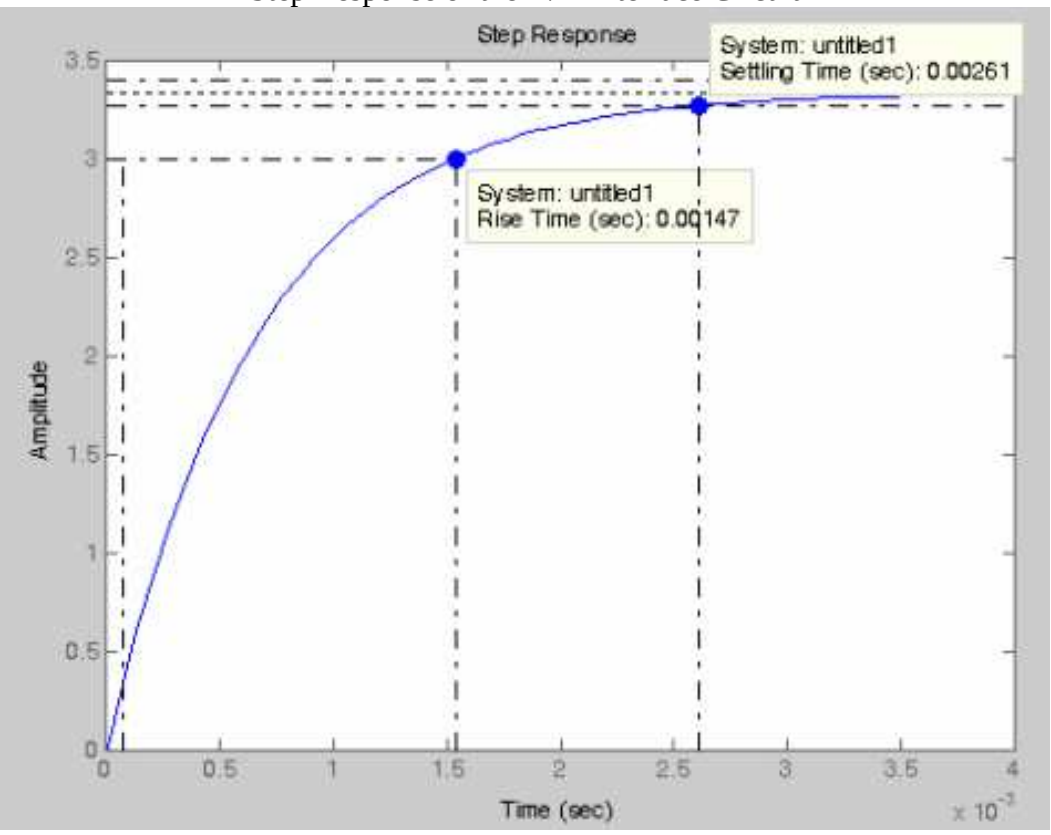

Figure 46. The step response of the A/D interface circuit. The rise and settling times are within 2ms and 5ms respectively.

Bode Plot of the A/D Interface Circuit

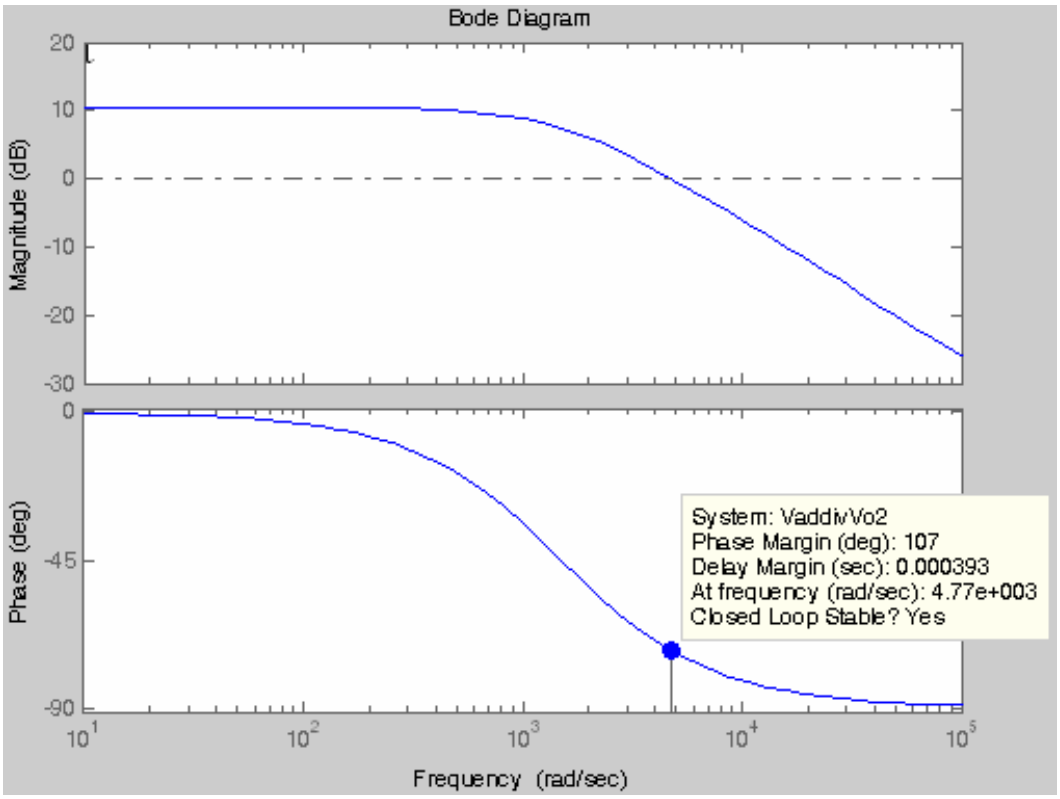

Figure 47. The Bode plot of the A/D interface circuit. The system is stable with an infinite gain margin and a phase margin of 107°.

The rise time and settling times were equal to 1.47ms and 2.61ms respectively. The Bode plot of the transfer function was also found in Matlab (Appendix C). The Bode plot of the A/D Interface circuit (figure 47) displays similar results to the LED Driver circuit. The system is stable with a phase margin = 107° and an infinite gain margin [79].

CHAPTER 6: IMPLEMENTATION AND INTERPRETATION

This chapter highlights the process of implementing the toner density sensor in the mono laser printer. Section 1 of this chapter (sensor development), explains the process to implement the sensor design into a tangible opto-electronic device. It also describes the placement of the sensor in the printer. Section 2 is the actual sensor testing. The three main parts within this section, EMI, qualification and environmental testing discuss testing procedures and provides the results. The EMI testing was performed to develop a design solution which reduced EMI affecting the toner density sensor's output. Qualification and environmental testing is required to verify the sensor's performance and/or durability under extreme conditions. Lastly, section 3 verifies the sensor's effectiveness in reducing print darkness variation.

This chapter demonstrates that the newly designed TDS met the goals of greatly reducing print darkness variation and EMI affecting the TDS output signal.

6.1 Sensor Development

Once the design was complete, the sensor's PCB layout was completed in Mentor Graphics. The resistors and capacitors all have 0603 [81], [82] sizes to maintain enough space on the sensor PCB for LED and photodiode leads and the dual op amp. The PCB was then sent to a local PCB parts assembly company where a "first-pass" sensor PCB was developed. PCB components were purchased and soldered unto the PCB for testing.

First-Pass TDS PCB

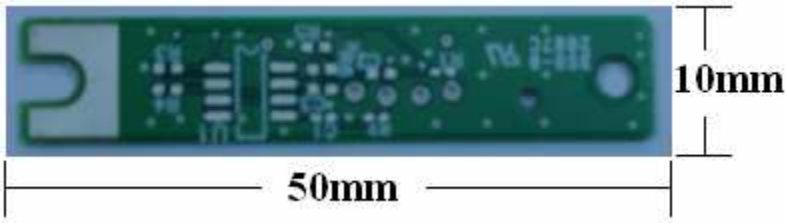

Figure 48. The first-pass TDS PCB. The TDS PCB was developed for an assessment of the TDS output to optimize the signal.

The optical housing was designed by a mechanical engineer with polycarbonate resin thermoplastic. This material is stronger and more durable than glass and Plexiglas. The polycarbonate material transmits 85% light with wavelengths greater than 700nm (IR range) at the optical window.

The connector and wires are to bridge between the printer's system card and the sensor. The five pin JST connector was picked based on availability and any durable connector that supports four terminals can be used. All of the resistors and capacitors possess a 1% tolerance for greater accuracy. Figures 49a-c displays the 2nd sensor fabricated.

The Toner Density Sensor Developed

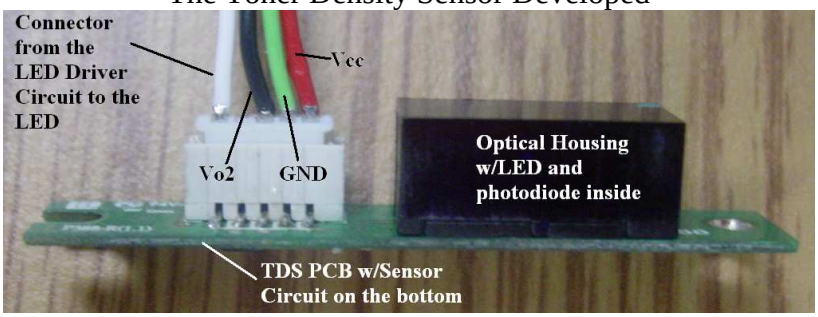

Figure 49a. The toner density sensor developed. The TDS sensor implemented in the printer. The initial design was a "first pass" to verify sensor performance in the printer. The white connector connects the sensor circuit to external circuits: the LED Driver circuit and the A/D Interface circuit placed on the printer's system card.

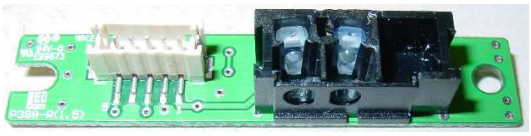

Figure 49b. The TDS sensor with optical housing cover removed. The photodiode is on the left and the LED is on the right. Light is emitted and detected by these components.

Figure 49c. The TDS PCB. A series of resistors and capacitors combined with a rail-to-rail output (RRO) dual op amp generates a measurable signal.

Figure 49d. The final TDS PCB. The PCB layout changed due to avoid high failure rate when IR reflow soldering. The PCB color was changed to avoid confusion with the previous version.

The sensor's layout had to change considering that optical components have lower failure rate when IR reflowed soldered [83] than hand soldered. Optical components are very susceptible to failure under high temperatures for durations longer than 3-5s (as stated in chapter 5.2). In addition, hand soldering optical components may have a high percentage of human error such as weak lead connections, shorting other components, poor look, etc. IR reflow soldering was implemented for TDS manufacturing instead of wave soldering since wave soldering requires greater temperatures. However, it was found that the current layout can create high failure rates (due to the positioning of components). Therefore, capacitors and resistors were rotated 90° to allow for faster and more efficient soldering in manufacturing. Figure 49d displays the final layout of the TDS PCB. The previous layout was adequate only for small volumes and prototyping.

However, manufacturing millions of these sensors required the layout change for the TDS PCB.

Some components of the printer were modified to fit the sensor. Figure 26 (chapter 5 section 2) displays the TDS in the printer. The sensor sits under the paper path 18mm from the PC drum. The TDS is powered (via V_{CC} = +5V) only when performing a calibration.

Teams at Lexmark supplied the necessary A/D converter, developed the code, and mechanical designs required to run the TDS and the calibration cycle. Several iterations of running the sensor were utilized to determine the necessary changes to code and the mechanical design surrounding the TDS. After final changes, actual testing of the "first-pass" TDS circuit began. Several circumstances were encountered with application of the TDS. One main problem encountered early in testing was electromagnetic interference (EMI) experienced by the sensor due to the printer (section 2.1). As a result, design changes were made to address the issue. It was the first change made to the sensor since a measurable signal was not detected accurately at the output due to the noise. The second problem was the sensor's response in extreme environmental conditions. These two problems, in addition to the qualification testing are addressed in section 2.3 of this chapter. At the end of the chapter (section 3), final results are displayed showing differences in print darkness variation as a result of implementing the toner density sensor.

6.2 TDS Testing

This section outlines testing in three parts: EMI reduction, qualification and environmental stress testing. These tests determined the performance of the TDS under a

variety of conditions.

6.2.1. Reduction of TDS Electromagnetic Interference (EMI)

Actual TDS testing began to show some drawbacks to the initial design. The first problem to occur was arcing between the transfer roll and the TDS. Whenever the transfer roll was powered on (POR), a visible arc appeared until the transfer roll stopped running. Since transfer occurs in the >±1000V range and the TDS maximum output is 5V, a large potential was generated between the two components. To address this problem, the sensor was moved back 2mm from 16mm to 18mm. This reduced the arcing problem until the printer was powered on (POR). An investigation revealed that when the TDS was POR, the signal displayed was a filtered DC signal. However, when cartridge components were POR, the noise encapsulated the entire TDS output signal (V_{O2}). Figure 21 (chapter 4 section 2) displays the noisy output of the TDS. The initial solution was to add a conductive shield grounding EMI from the sensor (displayed in figure 50).

TDS with Conductive Shield (EMI Shield)

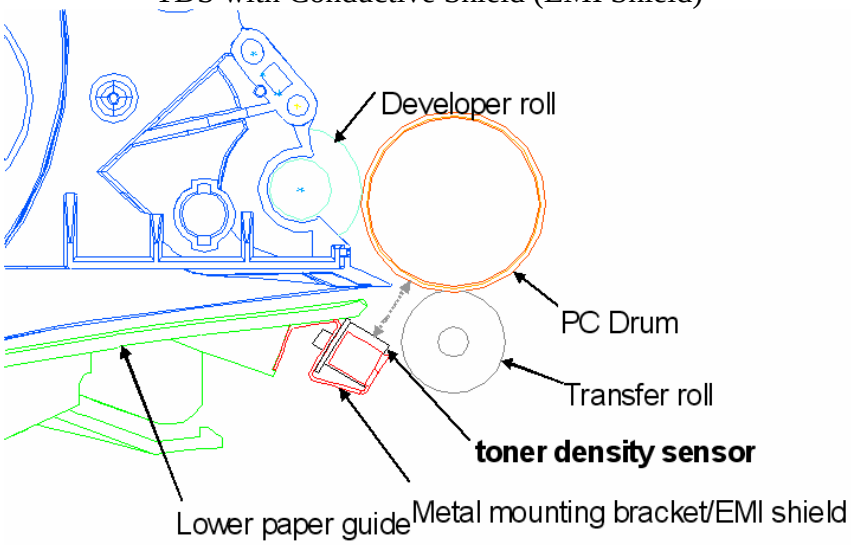

Figure 50 [63]. The TDS with the conductive EMI shield. The conductive shield was removed since arcing occurred between the transfer roll and the sensor.

The conductive shield blocked EMI from the sensor; however, arcing occurred again when the transfer roll was POR. It was then decided to make changes to the sensor circuit design to greatly reduce the noise. The design change required a new TDS PCB. Observing the FFT (displayed in figure 28 chapter 5 section 2), the frequencies needing the most filtering were displayed in table 1. However, once the sensor circuit from figure 43 (chapter 5 section 5) was implemented, the circuit's response time did not meet specifications. Therefore, to verify the concentration of noise to mitigate EMI and maintain a settling time <10ms, capacitor (C_3) was removed. Capacitor (C_4) mitigated most of the noise shown in figure 27 (chapter 5 section 2); however, ~700mV of noise was still present (displayed in figure 50). A simple first-order filter did not mitigate the noise experienced by the TDS. After this investigation, it became obvious for the need for a second-order Butterworth filter (as recommended by Matlab).

Sensor Output Noise Variation of V_{REF}

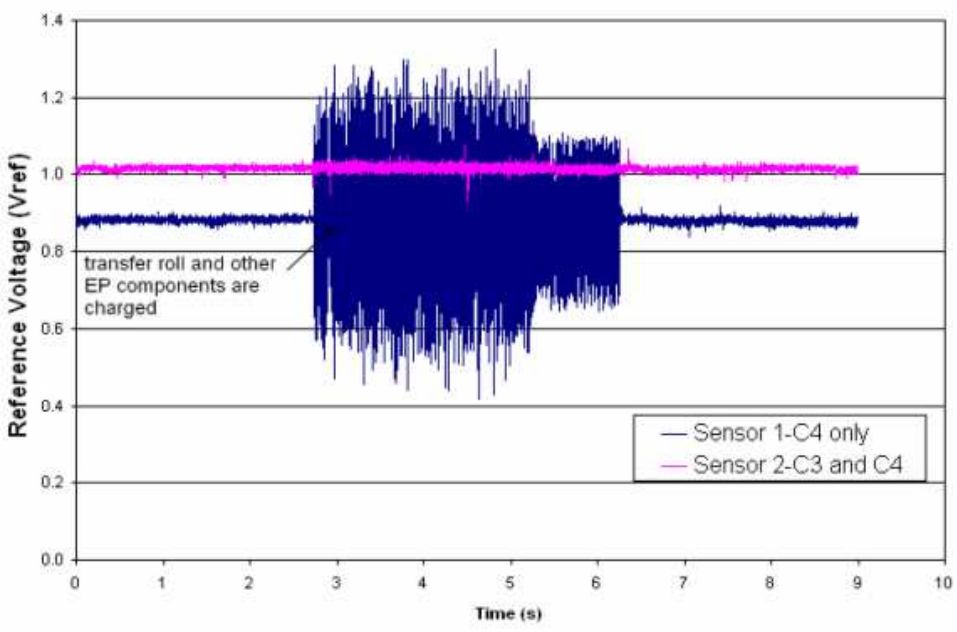

Figure 51. Sensor output noise variation of V_{REF}. The noise amplitude was greatly reduced by capacitor C_4; however, a considerable amount of noise continued to exist. The addition of C_3 reduced the noise for accurate output filtering.

The noise was existent without C_3. EMI was mitigated with C_3 included; however, the response was slower. Therefore, an additional resistor of 1kΩ (R_9) was added to the sensor PCB circuit (as displayed in figure 52) and the capacitor was reduced to 1µF as it was found that the sensor response improved with this value. R_6 was changed from 140kΩ to 137kΩ.

The Finalized TDS PCB Circuit Design

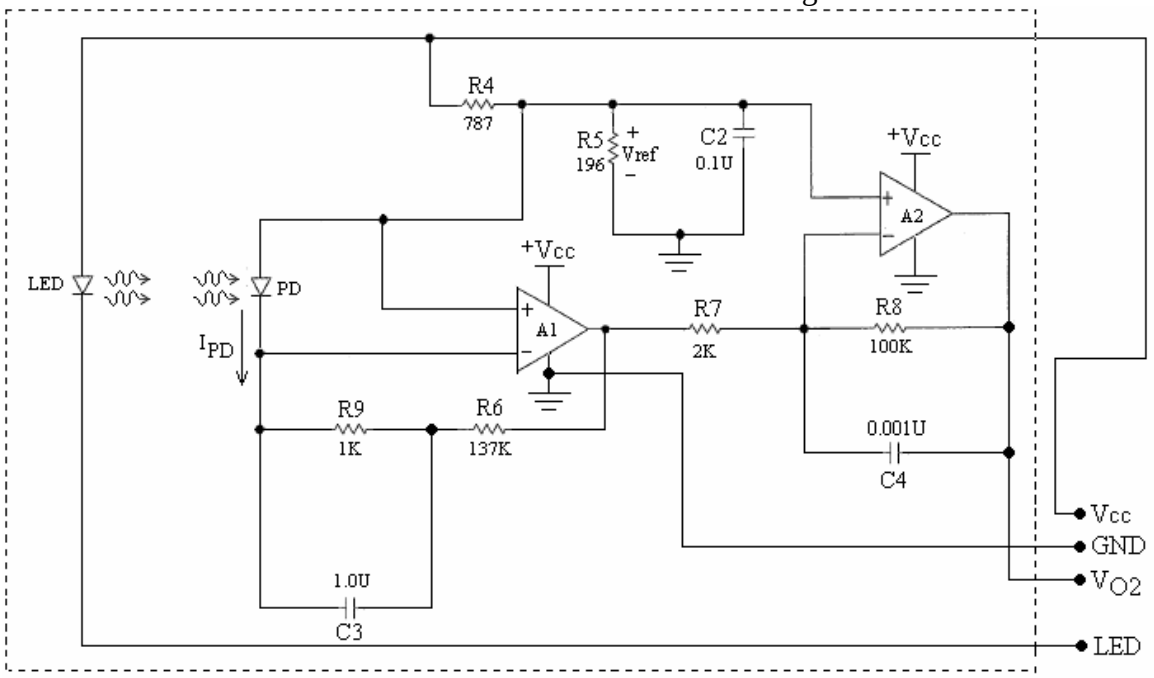

Figure 52. The modified TDS PCB circuit design. The original circuit design was modified with two additional capacitors and one resistor.

The circuit design change kept the noise amplitude down to under 50mV! Appendix B details the calculations to develop the filtered sensor PCB circuit.

The sensor layout was completed in Mentor Graphics and re-sent to the local PCB company for fabrication (figure 49d). After filtering modifications were completed with the sensor PCB, testing was repeated.

To address the sensor getting contaminated with paper dust and toner, a wiper

mechanism was designed to sweep the optical window of the TDS for accurate detection of IR light. The final equation for V_{O2} was derived to be:

$$V_{O2} = V_{REF} + I_{PD} * \frac{R_6 R_8 R_9 C_3 s + (R_6 R_8 + R_8 R_9)}{R_7 R_8 R_9 C_3 C_4 s^2 + (R_7 R_8 C_4 s + R_7 R_9 C_3) s + R_7} \quad \text{Eq. 51}$$

When there is no photodiode current (I_{PD}), there is no light detection (i.e. I_{LED} = 0). The PWM input signal is equal to zero and V_{O2} is equal to the reference voltage (V_{REF}). As long as V_{CC} = 5V DC is supplied to the sensor, the sensor will provide a ~1V output. If V_{CC} is zero, obviously, V_{O2} is also equal to zero. The Matlab results for the step response and Bode plot are displayed in figures 53 and 54.

Step Response of the Finalized TDS PCB Circuit

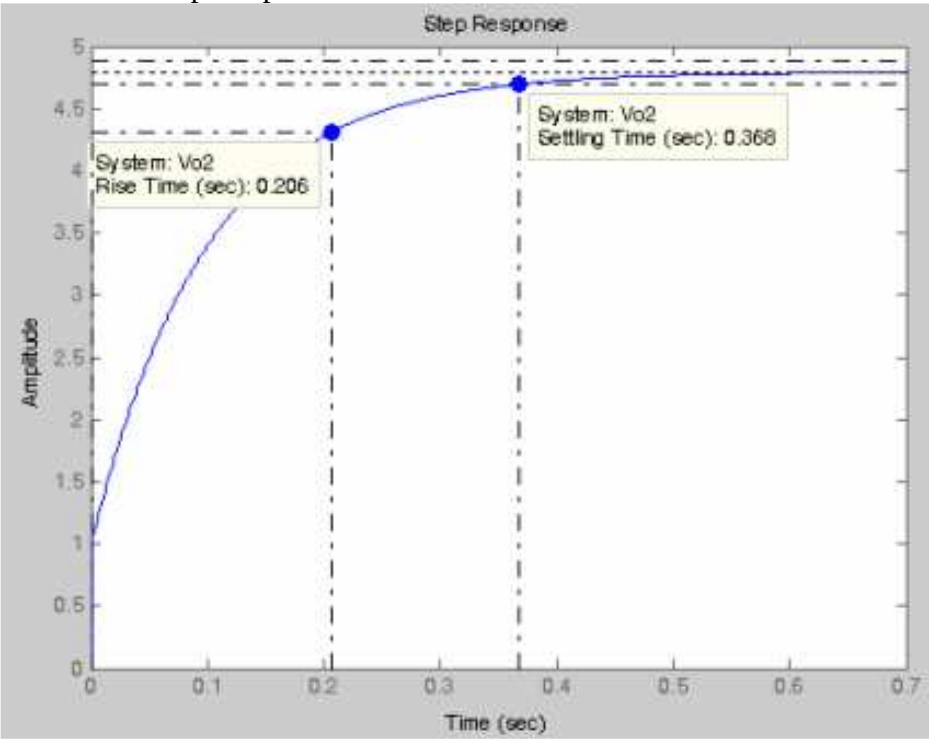

Figure 53. The modified sensor circuit step response. The rise time and settling time are within 2ms and 5ms respectively.

The circuit shows favorable results once changing the sensor design. The response time characteristics are within specifications. The Bode plot of the sensor PCB circuit is

displayed in figure 54.

Bode Plot of the Finalized TDS PCB Circuit

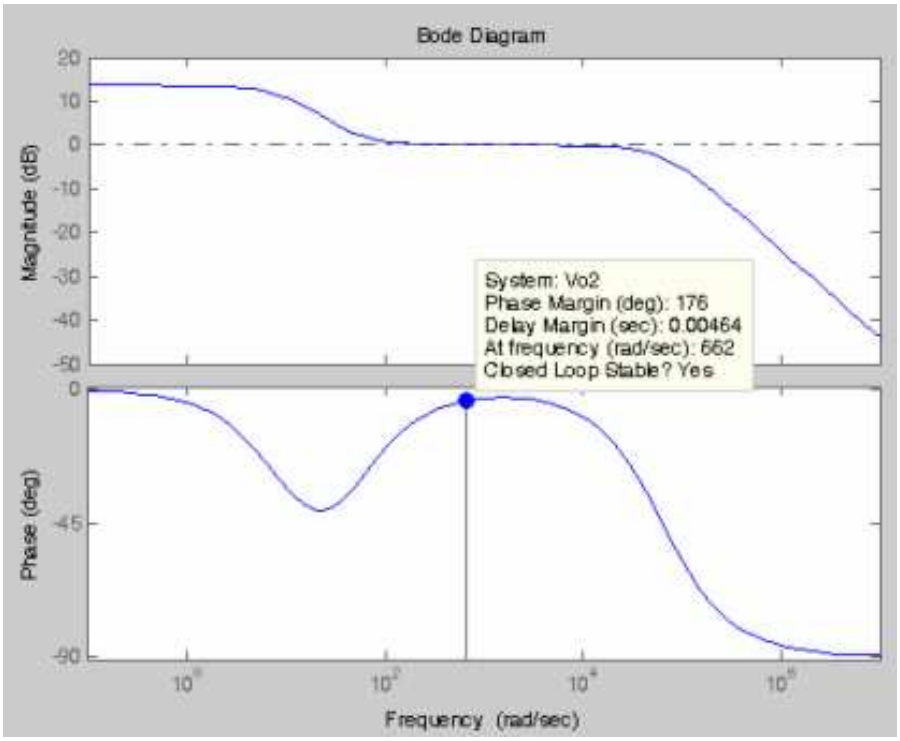

Figure 54. The Bode plot of the sensor circuit. The circuit is closed-loop stable.

The results show that the rise time and settling time are within specifications (2ms and 5ms respectively). Therefore, the goal of eliminating EMI while maintaining a fast response is achieved with the design displayed in figure 52. The circuit displayed in figure 55 is a graph of the TDS cycle used to adjust print darkness.

With the modified circuit, EMI is no longer noticeable and the TDS cycle occurs with success. Once the TDS cycle is complete (TDS calibration captured in figure 55), the algorithm utilizes the data to adjust the EP component parameters for adjustment of print darkness. Once the sensor demonstrated that it functioned effectively under nominal conditions, other conditions are applied to assess the sensor's function under various stress conditions.

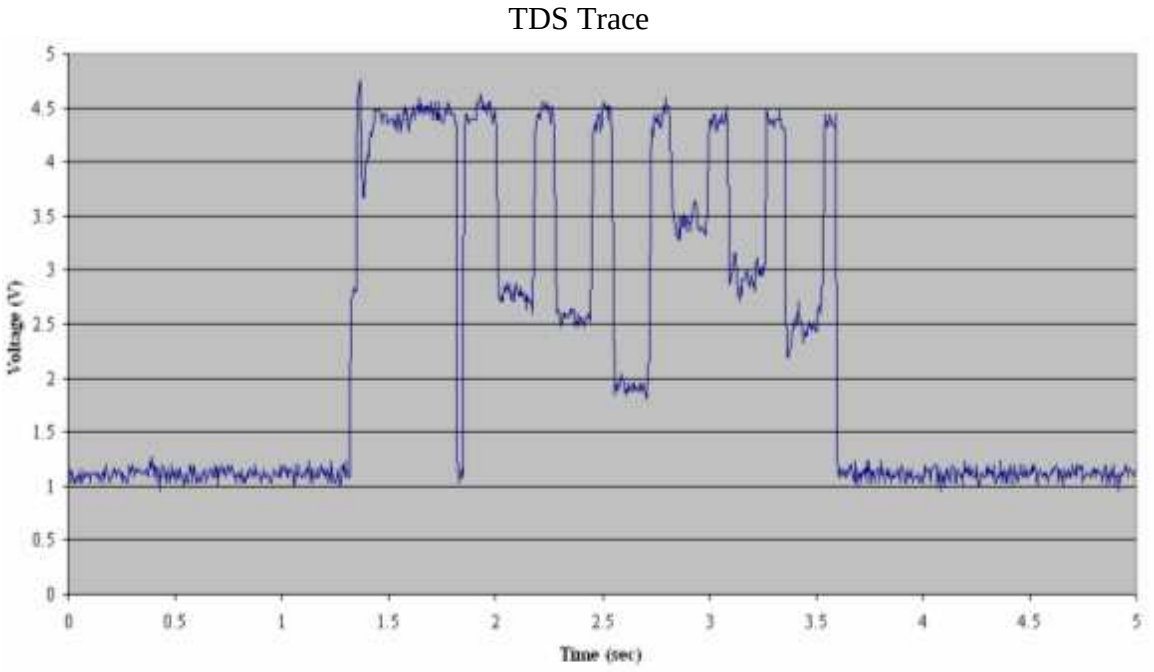

Figure 55. Trace of the TDS calibration cycle. The TDS calibration cycle with noise filtered by the finalized sensor circuit. The patches mentioned in chapter 4 are shown in the trace. The three patches (light, darker, and darkest are read from the PC drum twice in this graph. The lightest patch has the least of a voltage drop (@2sec and the darkest patch is read @2.5sec). The cycle lasts approximately 2.5s.

6.2.2. TDS Qualification Testing Summary

A variety of tests were performed to verify the TDS durability under various stress cases. Four characteristics were observed in qualification testing the TDS: the TDS output (V_{O2}) versus LED forward current (i_{LED}) linearity, the rise time and settling time, the TDS output change over life, and TDS failure during an ESD event. Test results confirm that the TDS is operational under these various stress cases. Since the original design, the maximum sensor output was finalized to 4.8±0.3V (instead of 4.3±0.7V). The minimum sensor output was finalized to 1.0±0.3V (instead of 1.0±0.7V). The change in minimum and maximum output voltages were simply based on tightened tolerances and actual resistor values available. In addition, the change allowed for an

increase in the maximum voltage based on op amp specifications (RRO op amp with <0.2V of the supply voltage 5.0V). The rise and fall times were maintained at 2ms and 5ms respectively. Using a test circuit (displayed in figure 56), the four tests were performed.

TDS Pulse Power Test Circuit

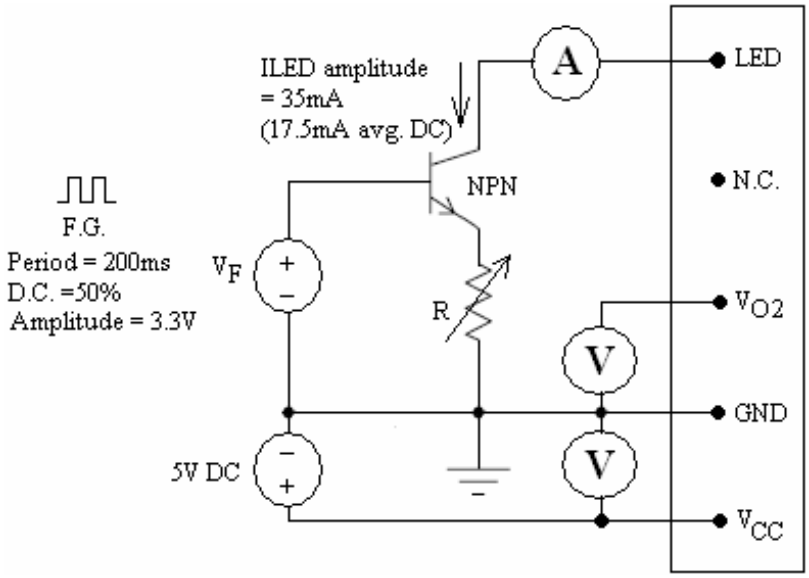

Figure 56. The TDS pulsed power test circuit. The circuit is utilized to capture pulsing TDS output voltage (V_{O2}) using an oscilloscope.

The circuit sends a square wave which pulses LED current. Both the power supply and function generator are on for at least ten minutes prior to taking measurements (to allow test equipment to reach steady state). The resistor is adjusted to generate LED forward current amplitude of 35mA. The NPN transistor is in active mode and thus the emitter current is approximately equal to the collector current. The current through the collector (I_{LED}) is a pulsing light source that is reflected by the PC drum and then detected by the photodiode to convert to a measurable pulsing output voltage (V_{O2}) of the same

frequency as the square wave input. V_{O2} is captured by an oscilloscope. Test results conclude that the sensor meets the specified limit of a rise time of 2ms and a settling time of 5ms nominally.

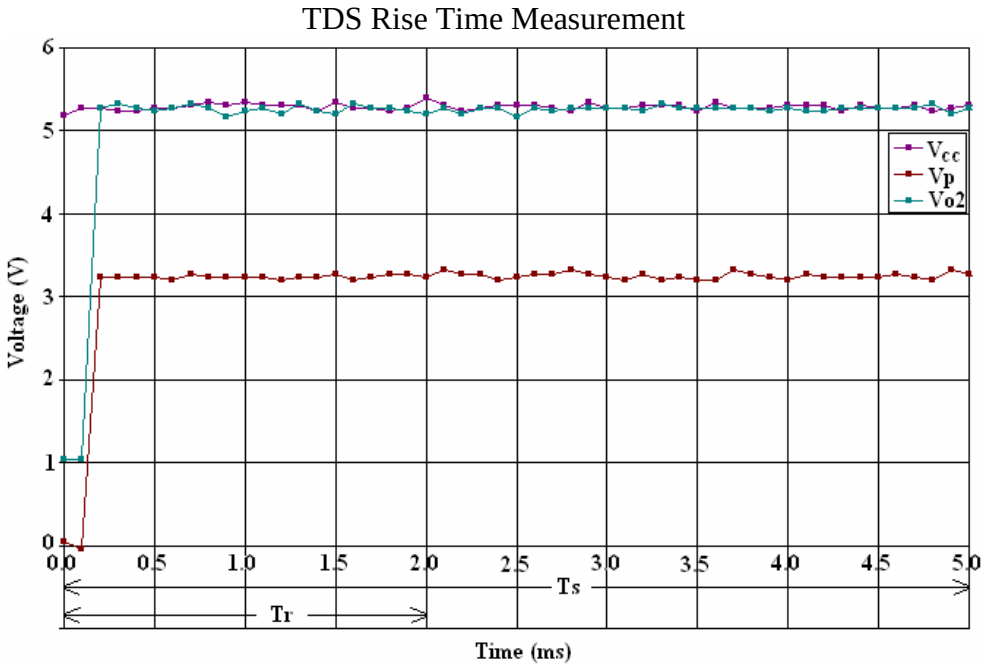

Figure 57. Measured rise time of the TDS. The TDS output (V_{O2}) rise time <2ms. The settling time is also within 5ms. Vp=Vpwm.

The TDS output displays the linear characteristic required to run the sensor effectively as theoretically specified in the Design chapter (chapter 5 section 5). The slope of a given sensor between 5mA and 15mA were compared. The equation utilized to determine a comparison for a slope within the margin of error for print darkness calibration is provided by the following:

$$Slope = \left(\frac{V_{O2\text{-}15} - V_{O2-5}}{15mA - 5mA} \right) \quad \text{Eq. 52}$$

$$Slope_1 = \left(\frac{V_{O2\text{-}10} - V_{O2-5}}{10mA - 5mA} \right) \quad \text{Eq. 53}$$

$$Slope_2 = \left(\frac{V_{O2\text{-}15} - V_{O2\text{-}10}}{15mA - 10mA} \right) \quad \text{Eq. 54}$$

The slopes are compared to determine the error. The TDS V_{O2} vs. I_{LED} slopes must not exceed the specified error of 0.05 (as stated in equations 55 and 56).

$$\Delta Slope_1 = \left| Slope - Slope_1 \right|, \quad \Delta Slope_1 \leq 0.05 \quad \text{Eq. 55}$$

$$\Delta Slope_2 = \left| Slope - Slope_2 \right|, \quad \Delta Slope_2 \leq 0.05 \quad \text{Eq. 56}$$

Printer calibration relies heavily on the TDS linear characteristic and thus, the linear relationship must be as close to linear as possible between 5mA and 15mA. Test results display that the sensor was greatly within the error specified.

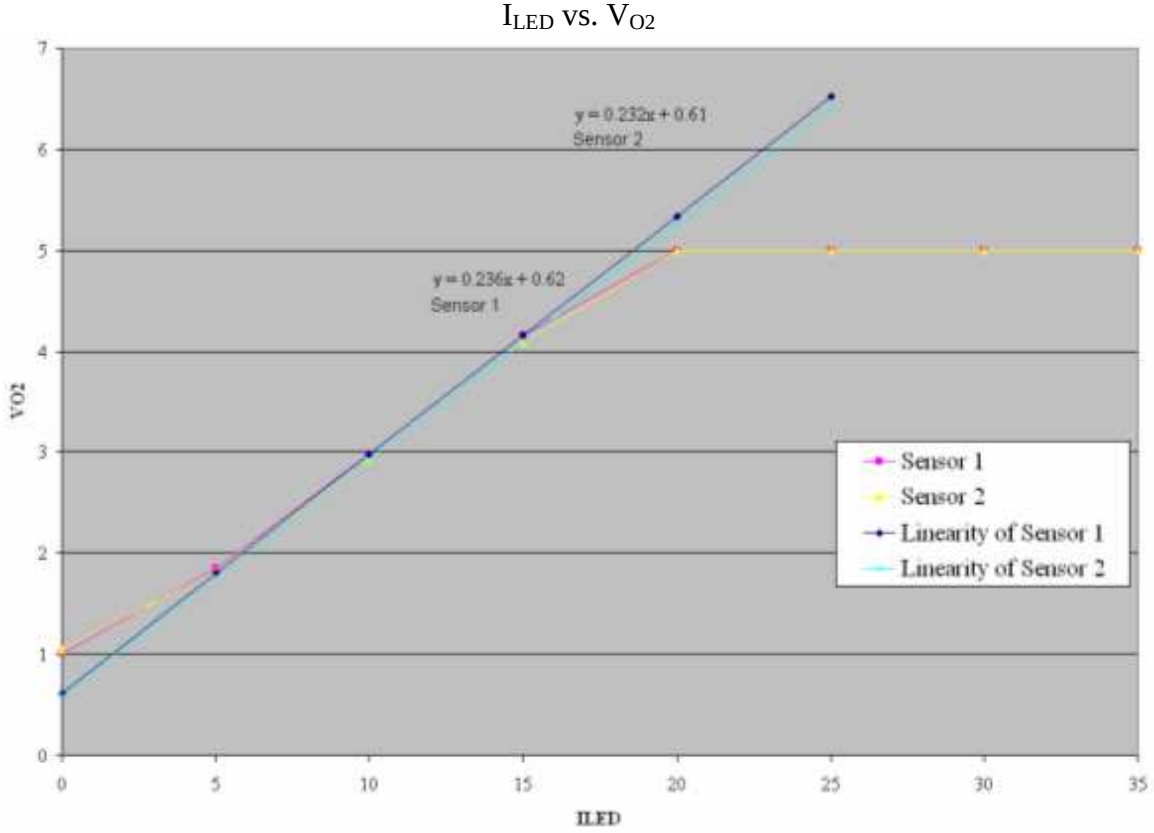

Figure 58. TDS I_{LED} vs. V_{O2}. TDS relationship between input current (i_{LED}) and output voltage (V_{O2}) measured.

All ten sensors ran >2 million times in the TDS life test (simulated by the pulsing test circuit) and maintained the specified output of 4.8V±0.3V without any occurrence of sensor failure or sensors falling out of spec. Therefore, the TDS is robust throughout the one million page yield printer (assuming a calibration for every page ran, which is the most extreme case). Lastly, the sensor works well under ESD (electrostatic discharge). The sensors were tested individually and in the printer during operation with voltages of 2kV, 4kV, 6kV and 8kV. For every voltage level, an ESD signal was pulsed every second 100 times and repeated. The sensors tested maintained successful operation and none of the sensors failed or resulted in poor operation. There were spikes of voltage in the sensor's output and it increased with ESD voltage level; however, these spikes can be flagged in code and does not affect the accuracy of the TDS while in operation.

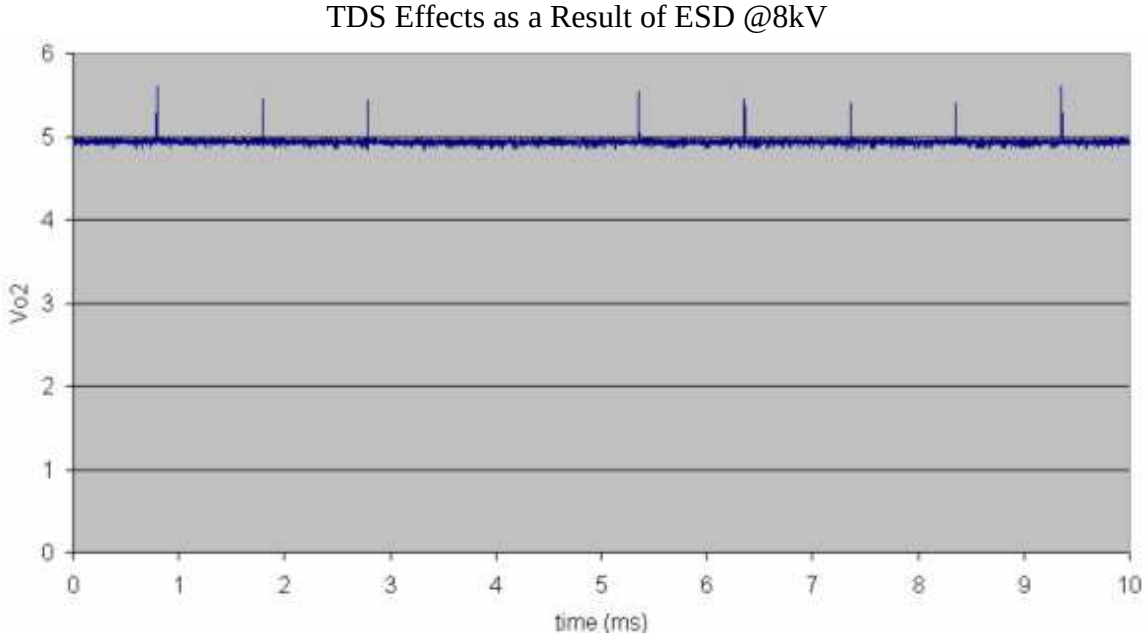

Figure 59. The TDS stressed to the maximum ESD test voltage of 8kV. The spikes can be filtered in code.

The last range of tests performed was to place the sensors in the printer for

environmental stress tests.

6.2.3. TDS Environmental Stress Testing

The TDS was tested under a variety of conditions to verify its performance through environmental stress cases during calibration as well as after being shipped or stored in extreme weather conditions. The sensor was placed in environments from 90°F and 45% relative humidity (RH) to 60°F and 8% RH. The sensor performed very well. However, when the sensor was in 90°F and 90% humidity, the sensor displayed a distorted output. When simply testing the reference voltage (V_{REF}) and maintaining V_{CC} =5V and V_{pwm} =0 (i.e. I_{PD}=0), V_{REF} displayed the output observed.

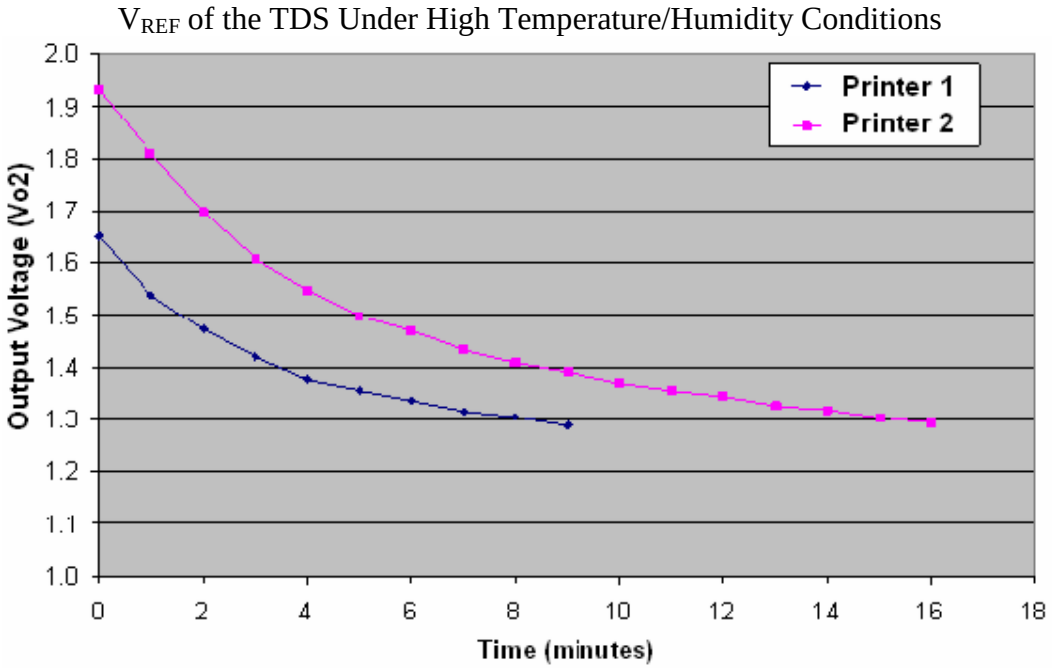

Figure 60. V_{REF} of the TDS under high temperature/humidity conditions. The baseline voltage is supposed to maintain a constant voltage of 0.8+/-0.3V; however, the sensor output changed over time. The characteristic shown is due to moisture around the sensor. As the printer ran (drying the air around the sensor), the sensor gradually dropped to its steady state voltage [86], [87].

In some of the data, the sensor took over 30 minutes to return to steady state! It was

discovered that the sensor is very sensitive to extreme weather environments. Considering that there are consumers that live in these extremely humid environments (in locations such as Southeast Asia), a solution had to be determined.

It was found that the electronic components on the printed circuit board (PCB) were very susceptible to error under humid environments. Moisture is getting unto the PCB causing these distorted results. The solution was to apply a sealant to the TDS PCB. The sealant is designed to keep out moisture under extreme environments which (as a result) became a great, cost-effective solution. After the addition of the sealant, V_{REF} displayed a normal steady DC voltage.

V_{REF} of the TDS Under High Temperature and Humidity Conditions with Moisture Sealant Applied to the PCB

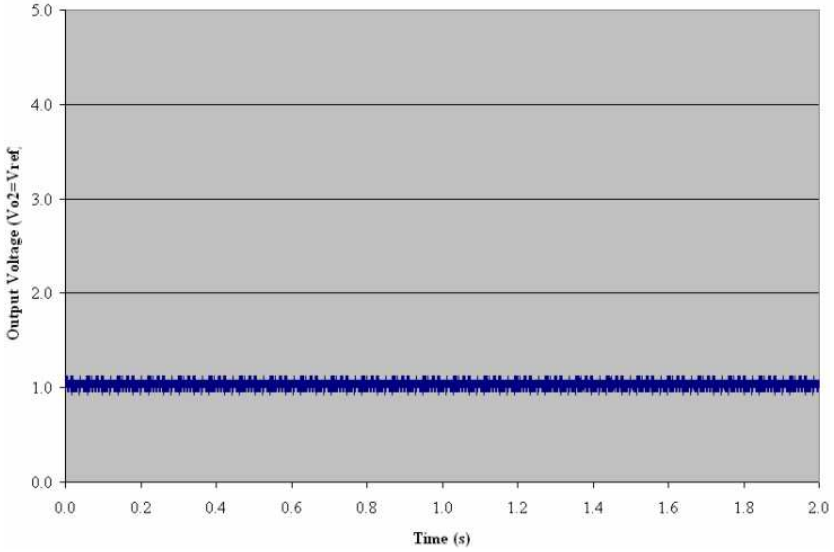

Figure 61. V_{REF} of the TDS under high temperature and humidity conditions with moisture sealant applied to the PCB. The baseline voltage maintains a constant voltage of 0.8+/-0.3V once applying the moisture sealant.

The sealant coats all of the electronic components of the sensor and now the sensor functions properly under more extreme weather conditions.

6.3 TDS Print Darkness Variation Testing

After the TDS passed a variety of tests for proper function and displayed favorable results when tested under various extreme environments conditions, the sensor was finally put to the test in the printer (Lexmark T652) again for print darkness variation comparison. The newly developed Lexmark T652 cartridge was ran through life for print darkness variation and was compared to the previous generation Lexmark T641 cartridge and the HP 4250 (competitor printer) cartridge. Three printers for each model were tested with three cartridges per printer (equaling nine cartridges per printer model). The following results are displayed in figure 62. Print darkness variation samples between the Lexmark T641 (figures 22 and 24 from chapter 5 section 1) and the T652 were compared (figures 63 and 64) to the nominal print sample (figure 23 chapter 5 section 1). Figures 22-25 are displayed with Figures 63 and 64 for comparison.

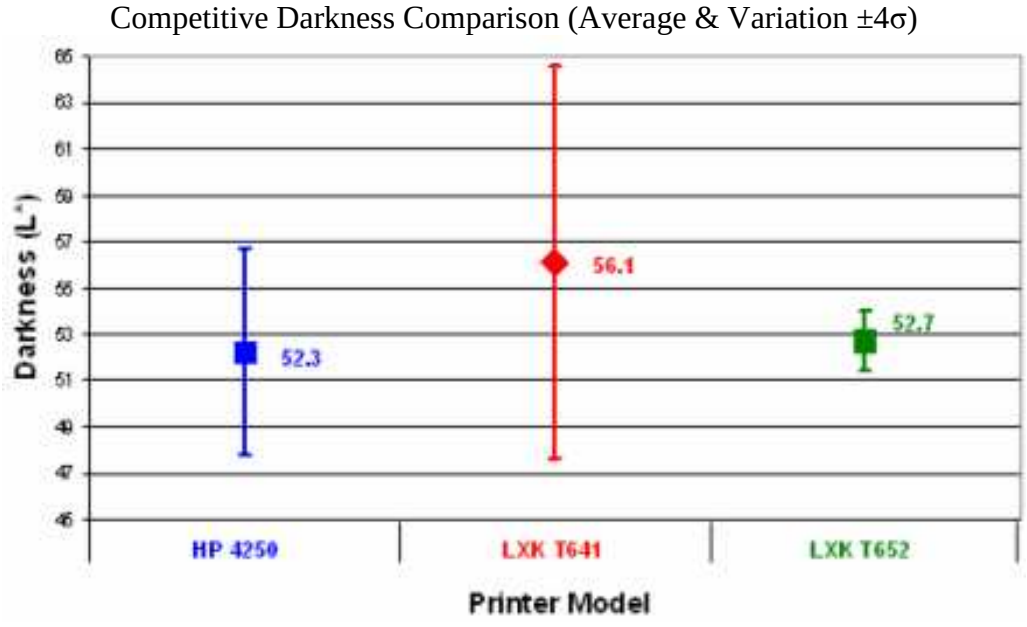

Figure 62 [63]. Competitive darkness comparison between printer cartridge models. The TDS was implemented in the Lexmark E series though tested in the Lexmark T series printer. Notice the reduction in print darkness!

The print darkness variation was over ±8L* in the previous generation printer. The HP 4250, has a print darkness variation of ±4L*. The print darkness variation with the toner density sensor in the new Lexmark T652 is now less than ±2L* over the life of a cartridge! The goal of reducing print darkness variation to <±5L* was achieved. The sensor was finally implemented in the new low-end Lexmark E series printer.

Lightest Sample of Print Darkness for the Previous Generation Printer

Figure 22 [63]. The lightest sample of print darkness for the previous generation printer. The TDS was not implemented in the printer used to produce this print sample. (Print defects may appear as a result of scanning the original print sample into this document for display.)

Darkest Sample of Print Darkness for the Previous Generation Printer

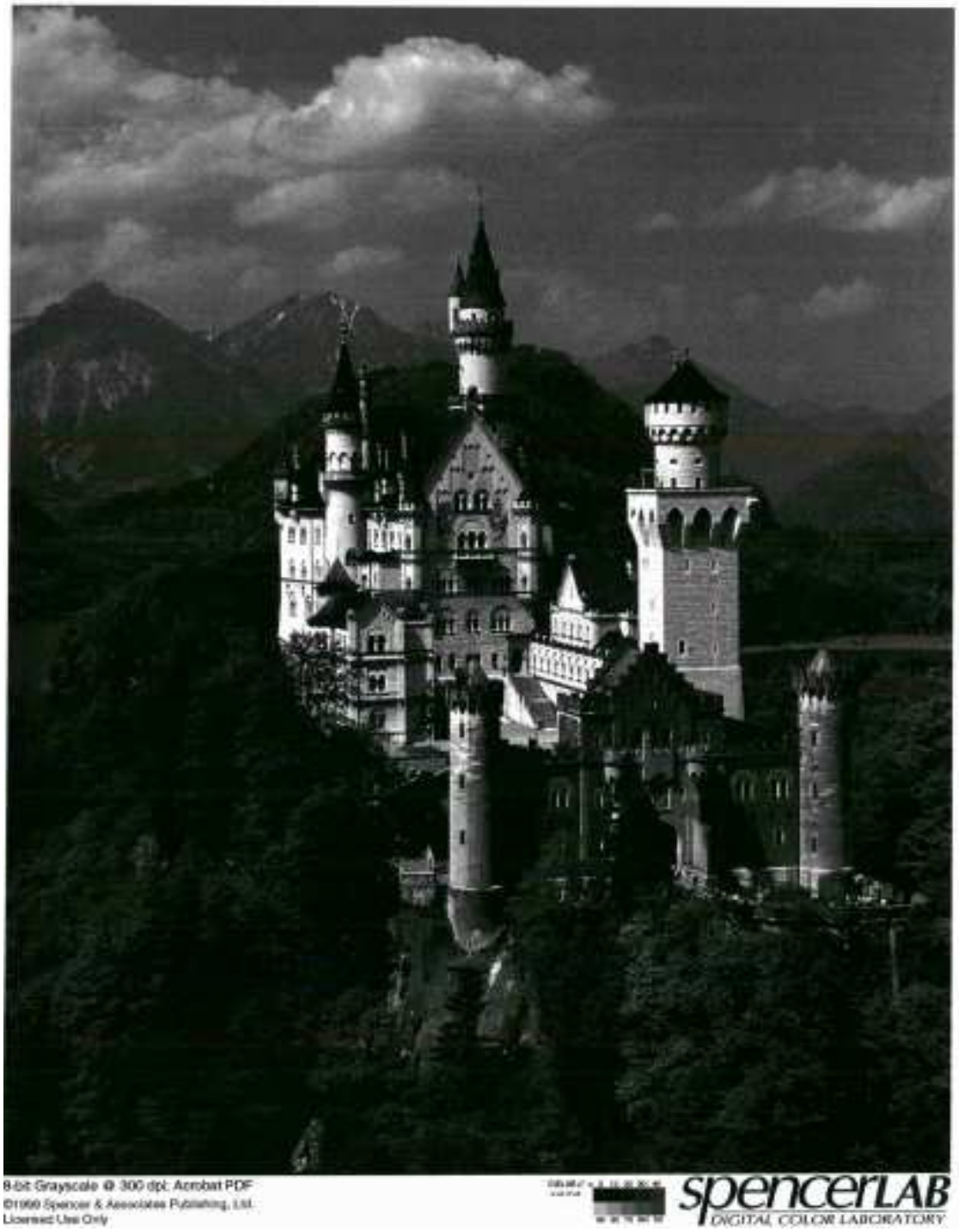

Figure 24 [63]. The darkest sample of print darkness for the previous generation printer. The TDS was not implemented in the printer used to produce this print sample. (Print defects may appear as a result of scanning the original print sample into this document for display.)

Print Darkness of a Nominal Print Sample

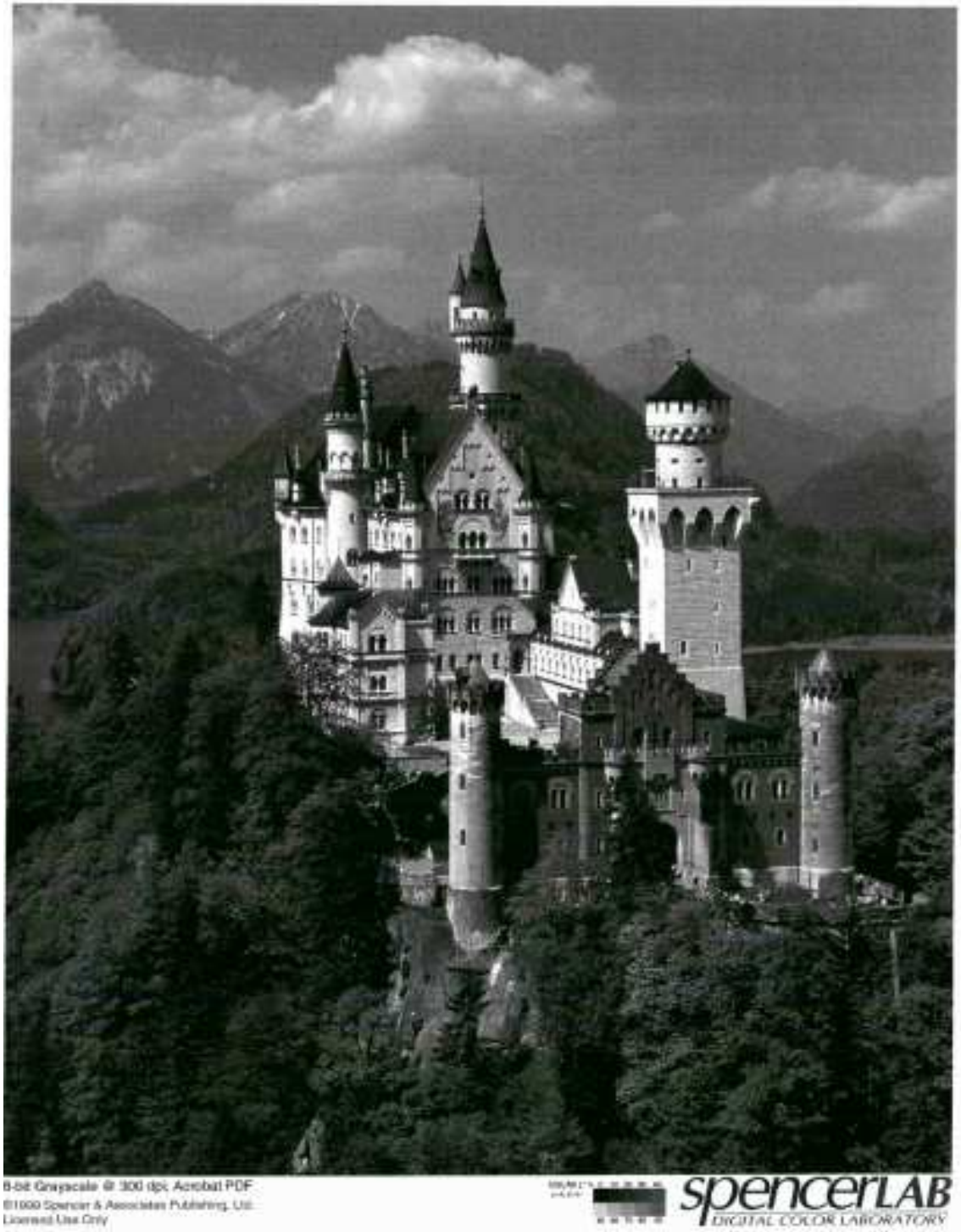

Figure 23 [63]. Print darkness of a nominal print sample. The nominal print sample is utilized to compare dark and light samples. (Print defects may appear as a result of scanning the original print sample into this document for display.)

Lightest Sample of Print Darkness for the Current Generation Printer

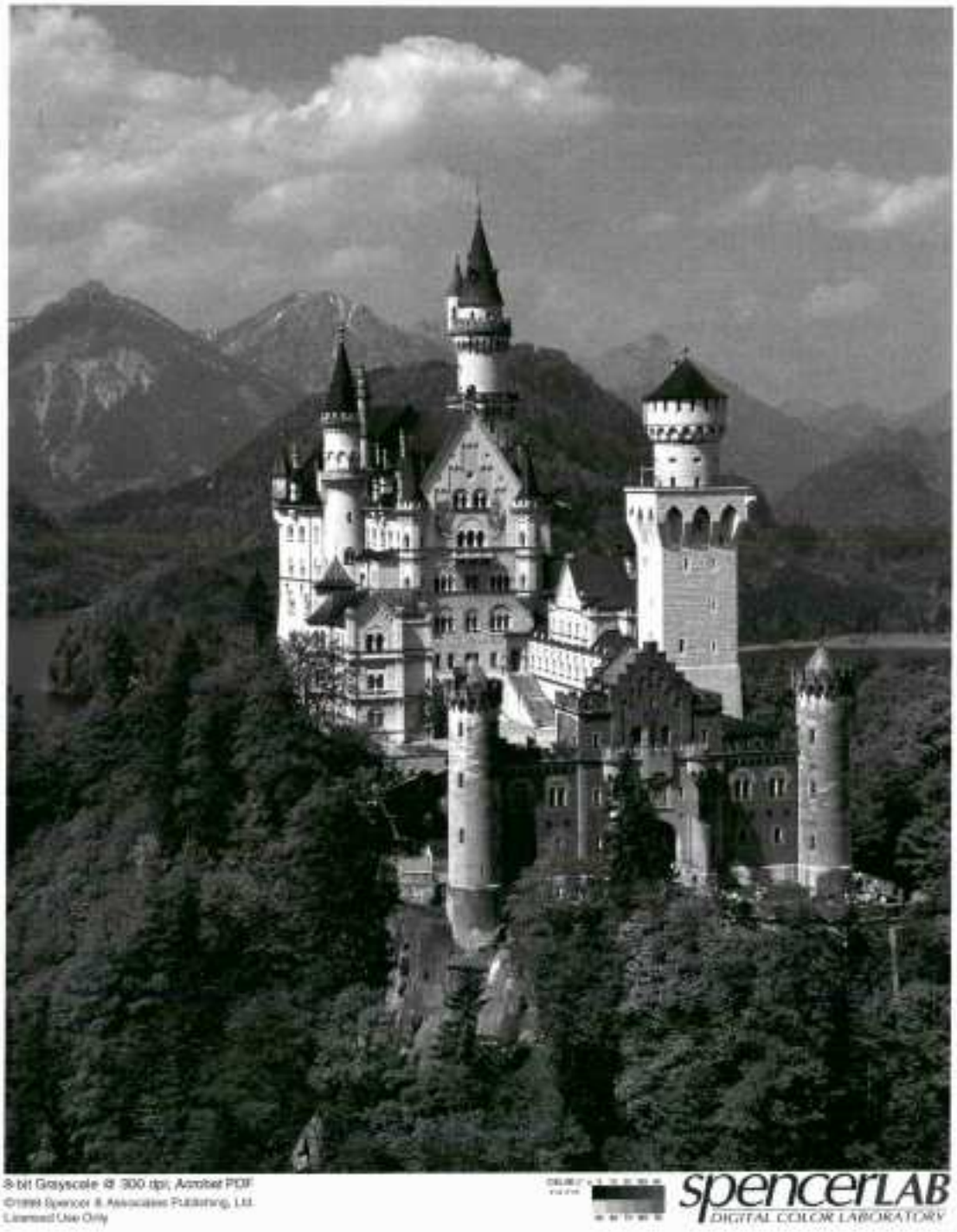

Figure 63 [63]. The lightest sample of print darkness for the current generation printer. The TDS was implemented in the printer used to produce this print sample. (Print defects may appear as a result of scanning the original print sample into this document for display.)

Darkest Sample of Print Darkness for the Current Generation Printer

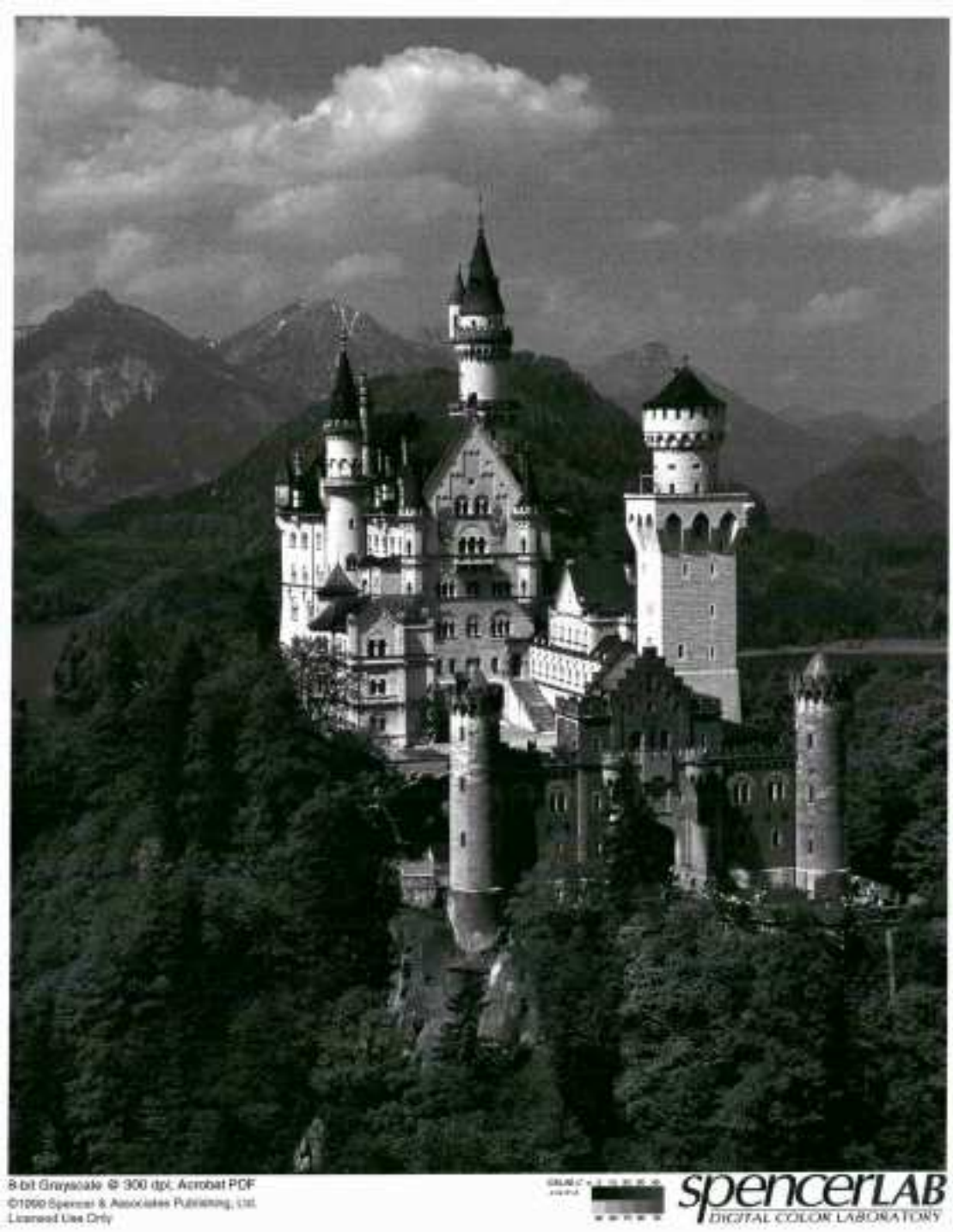

Figure 64 [63]. The darkest sample of print darkness for the current generation printer. The TDS was implemented in the printer used to produce this print sample. (Print defects may appear as a result of scanning the original print sample into this document for display.)

CHAPTER 7: ASSESSMENT

The toner density sensor design greatly improved print quality. The main focus of the research was to reduce print darkness variation and to mitigate EMI experienced by the TDS. Print darkness variation decreased by more than half! Certainly, there were some problems during the implementation of the sensor in the printer. The EMI issue was one of the main problems. The second order Butterworth filter design (suggested by Matlab) for the TDS PCB circuit implemented by a series of two active low pass filters (mentioned in chapter 6.2.1) greatly reduced the EMI experienced by the sensor to a negligible measure (<50mV). The circuit analysis made selecting resistor and capacitor values fairly easy to choose. The closed-loop system for all the circuits required to run the sensor (i.e. the LED Driver circuit, the Sensor PCB circuit and the A/D Interface circuit) are stable and displayed rise and settling times within specifications.

An implementation issue that also occurred was inaccurate data captured by the TDS due to moisture in the environment. The problem was difficult to diagnose since the sensor functioned properly when tested in controlled warm temperature (~78°F) and high percent relative humidity (~80%). The addition of the sealant required retesting of the TDS under the variety of tests mentioned in chapter 6 (i.e. TDS environmental tests, TDS life test, and ESD test) to verify the sealant's strength under varying conditions. After the addition of the sealant, test results continued to display very favorable results.

The TDS works well in the EP system; however, it is unsure how much print

darkness variation is contributed by fusing. The TDS is utilized before the fusing process; therefore, print variation can possibly be improved if additional sensing was placed after the fusing process. The other concern is that the TDS was implemented on only one side of the PC drum. PC drum is not entirely uniform. The PC drum may cause erroneous data if it is damaged or very rough in the area of the TDS reflective window (w.r.t. to the rest of the PC drum).

Halftoned samples are showing excellent results with the TDS (figures 63 and 64). It has also been proven that the TDS works well with error diffused samples as well [63]. Since the normalized TDS output is utilized to measure print darkness of toner on the PC drum prior to transferring to media (without the use of look-up tables), future algorithm adjustments become much easier. With the assumption of a normal PC drum, the TDS captures accurate real-time data in a vast range of environmental conditions, ESD conditions, and EMI conditions.

Overall, the toner density sensor greatly improved print quality by reducing print darkness variation. The sensor is a great asset to the printing system and has since its implementation, established its place as a great prink darkness calibration tool for future generation printers.

CHAPTER 8: CONCLUSION/FUTURE WORK

The newly designed toner density sensor has demonstrated that it is a great device for application in reducing print darkness over the life of a cartridge. L* variation was reduced by 75% with the TDS implementation (from ±8L* to <±2L)! The second goal of the TDS is to reduce EMI affecting the TDS output signal once implemented. The new design has successfully performed this task and the sensor provides a fast response unnoticed by the user. Cartridge-to-cartridge variation is greatly reduced with a normalized TDS calibration algorithm. If a part is changed within a given cartridge, toner size change over the life of a given cartridge, or media type changes, print darkness is still accurately captured since the TDS captures real-time data. Environmental (or ship/store weather) conditions, and ESD doesn't significantly affect the sensor's performance. The toner density sensor has established itself for future printer generations to come.

There are some noticeable areas where print quality can potentially be improved. The TDS only measures reflectance on one small portion of the width of the PC drum and not the whole length of the drum. It is unknown if PC drum is uniform-enough to not affect the actual print darkness calibration scheme. Future investigations of PC drum uniformity and its relationship with TDS output will be reviewed. In addition, the fuser's affect on print darkness variation has not been observed. A future investigation of print darkness variation regarding the fuser is also considered for future investigation.

Some other future work may include the application of neural networks and pattern recognition in conjunction with the TDS for printer calibration [88], [89], [90] or calibrating multiple halftones in a MFP printer [91]. This is considering that EMI issues will continue to persist as print process speeds change with each printer generation. With any of these methods, the TDS can significantly compliment these processes as it is a great asset to current printer calibration processes and sub-processes.

REFERENCES

[1] http://www.cie.co.at/index_ie.html

[2] http://www.digibarn.com/collections/printers/xerox-9700/index.html

[3] http://thelongestlistofthelongeststuffatthelongestdomainnameatlonglast.com/first362.html

[4] G. Starkweather, “Electronic Color-Printer Technologies”, Color Research and Application, vol. 11, 1986, pp. 73-74.

[5] R. Shaffert, Electrophotography, Focal Press Limited, London, 1969, pp. 1-376.

[6] C. Elzinga, T. Hallmark, R. Mattern, J. Woodward, “Laser Electrophotographic Printing Technology”, IBM Journal of Research Development, vol. 25, no. 5, September 1981, pp. 767-773.

[7] L. Schein, “Ben Franklin and Electrophotography”, Journal of Vac. Science and Technology, vol. 25, no. 4, July-August 2007, pp. 1256-1260.

[8] S. Otsuka, “Technology Trends in Materials for Electrophotography”, Proc. Of SPIE, vol. 1670, 1992, pp. 128-137.

[9] A. Tam, R. Balanson, “Lasers in Electrophotography”, IBM Journal of Research Development, vol. 26, No. 2, March 1982, pp. 186-197.

[10] A. R. Melnyk, D. M. Pai, “Organic Photoreceptors: An Overview”, SPIE vol. 1253 Hard Copy and Printing Materials, Media, and Process, 1990, pp. 141-154.

[11] K. Takagi, “Analysis of Imaging Density Degradation by Dynamics of Toner Charging and Mass Transfer in the Toner Development Process”, Journal of Imaging Science and Technology”, vol. 49, no.2 , March-April 2005, pp. 196-203.

[12] A. R. Meinyk, D. M. Pai, “Organic Photoreceptors: An Overview”, Proc. Of SPIE, vol. 1253, 1990, pp. 141-154.

[13] M. Lee, J. Ayala, B. Grant, W. Imaino, A. Jaffe, M. Latta, S. Ricke, “Technology Trends in Electrophotography”, IBM Journal of Research Development, vol. 28, no. 3, May 1984, pp. 241-251.

[14] D. Kacker, “Electrophotographic Process Embedded in Direct Binary Search”, IEEE Transactions on Image Processing, vol. 11, no. 3, March 2002, pp. 243-257.

[15] Y. Hoshino, T. Tanaka, M. Omodani, "Electrophotographic Color Printer", Review of the Electrical Communications Library, vol.35 no. 4, 1987, pp. 421-426.

[16] M. Wu, D. Huang, J. Horng, "Tribo-Charge and Particle Size Characteristics of Toners in a Laser Printer", Proc. Of SPIE, vol. 1670, 1992, pp. 146-152.

[17] J.H. Anderson, "Humidity Dependence of Tribocharging of Toner Surface Treated with Hydrophobic and Hydrophylic Silica", Journal of Dispersion Science and Technology, 2004, vol. 25, No. 4, pp. 435-437.

[18] P. Ding, A. W. Pacek, K. Abinhava, S. Pickard, M. R. Edwards, A. W. Nienow, "A Process for the Manufacture of Chemically Produced Toner (CPT). Evolution of Structure and Rheology" Industrial and Engineering Chemical Research Journal, 2005, vol. 44, No. 16, pp. 6004-6011.

[19] R. Ulichney, "Digital Halftoning", The MIT Press, Cambridge Massachusetts, 1987 pp. 1-319.

[20] R. Ulichney, "A Review of Halftoning Techniques", SPIE Conference on Color Imaging: Device-Independent Color, Color Hardcopy, and Graphic Arts, V, San Jose California, January 2000, SPIE vol. 3963, pp. 378-391.

[21] M. Mese, P. Vaidyanathan, "Look-Up Table (LUT) Method for Inverse Halftoning", IEEE Transactions on Image Processing, vol. 10, no. 10 October 2001, pp. 1566-1578.

[22] G. Goertzel, G. Thompson, "Digital Halftoning on the IBM 4250 Printer", IBM Journal of Research Development, vol. 31, No.1, January 1987, pp. 2-15.

[23] T. Pappas, D. Neuhoff, "Printer Models and Error Diffusion", IEEE Transactions on Image Processing, vol. 4, No. 1, January 1995, pp. 66-80.

[24] L. Schaaf, William Henry Fox Talbot, Phaidon Press, London, 2008, pp. 1-15.

[25] D. Lau, G. Arce, Modern Digital Halftoning, 2nd Edition, Marcel Dekker, New York, 2001, pp. 1-25.

[26] S. Graham, "Comparison of Selected Digital Halftoning Techniques", Microprocessors and Microsystems, vol. 15, no. 5, June 1991, pp. 249-255.

[27] S. Wang, "Algorithm-Independent Color Calibration for Digital Halftoning", The Fourth IS&T/SID Color Imaging Conference: Color Science, Systems and Applications, 1996, pp. 75-77.

[28] Anon, “Improved Halftoning Based on Error Diffusion”, Research Disclosure, 2006, pp. 547-548.

[29] G. Sharma, “Digital Color Imaging Handbook”, CRC Press LLC, 2003, pp. 1-41, 271-312.

[30] http://www.hunterlab.com/appnotes/an07_96a.pdf

[31] R. Bala, V. Monga, G. Sharma, J. Van de Capelle, “Two-Dimensional Transforms for Device Color Calibration, Processing of SPIE: Color Imaging: Processing, Hard Copy and Applications IX, vol. 5293, San Jose, 19-22, Jan 2004, pp. 250-261.

[32] http://en.wikipedia.org/wiki/Lab_color_space

[33] G. Starkweather, “Metrication for Color Imaging Devices”, Proc. Of SPIE, vol. 3648, January 1999, pp. 142-147.

[34] S. Wang, “Feedback for Printer Color Calibration”, International Conference on Digital Printing Technologies, Conference on Digital Printing Technologies,1999, pp. 327-330.

[35] K. Knox, C. Hains, and G. Sharma, “Halftone-Independent Calibration of Black and White Printers”, SPIE, vol. 2657, 1996, pp. 432-436.

[36] H. Kang, P. Anderson, “Neural Networks Applications to the Color Scanner and Printer Calibrations,” Journal of Electronic Imaging, vol.1, April 1992, pp. 125-135.

[37] Y. Wu, “Printer Color Calibration Using an Embedded Sensor”, Color Imaging XII: Processing, Hardcopy, and Applications, Proc. Of SPIE-IS&T Electronic Imaging, SPIE vol. 6493, 2007.

[38] Y. Wu, “Combine 1-D and 3-D Color Calibration Methods for Ensuring Consistent Color Reproduction”, Proc. Of SPIE-IS&T Electronic Imaging, vol. 5293, 2004, pp. 242-249.

[39] P. Graf, W. Von Tluck, “Sensors in Lasers Printers”, Sensors and Actuators, vol. 3, 1982-1983, pp. 41-50.

[40] http://www.oce.com/se/About/Technologies/Technologymilestones.htm

[41] R. W. Pries, “The Toner Patch Sensor”, IBM Technical Disclosure Bulletin, vol. 26, no. 4, 1983, pp. 1910-1911.

[42] Y. Takeda, “Sensing and Process Control System for Color MFP”, 2004 International Conference on Digital Printing Technologies.

[43] H. Ren, L. Stauffer, S. Rodriguez, T. Ives, “Investigation of the Behavior of Optical Based Toner-Level Sensing”, 21st International Conference on Digital Printing Technologies Final Program and Proceedings, Society for Imaging Science and Technology, 2005, pp. 169-172.

[44] Anon, “Paper-Position Sensor”, IBM Technical Disclosure Bulletin, vol. 28, no. 4, 1985, p. 1681.

[45] W. Goff, J. Rakes, “Paper Sensor”, IBM Technical Disclosure Bulletin, vol. 25, n. 11a, April 1983, p. 5600.

[46] J. Mc Kenney, J. van den Berg, “Printer Paper Top of Form and End of Form Sensor”, IBM Technical Disclosure Bulletin, vol. 27, n. 4b, September 1984, pp. 2535-2538.

[47] F. Yam, Z. Hassan, “Innovative Advances in LED Technology”, Microelectronics Journal, vol. 36, 2005, pp. 129-137.

[48] D. Halliday, R. Resnick, J. Walker, Fundamentals of Physics, 4th Edition, John Wiley and Sons, Toronto, 1993, pp. 1210-1225.

[49] S. Matsik, M. Rinzan, D. Esaev, A. Perera, “Effect of Doped Substrate on GaAs-AlGaAs Interfacial Work function IR Detector Response Through Cavity Effect”, IEEE Transactions on Electron Device, vol. 52, no. 3, March 2005, pp. 413-418.

[50] A. Yariv, Optical Electronics in Modern Communications, 5th Edition, Oxford University Press, New York, 1997, pp. 570-578.

[51] http://nptel.iitm.ac.in/courses/Webcourse-contents/IIT-Delhi/Semiconductor%20Devices/LMB2A/2a.htm

[52] C. Pollock, Fundamentals of Optoelectronics, Richard D. Irwin, Inc., Chicago, 1995, pp. 463-490.

[53] H. Kressel, J. K. Butler, Semiconductor Lasers and Heterojunction LEDs, Academic Press, New York 1977.

[54] H. C. Casey, M. B. Panish, Heterostructure Lasers, Academic Press, New York, 1978.

[55] R. D. Dupois, P. D. Dapkus, “Room-temperature operation of $Ga_{(1-x)}Al_xAs/GaAs$ Double-Heterostructure Lasers Grown by Metalorganic Chemical Vapor Deposition”, Applied Physics Letters, vol. 31, no. 7, 1977, p. 466.

[56] G. Stringfellow, Organometallic Vapor-Phase Epitaxy: Theory and Practice, 2nd Edition, Academic Press, San Diego, 1999.

[57] A. Rogalski, "Infrared Detectors: An Overview", Infrared Photonics and Technology", vol. 43, 2002, pp. 187-210.

[58] R. Emmons, S. Hawkins, K. Cuff, "Infrared Detectors: An Overview", Optical Engineering, Jan-Feb 1975, vol. 14, no. 1, pp. 21-30.

[59] H. Norton, Sensors and Analyzers Handbook, Prentice Hall, Inc, New Jersey, 1982, pp. 397-426.

[60] P.K. Gurram, S. A. Dianat, "Comparison of 1-D, 2-D, and 3-D Printer Calibration Algorithms with Printer Drift", Society for Imaging Science Technology 21st International Conference on Digital Printing Technologies Final Program and Proceedings, 2005, pp. 505-510.

[61] S. Hullfish, J. Fowler, Color Correction for Digital Video: Using Desktop Tools to Perfect Your Image, CMP Books, San Francisco, 2003.

[62] Y. Wu, "Fast Printer Color Calibration Using Pre-Build Linearization Tables", Color Imaging X: Processing, Hardcopy, and Applications, Proc. Of SPIE-IS&T Electronic Imaging, SPIE, vol. 5667, 2005, pp. 401-408.

[63] Lexmark International Incorporated.

[64] A. Oppenheim, R. Schafer, Discrete-Time Signal Processing, 2nd Edition, Prentice-Hall, Upper Saddle River, New Jersey, 1999, pp.1-600.

[65] W. Hunley, J. Bechtel, Infrared Optoelectronics: Devices and Applications, Marcel Dekker, Inc., New York, 1987.

[66] A. Goel, H. Shah, "Gallium Arsenide-On-Silicon Technology: An Overview", Midwest Symposium on Circuits and Systems, 1989, p 1259-1262.

[67] J. Summers, L. Ng Thow Hing, "An Overview of Gallium Arsenide MMIC Processes", GEC Journal of Research, vol. 4, no. 2, 1986, pp. 104-113.

[68] Texas Instruments Ltd., Optoelectronics: Theory and Practice, McGraw-Hill Book Company, Texas Instruments Limited, New York, 1978.

[69] E. Schubert, Light-Emitting Diodes, 2nd Edition, Cambridge University Press, New York, 2006.

[70] G. Elion, H. Elion, Electro-Optics Handbook, Marcel Dekker, Inc., New York, 1979.

[71] http://www.semicon.panasonic.co.jp/ds2/SHC00011CED.pdf

[72] http://optodatabook.liteon.com/DataBookFiles/10922/E302.pdf

[73] http://media.digikey.com/pdf/Data%20Sheets/Sharp%20PDFs/pd480pi.pdf

[74] J. Lenk, Circuit Encyclopedia and Troubleshooting Guide, Vol. 3, McGraw-Hill, New York, 1996.

[75] A. Sedra, K. Smith, Microelectronic Circuits, Oxford University Press, New York, 1998, pp. 59-331.

[76] A. Malvino, Transistor Circuit Approximations, McGraw-Hill, New York, 1973.

[77] E. Wolfendale, Transistor Circuit Design and Analysis, CRC Press, Cleveland, Ohio, 1966.

[78] G. Franklin, J. Powell, Feedback Control of Dynamic Systems, 3rd Edition, Addison-Wesley Publishing Company, Inc., Reading, Massachusetts, 1994, pp. 1-131.

[79] J. Bird, Electrical Circuit Theory and Technology, 3rd Edition, Elsevior Ltd., Oxford, 2007.

[80] http://focus.ti.com/lit/ds/symlink/tlv2770a.pdf

[81] R. Prasad, Surface Mount Technology: Principles and Practice, Van Nostrand Reinhold, New York, 1989.

[82] J. Hwang, Modern Solder Technology for Competitive Electronics Manufacturing, McGraw-Hill, New York, 1996.

[83] L. Marks, J. Caterina, Printed Circuit Assembly Design, McGraw-Hill, New York, 2000.

[84] R. Ozenbaugh, EMI Filter Design, Marcel Dekker, Inc., New York, 2001.

[85] M. Gupta, Electrical Noise: Fundamentals and Sources, John Wiley and Sons, Inc., New York 1977.

[86] R. Tye, Thermal Conductivity, Academic Press, Inc., New York, 1969.

[87] T. Espinola, Introduction to Thermophysics, Wm. C. Brown Communications, Inc., Dubuque, Iowa, 1994, pp. 1-7.

[88] H. Kang, P. Anderson, “Neural Network Applications to the Color Scanner and Printer Calibrations”, Journal of Electronic Imaging, vol. 1, no. 2, pp. 125-135.

[89] K. Huang, S. Hsieh, H. Fu, “Cascade-CMAC Neural Network Applications on the Color Scanner to Printer Calibration”, IEEE International Conference on Neural Networks-Conference Proceedings, vol. 1, 1997, pp. 10-15.

[90] R. Duda, P. Hart, D. Stork, Pattern Classification 2nd Edition, John Wiley and Sons, Inc., Toronto, 2001.

[91] Patent Number: 509054, “Simultaneously Calibrating Multiple Halftones in a Printer”, September 2006.

APPENDIX A: LED DRIVER CIRCUIT STEP RESPONSE MATLAB CODE

```
%The following values are initially chosen for the TDS LED driver
circuit design.
%The values will be selected based on the rise time, settling time and
noise
%experienced by the printer once the design is implemented.

%VB=Vpwm*([Ao*F/D]*tf([D],[1 D]) where Vpwm = step input = tf([1],[1
0])
%VBdivVPwm=([Ao*F/D]*tf([D],[1 D])
%F=1/(r1*c1) and D=(r1+r2)/(r1*r2*c1)

Ao=3.3      %for 100% duty cycle

r1=1000
r2=10000
c1=1e-6

F=1/(r1*c1)
D=(r1+r2)/(r1*r2*c1)

VBdivVpwm=[Ao*F/D]*tf([D],[1 D])

step(VBdivVpwm)    %Vpwm = step input.  step(VBdivVpwm)= VB
```

APPENDIX B: CIRCUIT ANALYSIS OF THE TDS PCB CIRCUIT

Utilizing figure 52 from the Implementation and Interpretation chapter 6 section 2.1 provides the circuit for determining optimal resistor and capacitor values to maintain the rise and settling time of the circuit to 2ms and 5ms respectively. First, V_{O1} (output of op amp A1) is determined using Kirchoff's Voltage law.

$$-I_{PD} = \frac{V_{O1} - V_{REF}}{Z_{C3} // R_9 + R_6} \Rightarrow -I_{PD} = \frac{V_{O1} - V_{REF}}{\frac{\frac{1}{C_3 s} * R_9}{\frac{1}{C_3 s} + R_9} + R_6} = \frac{V_{O1} - V_{REF}}{\frac{\frac{R_9}{C_3 s}}{\frac{1 + R_9 C_3 s}{C_3 s}} + R_6} = \frac{V_{O1} - V_{REF}}{\frac{R_9}{1 + R_9 C_3 s} + R_6} \quad \text{Eq. 57}$$

$$\text{Where } V_{REF}(s) = \frac{V_{CC} F_s}{D_s}\left(\frac{D_s}{s + D_s}\right) \quad \text{Eq. 58}$$

$$D_s = \frac{R_4 + R_5}{R_4 R_5 C_2} \quad \text{Eq. 59} \qquad \text{and } F_s = \frac{1}{R_4 C_2} \quad \text{Eq. 60}$$

The equations are given by the resistor divider equation derived in chapter 5 section 4. Simplifying the circuit and isolating V_{O1} gives:

$$-I_{PD} = \frac{V_{O1} - V_{REF}}{\frac{R_6}{1 + R_6 C_3 s}} = \frac{(V_{O1} - V_{REF}) * (1 + R_6 C_3 s)}{R_6} \quad \text{Eq. 61}$$

$$-I_{PD}(R_6) = (V_{O1} - V_{REF}) * (1 + R_6 C_3 s) \quad \text{Eq. 62}$$

$$V_{O1} = V_{REF} - \frac{I_{PD}(R_6)}{(1 + R_6 C_3 s)} \quad \text{Eq. 63}$$

The output of the second op amp (A2) is determined using Kirchoff's current law.

$$\frac{V_{O1} - V_{REF}}{R_7} = \frac{V_{REF} - V_{O2}}{R_8 // Z_{C4}} \Rightarrow \frac{V_{O1} - V_{REF}}{R_7} = \frac{V_{REF} - V_{O2}}{\frac{R_8}{1 + R_8 C_4 s}} \Rightarrow \frac{V_{O1} - V_{REF}}{R_7} = \frac{(V_{REF} - V_{O2})(1 + R_8 C_4 s)}{R_8} \quad \text{Eq. 64}$$

Substitute the equation for V_{O1} (equation 63) into the equation above yields:

$$\frac{\left[V_{REF} - \frac{I_{PD}(R_6)}{(1+R_6C_3s)}\right] - V_{REF}}{R_7} = \frac{(V_{REF} - V_{O2})(1+R_8C_4s)}{R_8} \quad \text{Eq. 65}$$

$$V_{O2} = V_{REF} + \frac{I_{PD}R_8R_6}{R_7(1+R_6C_3s)(1+R_8C_4s)} \quad \text{Eq. 66}$$

$$V_{O2} = V_{REF} + I_{PD} * \frac{R_6R_8}{R_6R_7R_8C_3C_4s^2 + (R_6R_7C_3 + R_7R_8C_4)s + R_7} \quad \text{Eq. 67}$$

The Matlab code for the actual sensor circuit is displayed below. Equations 58 and 67 are the transfer functions utilized to get the step response and Bode plot of the modified TDS PCB EMI reduction circuit.

Matlab Code for the Initial EMI Reduction TDS PCB Circuit

```
%Designed EMI sensor circuit.

%Vref=Vcc*([F/D]*tf([D],[1 D]) Same transfer function as in the
%LED Driver Circuit design.
%F=1/(r4*c2) and D=(r4+r5)/(r4*r5*c2)

Vcc=5

ipd=0.55e-6;

r4=787
r5=196
r6=137000
r9=1000
r7=2000
r8=100000

c2=0.1e-6
c3=1e-9
c4=1e-9

F=1/(r4*c2)
D=(r4+r5)/(r4*r5*c2)

Vref=[Vcc*F/D]*tf([D],[1 D])

xfer=ipd*tf([(r6*r8)],[(r6*r7*r8*c3*c4) (r6*r7*c3+r7*r8*c4) r7])

Vo=xfer
```

```
Vo2=xfer+vref;
bode(Vo)
```

For the finalized TDS PCB Circuit, the analysis is displayed in equations 58-74. This replaces the analysis displayed in equations 61-67 above.

$$-I_{PD} = \frac{V_{O1} - V_{REF}}{\frac{R_9 + R_6 + R_6R_9C_3s}{1 + R_9C_3s}} = \frac{(V_{O1} - V_{REF}) * (1 + R_9C_3s)}{R_9 + R_6 + R_6R_9C_3s} \quad \text{Eq. 68}$$

$$-I_{PD}(R_9 + R_6 + R_6R_9C_3s) = (V_{O1} - V_{REF}) * (1 + R_9C_3s) \quad \text{Eq. 69}$$

$$V_{O1} = V_{REF} - \frac{I_{PD}(R_9 + R_6 + R_6R_9C_3s)}{(1 + R_9C_3s)} \quad \text{Eq. 70}$$

The output of the second op amp (A2) is determined using Kirchoff's current law.

$$\frac{V_{O1} - V_{REF}}{R_7} = \frac{V_{REF} - V_{O2}}{R_8 // Z_{C4}} \Rightarrow \frac{V_{O1} - V_{REF}}{R_7} = \frac{V_{REF} - V_{O2}}{\frac{R_8}{1 + R_8C_4s}} \Rightarrow \frac{V_{O1} - V_{REF}}{R_7} = \frac{(V_{REF} - V_{O2})(1 + R_8C_4s)}{R_8} \quad \text{Eq. 71}$$

Substitute the equation for V_{O1} (equation 70) into the equation above yields:

$$\frac{\left[V_{REF} - \frac{I_{PD}(R_9 + R_6 + R_6R_9C_3s)}{(1 + R_9C_3s)}\right] - V_{REF}}{R_7} = \frac{(V_{REF} - V_{O2})(1 + R_8C_4s)}{R_8} \quad \text{Eq. 72}$$

$$V_{O2} = V_{REF} + \frac{I_{PD}R_8(R_9 + R_6 + R_6R_9C_3s)}{R_7(1 + R_9C_3s)(1 + R_8C_4s)} \quad \text{Eq. 73}$$

$$V_{O2} = V_{REF} + I_{PD} * \frac{R_6R_8R_9C_3s + (R_6R_8 + R_8R_9)}{R_7R_8R_9C_3C_4s^2 + (R_7R_8C_4 + R_7R_9C_3)s + R_7} \quad \text{Eq. 74}$$

The Matlab code for the actual sensor circuit is displayed below. Equations 58 and 74 are the transfer functions utilized to get the step response and Bode plot of the sensor PCB circuit.

Matlab Code for the Step Response of the Sensor PCB Circuit

```
%Actual sensor circuit.

%Vref=Vcc*([F/D]*tf([D],[1 D]) Same transfer function as in the

%LED Driver Circuit design.
%F=1/(r4*c2) and D=(r4+r5)/(r4*r5*c2)

Vcc=5
ipd=0.55e-6;

r4=787
r5=196
r6=137000
r9=1000
r7=2000
r8=100000
 c2=0.1e-6
c3=1e-9
c4=1e-6

F=1/(r4*c2)
D=(r4+r5)/(r4*r5*c2)
Vref=[Vcc*F/D]*tf([D],[1 D])

xfer=ipd*tf([(r6*r8*r9*c3) (r6*r8+r8*r9)],[(r7*r8*r9*c3*c4)
(r7*r8*c4+r7*r9*c3) r7])

Vo2=Vref+xfer
step(Vo2)
bode(Vo2)
```

APPENDIX C: A/D INTERFACE CIRCUIT STEP RESPONSE MATLAB CODE

```
%The following values are initially chosen for the TDS A/D Interface
circuit design.
%The values will be selected based on the rise time, settling time and
noise
%experienced by the printer once the design is implemented.

%Vad=Vo2*([F/D]*tf([D],[1 D]) where Vo2 = step input = tf([1],[1 0])
%VaddivVo2=([Vo2a*F/D]*tf([D],[1 D])
%F=1/(r10*c5) and D=(r10+r11)/(r10*r11*c5)

Vo2a=5.0  %amplitude of Vo2
r10=10000
r11=20000
c5=0.1e-6

F=1/(r10*c5)
D=(r10+r11)/(r10*r11*c5)

VaddivVo2=[Vo2a*F/D]*tf([D],[1 D])
step(VaddivVo2)    %Vo2 = step input.  step(VaddivVo2)= Vad
```